Huge Magnetostriction of Magneto-rheological composite

Gildas Diguet

Université de Grenoble

Ecole doctorale de physique

THESE

Pour obtenir le grade de

Docteur ès Science de l'université de Grenoble

Préparée au sein du **Consortium de Recherche pour l'Emergence de Technologies Avancées** (CRETA CNRS-Grenoble) et du laboratoire **Matériaux : Ingénierie et Science** (MATEIS INSA-Lyon)

Spécialité:

PHYSIQUE des matériaux

Présentée par

Gildas DIGUET

Date de soutenance 13 janvier 2010

Huge Magnetostriction of magneto-rheological composite

Directeur de thèse : Eric BEAUGNON

Co-directeur de thèse : Jean-Yves CAVAILLÉ

Jury

M. Thierry BRETHEAU	Rapporteur
M. Iwao MOGI	Rapporteur
M. Jean-Yves CAVAILLÉ	Examinateur
M. Eric BEAUGNON	Examinateur
M. Yves BRECHET	Examinateur
M. Frank CLAEYSSEN	Examinateur
M. Georges BOSSIS	Examinateur

Remerciements

Je remercie la région Rhône-Alpes et particulièrement le Cluster MACODEV (Matériaux et Conception pour un développement Durable) pour le soutien financier apporté à ma thèse.

Ce travail s'est déroulé au sein des laboratoires MATEIS (Matériaux : Ingénierie et Science) de l'INSA-LYON et du CRETA (Consortium de Recherche pour l'émergence de Technologies Avancées) au CNRS-Grenoble. Je souhaite remercier ces 2 laboratoires pour leur accueil et particulièrement Mlle Antonia Riccobene et Marie-Dominique Bernadinis qui m'ont aidé pour la logistique.

Je tiens à remercier sincèrement mes 2 directeurs de thèse, Mr Eric Beaugnon et Mr Jean-Yves Cavaillé pour le temps et surtout la confiance qu'ils m'ont accordé au cours de ces 3 années (et un peu plus) de thèse. Je les remercie pour m'avoir envoyé dans des grandes conférences internationales à travers le monde : Rome (Italie), Sendai (Japon) et Nimègue (Pays-Bas) où j'ai pu rencontrer une communauté de chercheurs et confronter mes résultats à leur jugement. Ils m'ont laissé beaucoup de liberté dans mes travaux de thèse et ainsi permis d'acquérir une grande indépendance. Trouver des plages horaires dans leurs emplois du temps de ministres fut assez compliqué, néanmoins nous avons réussi à finaliser ce projet, ce manuscrit en est la cristallisation.

Je remercie les deux rapporteurs de thèse, Mr Thierry Bretheau et Mr Iwao Mogi qui est venu spécialement du Japon pour la soutenance. Je remercie aussi Messieurs Yves Brechet, Georges Bossis d'avoir accepté de faire parti du Jury. Ainsi que Mr Frank Claeyssen qui fut mon professeur de matériaux actifs pendant mon Master 2 Pro Ingénierie des Systèmes Magnétiques et mon superviseur lors de mon stage à Cedrat Tech ; il m'a donné le gout et l'intérêt pour les matériaux magnétostrictifs qui m'ont ensuite amené à choisir, plus tard, cette thèse.

J'adresse ensuite ma reconnaissance à Mr Pierre Mohlo qui a mis à ma disposition son électro-aimant mais aussi pour ses conseils et nos discussions pendant ces 3 années de thèse.

Je garde enfin un très bon souvenir des personnes que j'ai côtoyé : Tristan et Ghislain pour les aventures nocturnes au CRETA, les copines : Albin, Sophie et Justine pour les quizz questions pour un champion online, la quatrième copine : Eliza, Sylvain pour sa « grande patience » aux mots fléchés, Jérémy pour sa légendaire bonne humeur, Cuiping , Jinna, Haixia et Jan Jun qui m'ont fait découvrir la culture chinoise, Andrea pour « l'italian touch » du labo, Stef, Nath sans oublier Virginie et tous les lanceurs de boulettes. Je souhaite beaucoup de réussite à Alex (un jour, on arrivera à se voir à Rennes) et Bianca pour leurs thèses.

J'adresse un énorme merci à Thomas d'avoir été plus qu'un collègue de travail, je te souhaite bonne chance pour la suite même si je sais que tout ira bien pour toi. Et enfin, mes pensées vont vers mon très cher Cyril pour nos grandes discussions dans ta voiture, dans mon bureau ou chez toi (en l'absence de ta femme) avec Attila et Cobalt ; tu gardes toute mon estime et mon amitié.

Je tiens à remercier Philippe et sa bonne humeur ; j'ai grandement apprécié ta compagnie dans le bureau. Patricia pour ton excellente soupe les soirs de corrections de dernière minute avec Eric, Xavier et Jean-Louis pour vos aides aux mots fléchés, Sophie pour tes connaissances sur les matériaux

magnétiques durs, Catherine pour ton soutien moral les samedis en fin de thèse, Laureline pour nos profondes discussions et nos rire dans la cuisine avec Paul. Je tiens ainsi remercier Paul et Pierre-Fred pour l'aide lors de la réalisation de pièces nécessaires à mon dispositif expérimental, vos sympathies respectives qui ont rendu très agréables mon séjour dans ce labo.

Dans l'équipe MATEIS, je remercie très chaleureusement Jenny avec qui j'ai passé une super conférence et partagé un séjour mémorable au pays du soleil levant ; les 2 agréables voisins de mon bureau temporaire : Séverine et Laurent, et enfin Catherine, Jean-Marc et Joël.

Ma gratitude va aussi à Maela, David et Germain pour les vendredis soir aux thématiques variées qui ont changé mon état d'esprit grâce à nos fous rires intensifs. Et je n'oublie pas non plus Ion, Piotr, Oana, Danny et Meryll.

Un merci aussi à mes amis parisiens qui m'accueillent lors des voyages Grenoble-Rennes : Jérôme avec qui je passe toujours de bons moments que ce soit en Italie, en Belgique, à Grenoble ou Paris ; Julien qui partit tôt dans la Belle Province, Damien qui resta un peu plus sur Grenoble, Will qui a défoncé la porte des toilettes de mon appartement, Olivier qui nous enseigna la Salsa.

Catherine Dejoie reçoit aussi toute ma gratitude et reconnaissance pour les soirées autour de bières à partagé nos durs moments de fin de thèse de rédaction.

J'exprime ma gratitude à ma famille pour le soutien moral et de m'avoir poussé à aller toujours plus loin dans les études et dans le monde.

Et Mali qui est récemment entrée dans ma vie et m'a beaucoup apporté.

Je sers la science et c'est ma joie

Disciplus simplex - Leonard, de Groot & Turk

Summary

List of symbols:

H	Magnetic field [A/m]
H_0	Applied/External magnetic field [A/m]
H_d	Demagnetizing magnetic field [A/m]
B	Magnetic induction [T]
M	Magnetization [A/m]
m	Magnetic moment [Am^2]
F	Force [N]
f_v	Density of force per unit of volume [N/m^3]
Γ	Torque [Nm]
Γ_v	Density of torque per unit of volume [N/m^2]
ε	Strain [-]
σ	Stress [Pa]
τ	Shear stress [Pa]
E	Young's modulus [Pa]
ν	Poisson's ratio [-]
G	Shear modulus [Pa]

Introduction

This thesis is aimed to measure and explain the apparent magnetostriction of a composite when exposed to an external homogeneous magnetic field. The studied composite is composed of ferromagnetic particles (mainly Iron here) dispersed in an elastic matrix. An elongation up to 4.3% can be seen in 30% filled composite when exposed to a uniform magnetic field (Ref. Fig.III.6). The matrix is non-magnetic and Iron is weakly magnetostrictive (maximum strain around 10^{-5}). The composite deformation is 4 orders larger than the magnetostriction of the magnetic phase. None of the compounds used for the composite is (or too weakly) magnetostrictive. The observed phenomenon is a deformation due to an applied magnetic field, like the magnetostriction, which we will refer as magnetostriction in the following chapters, but it should be emphasized that it is not magnetostriction from the physical point of view. Their respective origins are totally different; magnetostriction is due to the magneto elastic coupling of a ferromagnetic crystal lattice whereas the observed magnetostriction is due to dipolar interactions.

The remote deformation of material needs a coupling between the referred material and the control field. Those materials are called active materials. Induction of the deformation has been studied since the discovery of magnetostriction and piezoelectricity two hundred years ago. Enhancement of properties has been explored through metallurgical approaches but magnetostriction is limited by the materials high elastic constants, generally some 100 GPa. Another solution has been found out more recently which consists in mixing magnetic particles in a soft elastic matrix. Organic elastomers are good candidates as matrix because of their low Young modulus. Materials made of injected ferromagnetic (or ferroelectric) particles in such polymer are called Magneto (Electro) Rheological Elastomers.

The rare-earth materials exhibit a 10^{-3} large magnetostriction, which is qualified “giant magnetostriction”. The apparent magnetostriction of these composite is larger than any magnetostrictive materials, so that it can be called “huge magnetostriction”. This result is achieved by the choice of the right compounds. Indeed, the matrix is elastically soft (with a low Young modulus) to ease the deformation and to provide a linear response whereas the particles are highly magnetic to maximize the magnetic force.

Mechanisms of this apparently huge magnetostriction are detailed in the following chapters. The origin of the elongation, the way particles get magnetized in a composite, the elastic response of the

matrix to the magnetic stress, or the effect seen from different filling factor or the quantity of added particles are described further.

The first chapter presents the starting point of all that follows in the thesis; all magnetic and mechanical laws that will be used forward in the manuscript are introduced here. Moreover, an introduction to MRE composite and their magneto-mechanical properties already known are gathered here.

The second chapter presents the materials preparation of material and their characterization used during the thesis. Devices, like magnetostriction and magnetization recorder, are also described in this chapter.

The third chapter deals with the origin of that apparent magnetostriction. It provides a model based on the interaction of the ferromagnetic particles dispersed in the soft matrix. Forces are calculated through the dipolar interaction and the strain is estimated using a finite element mechanical approach (FEM).

The fourth chapter treats the magnetization of the composite, as a homogeneous magnetic material. It will focus on the magnetic saturation and the magnetization slope. This slope is linked to the demagnetizing factor. Therefore, an effective demagnetizing factor will be introduced for such composites.

The fifth chapter presents the magnetostriction of the composite. The composite is treated as homogeneous with effective magnetic and mechanical properties. The way in which the filling factor impacts on the magnetic stress and the mechanical response, and thus on the effective magnetostriction is provided. Shape effect is also discussed in the same chapter.

The sixth chapter focuses on the magnetostriction composite filled with hard magnetic particles. Such particles are characterized by their magnetic remanence and hysteresis. Those parameters do influence the strain of the composite when they are placed in the presence of magnetic field.

The effect of temperature is discussed in the seventh (and last) chapter. Both magnetization and elastic modulus are indeed temperature dependent.

Chapter 1

Some background elements

I. Physics

The analysis of the strain of a composite placed in a uniform applied magnetic field is proposed in this thesis. This phenomenon is due to the magnetic interaction (chap.III). In this end, a brief and condensed presentation of magnetic laws which allowed us to calculate the magnetic interactions & magnetic stresses that act on the material. Magnetic field in the matter, forces and torques exerted on magnetic material are briefly described. It also describes the elastic laws used in the calculation of the strain.

I.1. Magnetostatic

Magnetic field and induction are linearly related as:

$$\vec{B} = \mu_0(\vec{H} + \vec{M}) = \mu_0(\vec{H}_0 + \vec{H}_m + \vec{M}) \qquad \text{eq.I.1}$$

With μ_0=4π10^{-7}, the vacuum permeability, *B* is the magnetic induction, *H* is the magnetic field H_m and H_0 are matter and external/applied field, *M* is the material magnetization.

I.1.1.Magnetic materials

The magnetic properties of media are affected by the presence of a magnetic field and acquire a macroscopic magnetization. Magnetization is defined as the density of magnetic moment, *m*, per unit volume:

$$\vec{M} = \frac{d\vec{m}}{dV} \qquad \text{eq.I.2}$$

In the case of linear materials, or at low magnetic field, the magnetization is set as:

$$\vec{M} = \chi\vec{H} \qquad \text{eq.I.3}$$

The susceptibility χ varies in a wide range depending on the kind of magnetic materials. Diamagnetism results in a negative and small susceptibility, typically χ_d is in the range of -10^{-6} to -10^{-5}, in contrast to the paramagnetic susceptibility, χ_p, which is positive, but still with low values; 10^{-6} to 10^{-3}. Industrial applications use the soft ferromagnetic materials which have much larger susceptibilities; χ_f will reach values 10^4 to 10^6 for Permalloy.

The response of a ferromagnetic medium to an external field can be summarized as follows. Increasing the magnetic field increases the magnetization via a first magnetization curve. Enhancing the field drives the magnetization in a state where all the magnetic moments are aligned in the direction of the applied field. This state of magnetization defines the saturated magnetization M_{sat}.

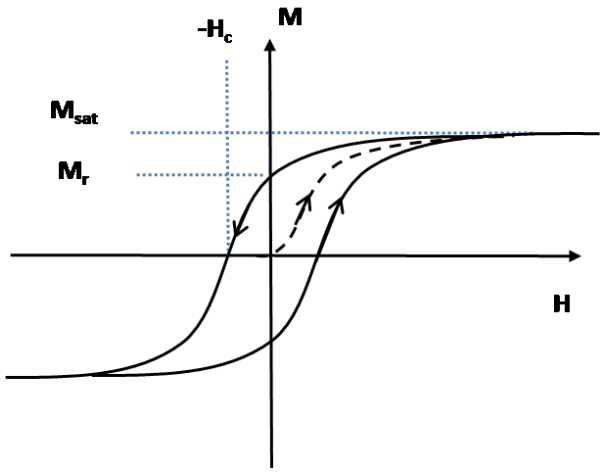

Fig.I.1Typical magnetization curve M(H)

Decreasing the magnetic field back to zero leads the magnetization to a non-null value. A remanent magnetization M_r appears due to defaults and magnetic anisotropy inside the materials. Bringing the magnetization to a zero state needs to decrease the applied field to negative values down to the coercive field H_c. A thin hysteresis is characteristic of soft materials, like Iron, unlike hard magnetic materials with a large hysteresis: those are currently used to make “magnets”.

I.1.2.Magnetic field in magnetized materials

The magnetic field inside a magnetized material is the superposition of the external field H_0 and the field which is generated by the magnetized body H_m:

$$\vec{H} = \vec{H}_0 + \vec{H}_m \qquad \text{eq.I.4}$$

Magnetic field, generated by magnetic materials, can be deduced from Coulombian model, which is an analogy to the field created by an electric dipole.

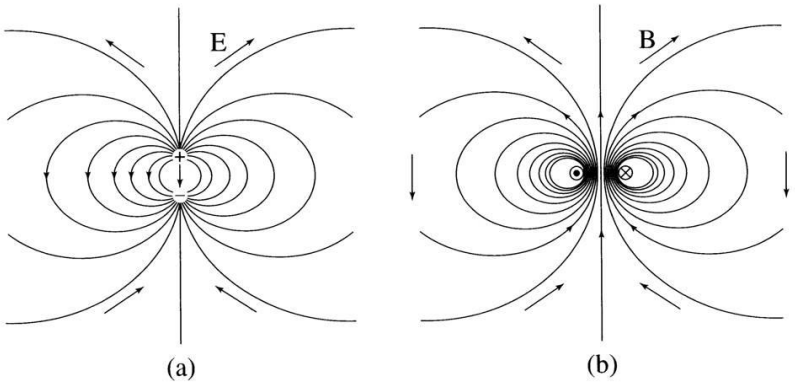

Fig.I.2 Equivalence of an electric dipole and the magnetic field created by a coil

The magnetic field is then:

$$\vec{H}_m = \int_V \frac{\mu_0}{4\pi} \frac{\rho\vec{r}}{r^3} dV \qquad \text{eq.I.5}$$

In that calculation, the equivalent charges have 2 origins; a volume density for non-homogeneous magnetized media, and a surface density:

$$\rho_V = -div(\vec{M}) \qquad \text{eq.I.6}$$

$$\rho_S = \vec{M} \cdot \vec{n} \qquad \text{eq.I.7}$$

Calculation of this magnetic field is an integral operation which is usually performed by FEM software. However, when the sample is an ellipsoid, the solution is analytically known; in the case of a sphere:

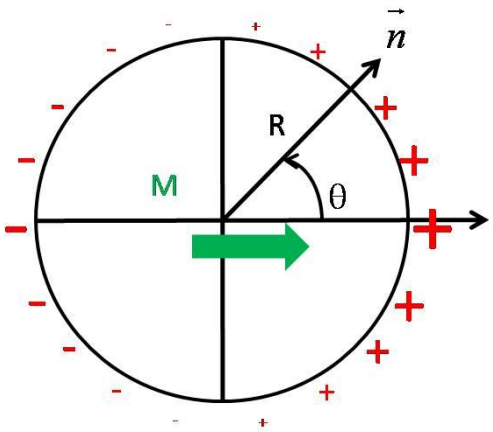

Fig.I.3a Map of the pseudo magnetic charge on the surface of a uniformly magnetized sphere

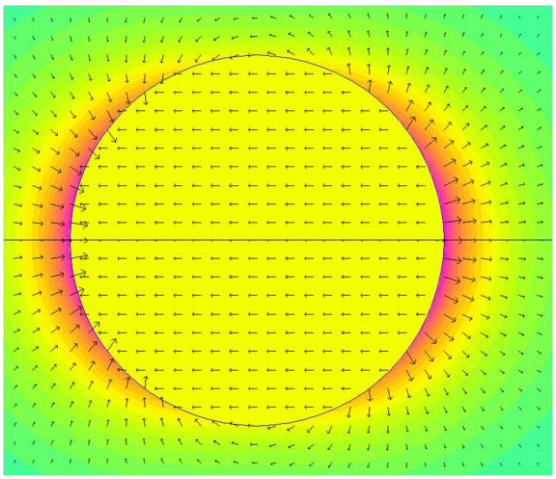

Fig.I.3b Map of the magnetic field of the sphere, using FEMM software

$$\vec{H}_m^{\text{int}}(r,\theta) = -\frac{\vec{M}}{3} \qquad r < R \qquad \text{eq.I.8}$$

$$\vec{H}_m^{ext}(r,\theta) = \frac{R^3}{r^3}\left[M\cos(\theta)\vec{n} - \frac{\vec{M}}{3} \right] r > R \qquad \text{eq.I.9}$$

This inner magnetic field, H_m^{int}, is also called demagnetizing field due to the reverse direction compared to the magnetization direction. Therefore, the effective magnetic field viewed by magnetic materials is less than the applied field. In the case of ferromagnetic materials, this magnetic field rules the magnetization curve versus the applied field. In the case of an ellipsoid, this demagnetizing field is uniform and proportional to the magnetization through a demagnetizing factor: its value is 1/3 for a sphere. Chapter IV will focus on this coefficient in other geometries and in the case of a composite made of ferromagnetic particles.

I.1.3. Magnetic interactions of a moment in a magnetic field

I.1.3.1. Magnetic force

The interaction energy of a magnetic moment *m* placed in an induction field *B* is defined as:

$$W = -\vec{m}\cdot\vec{B} \qquad \text{eq.I.10}$$

If the magnetic moment is placed in a non-homogenous field, the moment will experience a force **F** to decrease the interaction energy.

$$\vec{F} = -\vec{\nabla}(W) = (\vec{m} \cdot \vec{\nabla})\vec{B} \qquad \text{eq.I.11}$$

A body force f_v can be defined as the density of force per unit volume [Mag1]:

$$\vec{F} = \int_V \vec{f}_V dV \qquad \text{eq.I.12}$$

$$\vec{f}_V = (\vec{M} \cdot \vec{\nabla})\vec{B} \qquad \text{eq.I.13}$$

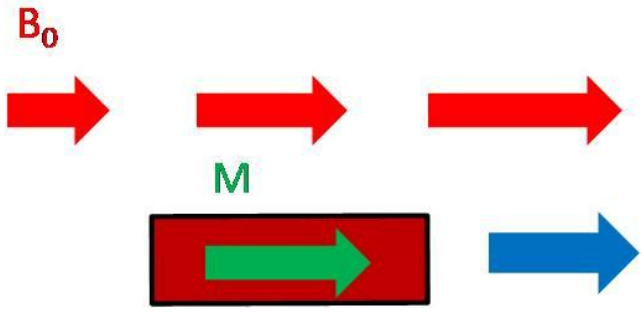

Fig.I.4 Magnetic force experienced by a magnet placed in a gradient of magnetic induction

Eq.I.11 (and eq.I.13) shows that a positive gradient of the viewed magnetic field results in a positive magnetic force; a magnetic moment experiencing such force will be displaced toward higher amplitude of magnetic field.

The body force expression can be expanded as:

$$\vec{f}_V = (\vec{M} \cdot \vec{\nabla})\vec{B} = \begin{bmatrix} M_x \frac{\partial B_x}{\partial x} + M_y \frac{\partial B_y}{\partial x} + M_z \frac{\partial B_z}{\partial x} \\ M_x \frac{\partial B_x}{\partial y} + M_y \frac{\partial B_y}{\partial y} + M_z \frac{\partial B_z}{\partial y} \\ M_x \frac{\partial B_x}{\partial z} + M_y \frac{\partial B_y}{\partial z} + M_z \frac{\partial B_z}{\partial z} \end{bmatrix} \qquad \text{eq.I.14}$$

I.1.3.2. Magnetic torque

In a uniform field, if the moment and the magnetic field are not parallel, a magnetic torque *Γ* will act to align the moment in the direction of the field, which reduces the interaction energy.

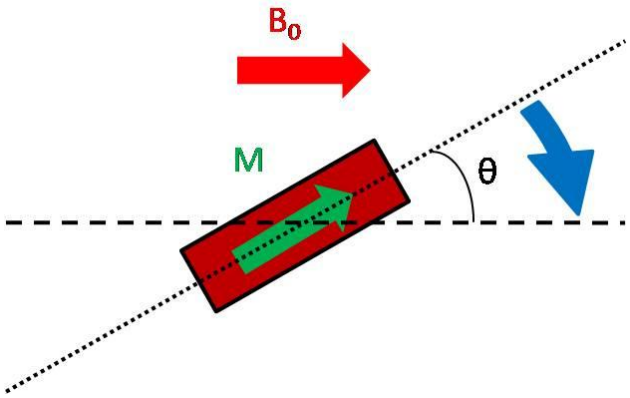

Fig.I.5 Magnetic torque on a magnet placed in uniform induction

$$\vec{\Gamma} = \vec{m} \times \vec{B} \qquad \text{eq.I.15}$$

Expanding this expression in respect with the angle θ, defined as the angle between the magnetization and the magnetic field, yields to:

$$\Gamma = mB\sin(\theta) \qquad \text{eq.I.16}$$

A density of magnetic torque *Γv*, per unit of volume, can be defined as [Mag1]:

$$\vec{\Gamma}_v = \vec{M} \times \vec{B} \qquad \text{eq.I.17}$$

This torque will rotate the magnet until the angle θ decreases to zero, i.e. until the direction of the magnetization is the same as the direction the magnetic field.

I.2. Mechanical constants

I.2.1.Elasticity

The material elastic response to external solicitations is described by a set of elastic constants. They are intrinsic to the material. For an isotropic material, two different constants are required to completely define its elastic behavior. In fact, three constants are often used, namely: Young modulus, Poisson ratio and shear modulus.

→ Young modulus

An elastic body is deformed whenever a force *F* is applied on it. The resulting displacement *dL* is linearly linked to the force, by a constant factor called the force (or spring) constant *k*. This is the Hooke law:

$$F = kdL \qquad \text{eq.I.18}$$

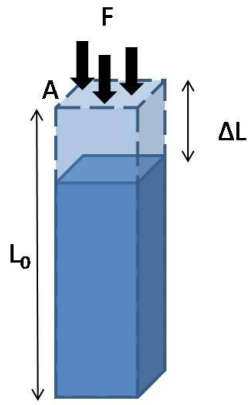

Fig.I.6 Deformation of an elastic material

In continuum mechanics, force and displacement are replaced by stress σ and strain ε, respectively defined as the force divided by its surface area *A* and the change in length *dL* divided by the current length *L*. If *dL* is small, then L can be replaced by L_0:

$$\sigma = \frac{F}{A} \qquad \text{eq.I.19}$$

$$\varepsilon = \frac{dL}{L_0} \qquad \text{eq.I.20}$$

Stress and strain are related, in the range of the Hooke law through the dimensionless factor *E*, the Young modulus:

$$\frac{\sigma}{\varepsilon} = \frac{kL_0}{A} = E \qquad \text{eq.I.21}$$

The Young modulus or longitudinal elastic modulus is defined as the ratio of the stress by the strain for body in tension or compression, as far as the behavior is linear.

Young modulus is an intrinsic elastic property of a given material and is also shape-independent. Iron modulus is close to 260 GPa whereas elastomers modulus have a much lower values, in the range of MPa.

→ Poisson ratio

Materials bodies pulled in one direction tend to contract in the transversal direction. The transversal strain divided by the axial strain, in the direction of the load, gives the Poisson ratio

$$\upsilon = -\frac{\varepsilon_{transveral}}{\varepsilon_{axial}} \qquad \text{eq.I.22}$$

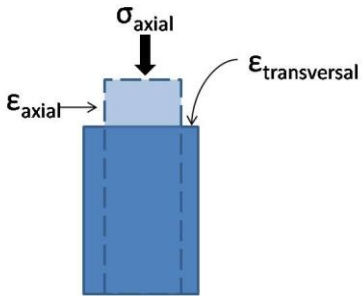

Fig.I.7 Transversal deformation of an elastic material, due to Poisson ratio

The minus sign, in eq.I.22, leads to a positive Poisson ratio value. This value ranges from 0 to 0.5. A 0.5 value induces a complete incompressibility of the material. Many metals have ν=0.27 – 0.35 unlike elastomers and rubbers which have ν=0.5.

→ Shear modulus

Stress is generally expressed by the stress tensor σ_{ij} with:

$$\sigma = \begin{bmatrix} \sigma_{xx} & \tau_{xy} & \tau_{xz} \\ \tau_{zy} & \sigma_{yy} & \tau_{yz} \\ \tau_{zx} & \tau_{zy} & \sigma_{zz} \end{bmatrix} \qquad \text{eq.I.23}$$

For $i \neq j$, σ_{ij} is shear stress, and is often written τ_{ij}. Similarly to the Young modulus which is defined as the ratio of the strain created by a perpendicular stress on a surface, the shear modulus G defines the ratio of the strain created by a tangential stress on a surface, the shear stress. Using the general law that linked the strain to stress [Lan1]:

$$\varepsilon_{ij} = \frac{1}{G}\tau_{ij} \qquad \text{eq.I.24}$$

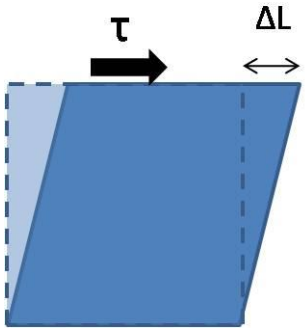

Fig.I.8 Deformation of an elastic material due shear stress

The shear modulus, Young modulus and the Poisson ratio are related as:

$$G = \frac{E}{2(1+\nu)} \qquad \text{eq.I.25}$$

The shear modulus of an incompressible medium (ν=1/2) is $G=E/3$.

I.2.2. Viscoelasticity

For purely elastic materials as above, the strain and the stress are linked by a timeless equation. However, for most elastomers, the response is linearly viscoelastic, i.e., is a combination of elastic and viscous components.

Elastic component: $\sigma = E\varepsilon$ eq.I.26

Viscous component: $\sigma = \eta \frac{d\varepsilon}{dt}$ eq.I.27

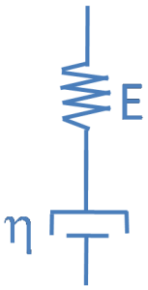

Fig.I.9a Maxwell model

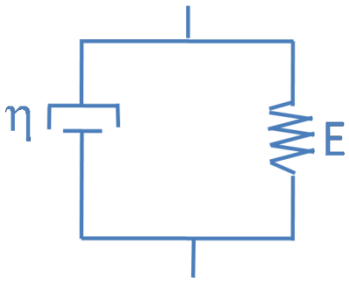

Fig.I.9b Voigt model

Empirical models have been built using 2 mechanical elements, namely: a spring and a dashpot. Maxwell model corresponds to a dashpot and a spring connected in series, giving the time dependant elongation below:

$$\frac{d\varepsilon}{dt} = \frac{\sigma}{\eta} + \frac{1}{E}\frac{d\sigma}{dt}$$ eq.I.28

Whereas the Voigt model, the spring and the dashpot are connected in parallel; the material is then ruled by the following time-dependent equation:

$$\sigma = \eta \frac{d\varepsilon}{dt} + E\varepsilon$$ eq.I.29

Both models introduce a relaxation constant:

$$\tau = \frac{\eta}{E}$$ eq.I.30

These materials exhibit a viscoelastic response to any stress.

II. Active materials

Active materials are defined as materials able to produce a mechanical effect (shear, contraction, elongation…) with an external non-mechanical stimulus such as magnetic field, electric field, temperature (as an example, actuators controlled by temperature were developed very successfully using shape memory alloys; the shape memory effect is a solid state phase transition which occurs in some metallic alloys and yields a change in the atomic arrangement. Low temperature phase is known as martensite and the high temperature is the austenite), etc … Active materials also could have the inverse property: being exposed to a stress, they change their polarization or magnetization. Such active materials are currently used as industrials device like actuators or sensors.

II.1. Piezoelectricity

Piezoelectricity results from the coupling between mechanical strain and electrical polarization that exists in some materials like crystals (quartz), ceramics (ex: PZT: Lead Zirconium Titanate) and also in polymers (polyvinylidene fluoride: PVDF). A stress applied to this crystal changes the electric polarization and inversely, an electric field E applied on this crystal deforms it.

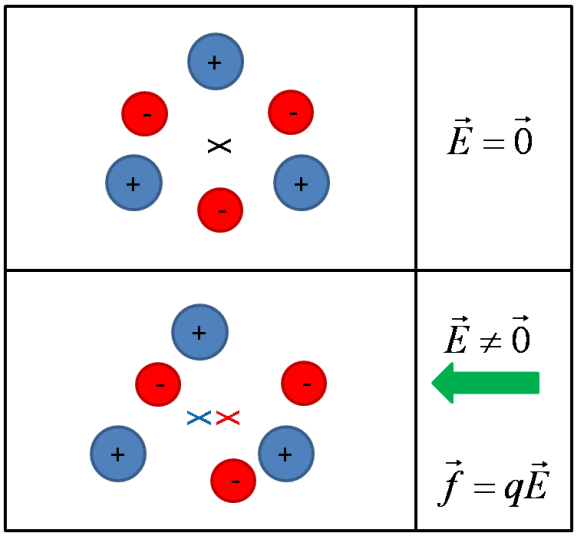

Fig.I.10 Piezoelectricity

This electromechanical ability has been discovered in 1880 by Jacques and Pierre Curie on a quartz crystal. The positive and negative charges, in a crystal lattice, are symmetrically distributed, so that the crystal is neutral. With an external electric field, charges are attracted or repulsed in the field's direction, according to their signs, which yields to an overall deformation (Fig.I.10, piezoelectricity). Piezoelectricity is mainly a linear function between strain, stress and the electrical field:

$$S = sT + dE \qquad \text{eq.I.31}$$

Where *S* is the strain, *T* the stress, *E* the electric field; *s* and *d* are coupling constants.

II.2. Magnetostriction

Magnetostriction effect was discovered by J. P. Joule in 1842 [Jou1] by noticing the elongation of an iron rod submitted to a local magnetic field. A material is said magnetostrictive when a change of magnetization results in a change of shape. Most of pure ferromagnetic media are magnetostrictive despite exhibiting a relatively small deformation (roughly 10^{-5}); metallic compounds and alloys are barely having a maximal magnetostriction larger than 10^{-4}. First applications of these materials were the sonar transducers although magnetostrictive materials were soon replaced by the piezoelectric PZT ceramic, for better physical properties.

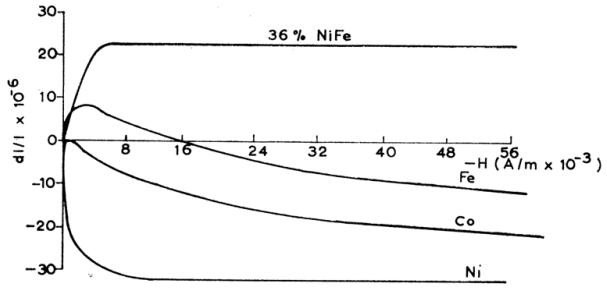

Fig.I.11a Magnetostriction versus magnetic field [Mag2]

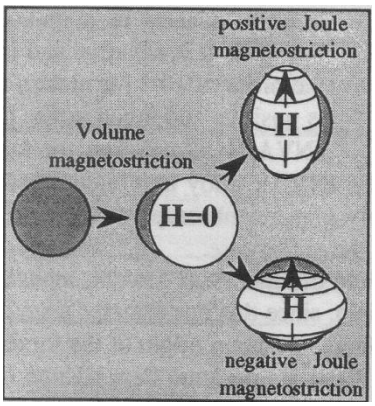

Fig.I.11b Volume and Joule magnetostriction [Tre]

Nevertheless, in the 1960's, Belov [Bel], discovered the giant magnetostriction, above 10^{-3}, for rare earth compounds $R_3Fe_5O_{12}$ (where R = Gd, Tb, Dy, Ho, Er or Yb), but only at low temperatures (below 100 °K). Clark [Tre] has then found out, in 1974, the giant magnetostriction at room temperature with a $Dy_{0.3}Tb_{0.7}Fe_2$, well-known as Terfenol-D; named after TERbium Iron (Fe) Naval Ordnance Laboratory and D for Dysprosium. This material is still the highest Joule magnetostrictive material at room temperature.

III. Magnetic Rheological Elastomers

MRE (Magnetic Rheological Elastomers), are composites made of ferromagnetic particles dispersed within a non-magnetic elastomer matrix. Such composites are used for their low elastic constant, some few MPa, which allows large strain. The magnetic interactions of the particles provide the force that changes the composite properties.

Those materials have elastic properties tunable by an external magnetic field. Indeed, the interactions between the particles lead to an apparent magnetic stress which changes their elastic behavior. This interaction is dependent on the inner distribution of the particles. The particles are usually randomly dispersed in the whole volume, in contrast to those which receive a magnetic treatment while the matrix is curing, leading to an anisotropic distribution of the particles. This latter category of MRE is often called "Field Structured Elastomer", (FSE). Chain-like, sheet-like, or more complicate structure belongs to the FSE kind [Mar1]. FSE and MRE exhibit different responses to a mechanical solicitation and also to a magnetic field. Kallio [Kal] uses the definition of isotropic MRE and aligned MRE.

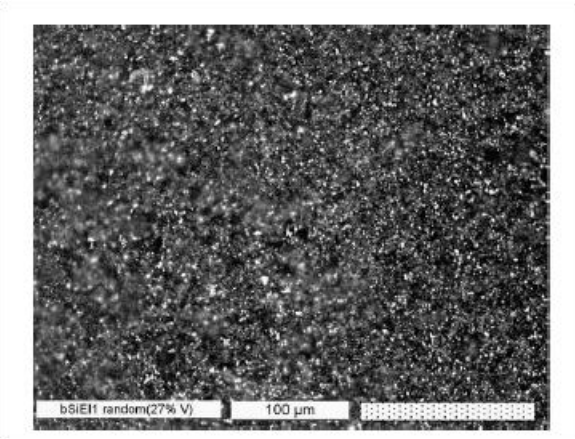

Fig.I.12a [Far] Randomly filled composite

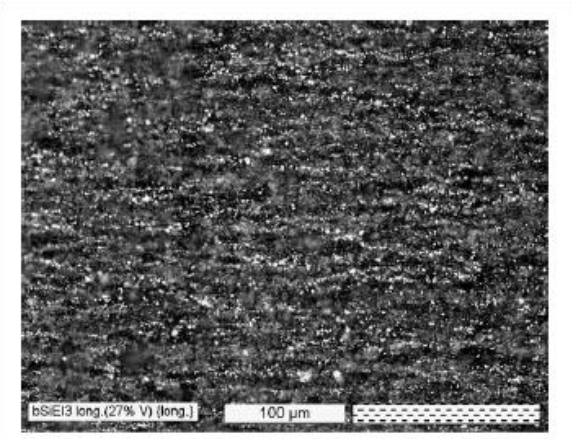

Fig.I.12b [Far] Structured composite

We have selected some articles which represent the state of the art in each sub-domain. Articles are briefly presented with the composition of the sample, when explicitly told, matrices and particles; the physical models are also provided using the author's notation and final results. Most of papers have been written on the possibility of magnetically tuning mechanical properties of the composite, by the application of a magnetic field, like the delta-E effect or the magneto-viscoelasticity. Fewer papers on the change of sample shape under magnetic field are presented as the sample is submitted to a field gradient or to a homogeneous field.

IV. Elastic tunable properties with a magnetic field

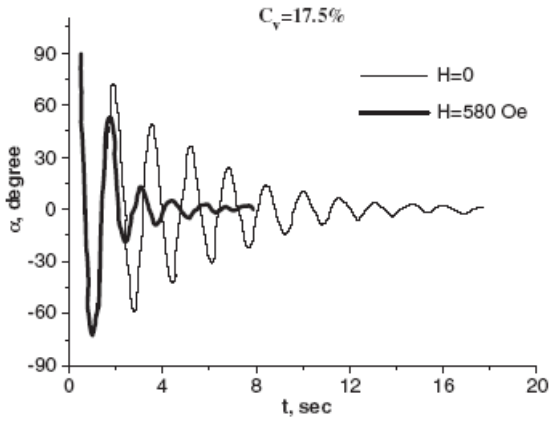

Fig. 6. Dependences of twisting angle α on time t in magnetic field and without field.

Fig.I.13 [Nik]Mechanical damping of a composite with and without magnetic field

The dependence of the mechanical damping on the external homogeneous magnetic field was shown by Nikitin & Al. [Nik]. His experiment was led on a cylinder filled by 2µm iron particles, which was twisted with and without magnetic field. When a magnetic field is applied, damping increases due to the interaction of the ferromagnetic particles. These interactions between the particles reinforce the stiffness of the materials. This result is extended by Varga & al. [Var], who also studied the magneto elasticity of elastomers, but there, as the effect of the particles distribution on the elastic modulus.

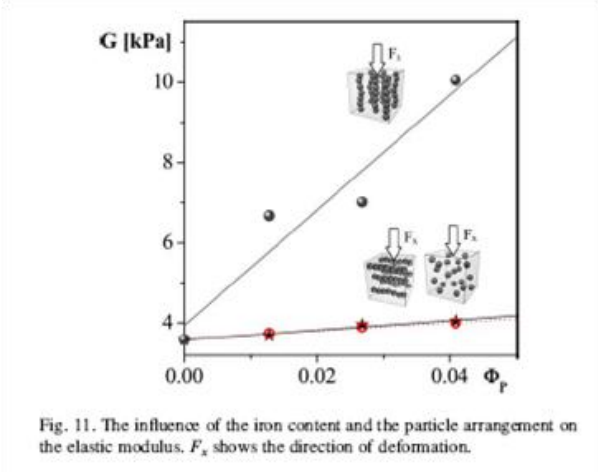

Fig. 11. The influence of the iron content and the particle arrangement on the elastic modulus. F_x shows the direction of deformation.

Fig.I.14 [Var] Changes of Young modulus for composite with different particles distributions

V. Shape change under magnetic field

Deformation of a MRE may be generated by the application of a magnetic field. Two cases, leading to composite strain, have been studied. First, applying a non-homogenous field, each magnetic particle is submitted to a force and, as a consequence, the material changes its shape to get closer to the higher field: the composite is strained.

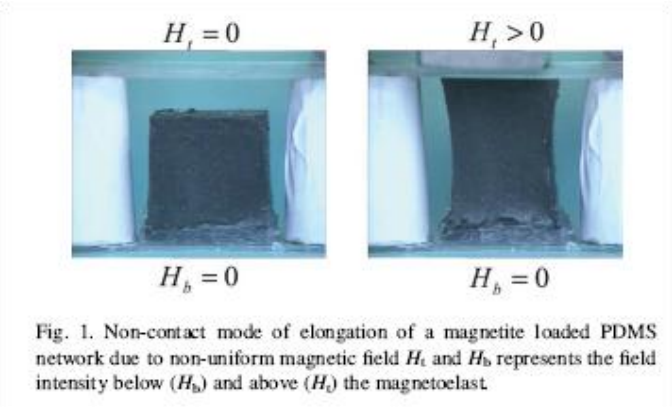

Fig. 1. Non-contact mode of elongation of a magnetite loaded PDMS network due to non-uniform magnetic field H_t and H_b represents the field intensity below (H_b) and above (H_t) the magnetoelast.

Fig.I.15 [Var] Length changes of a magneto elastomer due to an external gradient of magnetic field.

Secondly, with the application of a homogeneous field, the magneto elastomer can also deform due to inter-particles interactions. This effect was observed for both structured elastomers and randomly filled elastomers.

V.1. Changes resulting from a non-homogeneous field

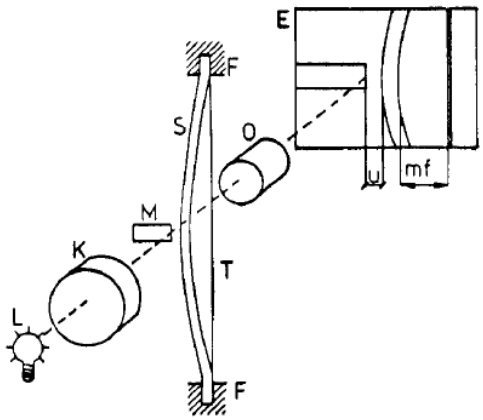

Fig. 7. Scheme of the measuring system: S ferroelast sample; F holder; T inextensible thread; M magnet; L light source; K condenser; O objective; E screen.

Fig.I.16 [Bed2] Bending of a long composite in the neighborhood of a magnet

Bednarek [Bed2] has studied the deflection of a silicone-steel composite beam fixed to its endpoints and submitted to a nearby magnet. Samples are prepared with a silicone matrix, used for its low Young modulus E_0=0.25 MPa, mixed with 0.10 – 0.15 mm steel particles. In this paper the magnetic force was estimated with the following expression:

$$P = \mu_0 \int_V (\mu_f - 1) H \left(\frac{\partial H}{\partial x} \right) dV \qquad \text{eq.I.32}$$

And the deflection is

$$f = \frac{Pl^3}{192 E_f I} \qquad \text{eq.I.33}$$

where μ_f is the relative permeability of the composite. H and $\partial H/\partial x$ stand for the magnetic field and gradient, respectively, created by the magnet. E_f stands for the effective Young modulus of the composite.

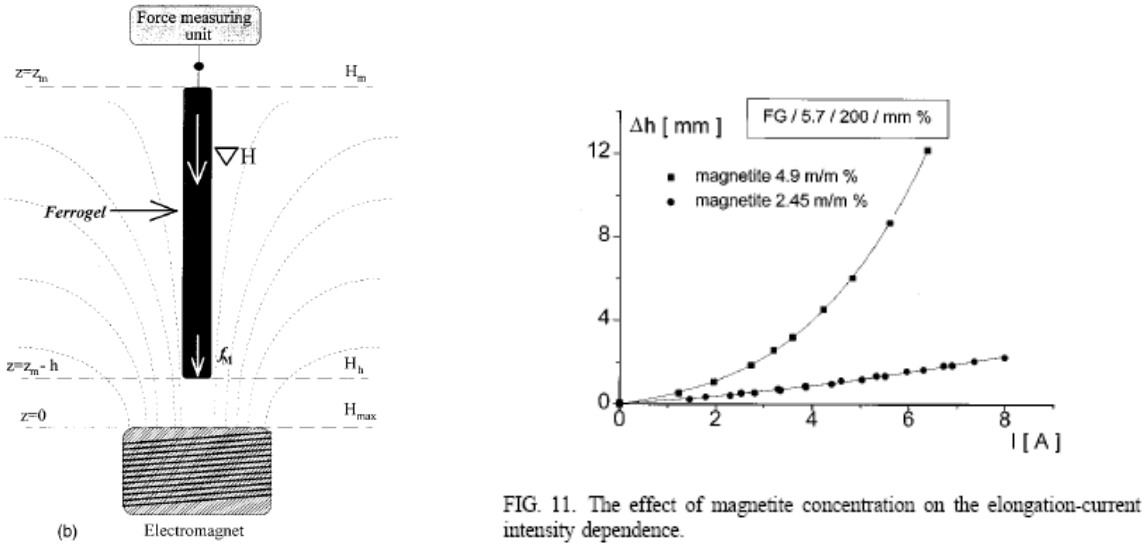

FIG. 11. The effect of magnetite concentration on the elongation-current intensity dependence.

Fig.I.17 [Zri1] *Stretching of a composite above an electromagnet*

In the same idea, Zrinyi [Zri1] has studied the elongation of a ferrogel within the field gradient created by an electromagnet placed under the composite. This ferrogel is a poly (vinyl alcohol), PVA, filled by magnetite (Fe_3O_4) particles with an average size of 10-12 nm. The composite was molded as a 120 mm long cylinder, with a content of magnetite close to 2-5 wt.% , and an effective elastic modulus of G=0.69 kPa. Experiments were carried out with an electromagnet creating a maximal

induction of 90mT (on the surface) and placed below the sample with a CCD camera shooting the displacement of the cylinder bottom. The force exerted on the sample is given as:

$$f_m = \int_V \mu_0 \vec{M} \left(\frac{\partial \vec{H}}{\partial z} \right) dV \qquad \text{eq.I.34}$$

Assuming that the magnetic field is small enough to restrict the magnetization in a linear approximation, $M = \chi H$; the mechanical behavior is also set as linear, using a Hookean law leading to the expression of the ferrogel length-change as :

$$\Delta h = h_0 \frac{\mu_0 \chi}{2G} (H_h^2 - H_m^2) \qquad \text{eq.I.35}$$

H_m and H_h are respectively the magnetic field viewed on the top and the bottom of the cylinder. In this experiment, Zrinyi reached a maximal displacement of 12mm i.e. roughly a 10% strain for this ferrogel. Such large strain is achieved with a very low elastic modulus of the composite: 0.69 kPa.

V.2. Changes resulting from a homogeneous field

As mentioned above, the response of a MRE to a magnetic solicitation highly depends on the distribution of the magnetic particles within the matrix. Field Structured Elastomers are stiffer than a randomly-filled Elastomers; their magnetostrictive behavior will also be different. In the first case, FSE will contract when a magnetic field is applied parallel to the chain-like columns: this is due to the attraction of the closest particles; on the contrary, randomly-filled elastomers will expand. These results are presented below.

V.2.1. Structured composite

Magnetostriction of FSE was intensively studied by Martin & Al. [Mar1]. The magnetostriction of the FSE is explained in this case by “the tendency of dipole pairs, aligned with the applied field, to approach each other, causing a contraction of the sample along the field and dipole pairs perpendicular to the field to push each other away, reinforcing the contraction along the field, due to the fact that Poisson ratio is close to ½ for these materials” as illustrated on Fig.I.18.

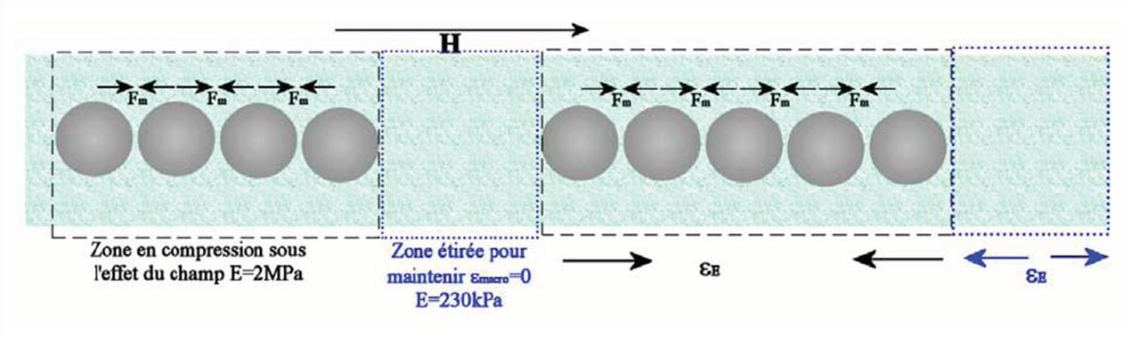

Fig.I.18 [Coq] Contraction of columns of particles due to inter-particles interaction.

Composites are prepared using 3-5µm irregular-shaped iron particles chosen to maximize the magnetic stress and a silicone matrix to maximize the elastic response. While curing, the structure was made using a triaxial magnetic field. Such field was used to provide information on the magnetostriction due to different particle structures and test for different magnetostriction behaviors. In Martin's model, the magnetostriction of composites depends on two parameters ψ_2 and ψ_4 describing the specific structures of the particles distribution and estimated from the formula of the dipolar field:

$$\vec{H}_{dip} = \frac{1}{4\pi}\left(\frac{3(\vec{m}\cdot\vec{r})\vec{r}}{r^5} - \frac{\vec{m}}{r^3}\right) \qquad \text{eq.I.36}$$

Summing the contribution of all particles dipolar field, the order parameters are defined as:

$$\psi_k = -\sum_{i\neq j}\left(\frac{a}{r_{ij}}\right)^3 P_k(\theta_{ij}) \qquad \text{eq.I.37}$$

r_{ij} is the distance of a pair particles within the composite, a is the particle radius, ϑ_{ij} is the angle between the vectors r_{ij} and the z-axis, P_k the kth Legendre polynomial function. Martin shows that magnetostriction of FSE is independent of the particle size. In the case of randomly-filled composite the ψ_2 parameter is null.

Martin also studied the effect of a compressive pre-stress on the contraction of the FSE. A pre-stress (compression along the particle alignment axis) reduces the inter-particle distance, which increases the inter-particle interactions and, finally, should increase the contraction. However, the contrary is observed in the measurements curves. The contraction of the composite is reduced because the pre-stress decreases the aspect ratio of samples which increases the demagnetizing energy of the composite.

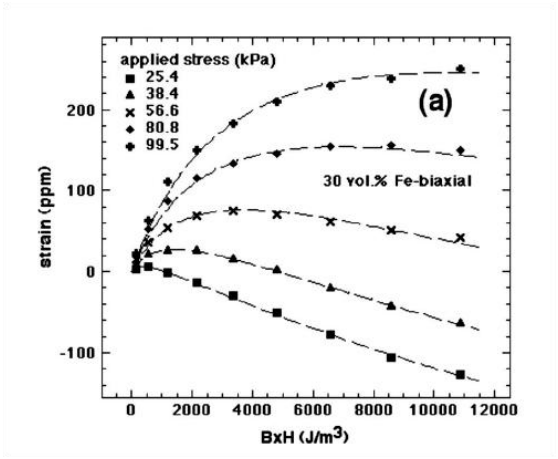

Fig.I.19a [Mar1] Magnetostriction (contraction) of FSE, with pre-stress

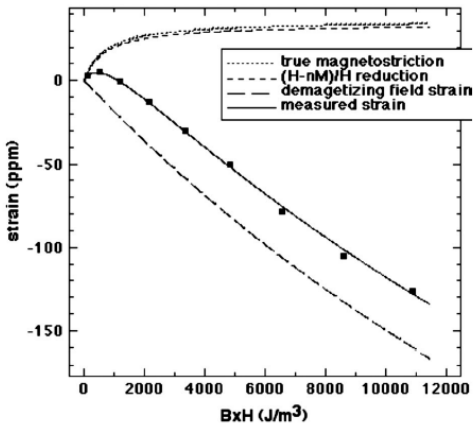

Fig.I.19b [Mar1] Correction of the demagnetizing strain on the magnetostriction (contraction) of FSE

In this way, Martin introduced an expression a demagnetizing field forces as a correction for its data:

$$F = \frac{1}{2}\frac{\mu_0 H_0^2 V}{(1+n\chi)^2}\left[\frac{\partial\chi}{\partial Z} - \chi^2\frac{\partial n}{\partial Z}\right] \qquad \text{eq.I.38}$$

This force brings the dependence on the composite susceptibility χ and on demagnetizing coefficient n.

In Martin's paper, the susceptibility of structured composites is written as:

$$\chi_w = \frac{3\phi\chi_p}{3+\chi_p(1-\phi+\delta_w\psi_2)} \qquad \text{eq.I.39}$$

With ϕ as the filling factor of particles in the composite, χ_p as the intrinsic susceptibility of the particles and δ_w as a constant linking the measurement axis and the chain-like axis. The 4th chapter will explain in depth this susceptibility behavior.

The first term of eq.I.38 depends on the derivative of the susceptibility over the z-coordinates. Since only the parameter ψ_2, evaluated, with the formula in eq.I.37, is a function of the distance (hence z), this first term is the force created by the structure of the composite. In the case of randomly filled composite the parameter ψ_2 is null, so the derivative of the susceptibility is null. If the first term stands for a structure force, the second stands for a force arising from the demagnetizing energy. Usually, the corresponding coefficient is not a function of space coordinates, but depends on the

aspect ratio of the sample. However, this second term brings a demagnetizing dependence on the magnetostriction, so a sample's shape dependence. Moreover, this susceptibility derivative sign is the opposite of the demagnetizing factor derivative. The 2 forces are opposite. The demagnetizing force is always acting on the sample. Studying contraction of FSE, this force was an undesirable effect; hence Martin hence uses long samples to avoid this demagnetizing effect during experiment.

A structured and a randomly-filled composite have different behaviors when exposed to an external magnetic field.

V.2.2. Comparison

Zhou [Zho] compared the displacement of the surface of a structured elastomer and of a randomly-filled elastomer, when exposed to a magnetic field. In this article, structured elastomers are called MRE whereas randomly-filled elastomers are called EFC (Elastomer Ferromagnet Composite). Displacement was measured using the white light speckle method. The maximal magnetic induction was 500 mT.

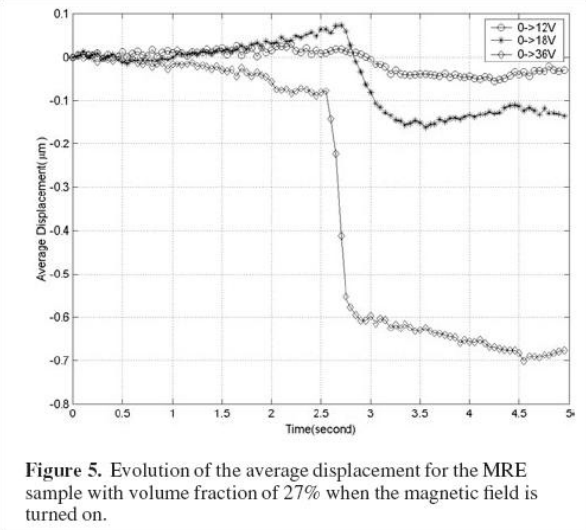

Figure 5. Evolution of the average displacement for the MRE sample with volume fraction of 27% when the magnetic field is turned on.

Fig.I.20a [Zho] Displacement of a structured composite

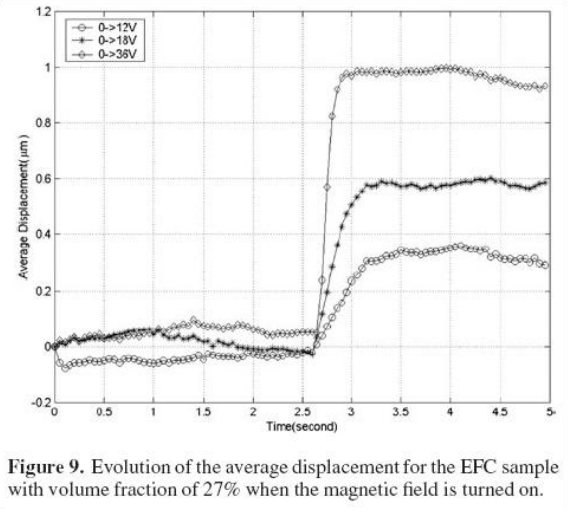

Figure 9. Evolution of the average displacement for the EFC sample with volume fraction of 27% when the magnetic field is turned on.

Fig.I.20b [Zho] Displacement of a randomly-filled composite

From these experiments, the difference in the behavior of the composite can be noticed whether they are randomly-filled or not. The displacement (the deformation) of FSE composite is negative

whereas, in the case of MRE composite, the displacement is positive. Moreover, the amplitude of displacement was found larger for a MRE than for a FSE, for composites with the same filling factor.

V.2.3. Randomly-filled composite

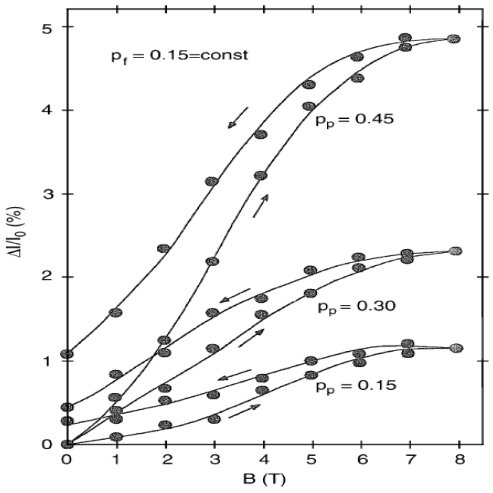

Fig. 4. Dependence of longitudinal magnetostriction $\Delta l/l_0$ on the induction of applied magnetic field B for samples of the composite with constant filling factor by ferromagnetic particles p_f and different porosity factors p_p.

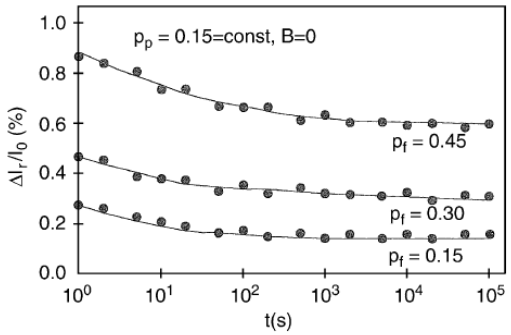

Fig. 5. Dependence of remanent magnetostriction $\Delta l_r/l_0$ on time t after switching off the magnetic field B for samples of the composite with constant porosity factor p_p and different filling factors by ferromagnetic particles p_f.

Fig.I.21 [Bed1]Magnetostriction of a randomly-filled composite

The strain of a randomly-filled composite, submitted to a homogenous magnetic field, was measured by Bednarek [Bed1]. Samples were prepared by mixing 0.1 – 0.15 mm iron particles into a silicone matrix characterized by an unfilled Young's modulus of E_0=0.25 MPa. This change of the composite length effect was tested for different filling factor and porosity into a superconductor magnet allowing a maximal induction of 8 T. The largest value recorded was **4.81%** for a composite filled by Pf=15% (vol.) particles, with a porosity Pp=45% (vol.) and an external field at the maximum value: 8 T. He also monitored the hysteresis for this phenomenon. Increasing the magnetic field and decreasing back to a null value didn't bring back the composite to its initial length. This so-called remnant magnetostriction is found to be a time-dependent function. Magnetostriction is affected by the composite viscoelastic behavior. About the phenomenon, Bednarek explained the shape change by the rotation of non-spherical particle due to the applied magnetic field and as a result, the whole sample will be strained along the field's direction. Guan [Gua1], which has measured a weak magnetostriction (184 ppm = 10^{-4}) of such a composite, also proposed the same explanation of the deformation.

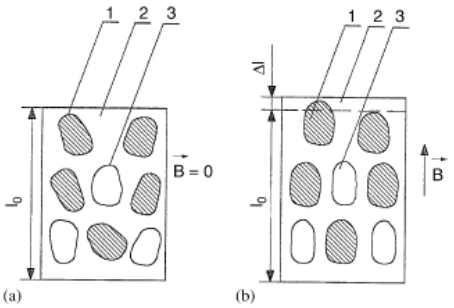

Fig. 7. Schematic presentation of the composite structure before switching on the magnetic field (a) and after switching on the magnetic field (b), explaining an origin of positive magnetostriction. The meaning of numbers is the same as in Fig. 1.

Fig.I.22a [Bed1] Bednarek's model for magnetostriction

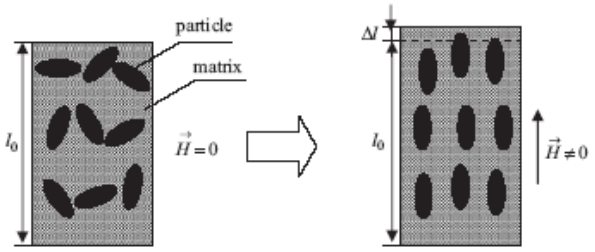

Fig. 7. The sketch of mechanism of MRE with interaction between magnetic particles and matrix under magnetic fields.

Fig.I.22b [Gua1]Guan's model for magnetostriction

Lanotte [Lao1] has developed this idea of rotation of ferromagnetic particles, inside an elastomer matrix. The prepared sample is constituted of 4 rectangular rods of silicone filled with 9% of Sm_2Co_7. Those ferromagnetic particles are hard magnetic particles, i.e. they keep their magnetization. Each of these rods has its particles oriented at 45° relatively to the rod axis. The 4 rods are then gathered into a 50 mm x 10 mm sample. This was used as a sensor, for oscillating strain monitoring, with frequencies ranging from 20 to 150Hz and maximal amplitude of 0.8 mm. When the strain is applied the rod reduces or extends his size, and the particles rotate positively or negatively respectively, to follow the matrix deformation. The axial magnetization shifts its value, which shifts the effective induction. This variation of induction is monitored via a pick-up coil, wounded around the elastomer. The measured signal was proportional to the strain amplitude. This experiment shows the possibility for MRE of being used as a linear strain sensor. This device was then tested as an actuator, using the inverse phenomenon. The pick-up coil acts here as the exciting coil which forces the magnetic particles to aligned towards its generated magnetic field with maximal amplitude of 0.2 Tesla. The force is proportional to the applied magnetic field and to the concentration of magnetic particles. The torque is, indeed, the product of the magnetic field and the magnetization which is the volume represented by all the magnetic particles inside the sample volume divided by that entire sample volume, i.e. the filling factor.

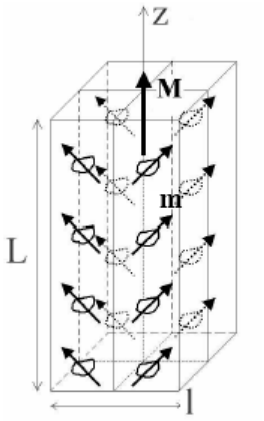

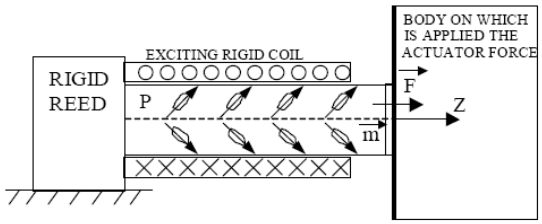

Fig. 7. Scheme of an elastomagnetic actuator. (P = composite sample as in Fig. 4).

Fig.I.23a Lanotte' sample [Lao1]

Fig.I.23b Lanotte' s device [Lao1]

Raikher [Rai] has performed a full calculation of the elongation of an incompressible ferromagnetic material sample, with an initial spherical shape, under the action of an external and homogenous magnetic field *H*. He uses the principle of conversion of magnetic energy to elastic energy. Following equations are given, in CGS units, as:

$$\delta E_{mag} = 2\pi \Delta N M^2 V \qquad \text{eq.I.40}$$

Where *ΔN* is the change of the demagnetizing factor of the sphere into an ellipsoid of semi-axis b<R<a.

$$\delta E_{elas} = \frac{2}{3} G V \frac{(a-b)^2}{R^2} \qquad \text{eq.I.41}$$

Summing and minimizing these energies leads to the expression of the strain:

$$\frac{a-b}{R} = \frac{4\pi(\chi H)^2}{15G} \qquad \text{eq.I.42}$$

With *χ* the material susceptibility.

Raikher operates another calculation based on variational equation with the hypothesis that the sphere will not necessarily change into an ellipsoid.

The sphere was supposed to be submitted to surface stress defined as:

$$\vec{n}\cdot\sigma\big|_{\Gamma} = 2\pi(\chi H_n)^2\vec{n}\big|_{\Gamma} \qquad \text{eq.I.43}$$

H_n is the normal magnetic field on the sphere boundary Γ, and $\vec{n}$ is the normal, outward, unit vector. Eq.I.43 shows that a sphere, having both magnetization and demagnetizing field homogenous and in the same direction, exhibits outward forces which results in the elongation of the sphere. Details of the calculation are provided in the article; the result of the magneto deformation of an incompressible sphere is:

$$\varepsilon = \frac{20\pi(\chi H)^2}{57G} \qquad \text{eq.I.43}$$

VI. Thesis subject

As presented in the above articles the magneto-elasticity is highly sensitive to the particles distribution. Magnetic field effect onto those composite, MRE or FSE, can be viewed as a tool to tune the stiffness of the composite, or to induce a deformation. Our interest is on the apparent magnetostriction of MRE.

Fewer works are carried out on that specific subject. Zhou has monitored the positive elongation of a randomly filled composite but did not explicitly give an explanation. Bednarek and Guan explained that this deformation comes from the non-spherical shape of the particles which rotate to get the same orientation as the magnetic field. But positive deformation does not necessarily require arising from rotation of elongated particles. Martin, who studied the deformation of composite with spherical particles in chains-like structure, introduced demagnetizing force acting on his composite, as a counter force which counters the contraction measurements. Focusing only on FSE composite, he didn't go farther with this. Moreover, he used long sample to reduce at maximum this additive force. Raikher published his theoretical paper on the conversion of demagnetizing energy into elastic energy which results into a positive strain.

This thesis focuses on modeling this phenomenon, from the particles scale, with the inter-particles interactions to the macroscopic scale of the composite. Magnetic and elastic effective media are introduced to have the important parameters which can enhance or limit the deformation. Our approach is also based on the demagnetizing energy conversion, but we give and measure, a

demagnetizing factor for a MRE composite with different shape and filling factor. Then using effective Young modulus of composite, we have the whole pieces to present a model of this kind of magnetostriction of composite.

MRE composite also provided many advantages:

- A larger positive effect, 5.10^{-2}, compared to the highest classical materials, 10^{-3}. So that randomly-filled composite offers a relative attractive value of deformation, under homogenous magnetic field.
- Those composite are easily manufactured, mixing magnetic particles in a matrix.
- Its compounds, particles and elastomers are extremely cheap.

References:

[Mag1]: Magnetism I-Fundamentals, E. du Tremolet de Lacheisserie, D. Gignoux, M. Schlenker, Springer-Verlag New York Inc. (2004), #ISBN-10: 0387229671, #ISBN-13**:** 978-0387229676

[Lan1]: Theory of elasticity, L.D. Landau and E. M. Lifshiftz, Pergamon Press, New York (1970)

[Jou1]: On the new class of magnetic forces, J.P. Joule, *Sturgeon's Annals of electricity, magnetism and chemistry* 8 (1842) p219

[Mag2]: Magnetism and Magnetic materials, J.C. Anderson, Chapman & Hall, London (1968)

[Tre]: Magnetostriction - Theory and Applications of Magnetoelasticity, E. du Trémolet de Lacheisserie, CRC Press 1993, #ISBN-10: 0849369347, #ISBN-13**:** 9780849369346 -

[Bel]: Magnetostriction of Rare-earth ferrite garnets at low temperature, K.P. Belov, V.I. Sokolov, *J. exptl. theoret. Phys.* (48) 979-981

[Mar1]: Magnetostriction of field-structured magnetoelastomers, J. E. Martin, R. A. Anderson, D. Read, G. Gulley, *Physical Review E* 74 (2006) 051507

[Kal]: The elastic and damping properties of magnetorheological elastomers, M. Kallio, PhD Thesis (2005) Tampere (Finland)

[Far]: Magnetoactive elastomer composite, M. Farshad, A. Benine, *Polymer testing* 23 (2004) 347

[Nik]: Experimental study of magnetoelastics, L.V. Nikitin, D.G. Korolev, G.V. Stephanov, L.S. Mironova, *Journal of Magnetism and Magnetic Materials* 300 (2006) 234

[Var]: Smart composites with controlled anisotropy, Z. Varga, G. Filipcsei, M. Zrinyi, *Polymer* 46 (2005) 7779

[Bed1]: The Giant linear magnetostriction in elastic ferromagnetic composites within a porous matrix, S. Bednarek, *Journal of Magnetism and Magnetic Materials* 301 (2006) 200

[Bed2]: Magnetoelastic properties of ferroelast within an organo-silicon polymer matrix, S. Bednarek, *Journal of Magnetism and Magnetic Materials* 166 (1997) 91

[Coq1] Propriétés élastiques et viscoélastiques de matériaux composites adaptatifs, E. Coquelle, PhD Thesis (2004) Nice

[Gua1]: Magnetostrictive effect of magnetorheological elastomer, Xinchun Guan, Xufeng Dong, Jinping Ou, *Journal of Magnetism and Magnetic Materials* 320 (2008) 158

[Zho]: Deformation in magnetorheological elastomer and elastomer-ferromagnet composite driven by a magnetic field, G.Y. Zhou, Z.Y. Jiang, *Smart Materials and Structures* 13 (2004) 309

[Lao1]: Sate of the art and development trends of novel nanostructured elastomagnetic composites, L. Lanotte, G. Ausanio, C. Hison, V. Iannotti, C. Luponio, C. Luponio Jr., *Journal of Optoelectronics and Advanced Materials* 6 (2004) 523

[Zri1]: Deformation of ferrogels induced by nonuniform magnetic field, M. Zrinyi, L. Barsi, A. Büki, *Journal of Chemical Physics* 104 (1996) 8750

[Rai]: Magnetodeformation effect in ferrogel samples, Y. L. Raikher, O. Stobolv, *Journal of Magnetism and Magnetic Materials* 258 (2003) 477

Chapter 2

Materials and characterization techniques

I. Sample preparation

In most of the cases, a soft matrix was used to get a smaller Young's modulus in order to increase the deformation. In some cases, a hard matrix was also used. The soft matrix was a bi-compound silicone provided from DALBE. The ratio hardener to silicone is roughly 2-5% depending on how fast the hardening should last. As received, it has a viscosity of 8000 mPa.s. The average time for polymerization is about 12h, and it presents in its elastomeric state a nominal strain up to 170%.

The hard matrix is an epoxy resin (Araldite), which is also a bi-component mixture hardening in a day.

The general method used was the injection of the particles in the matrix while it is liquid and viscous. This matrix viscosity creates the counter-force to the sedimentation on the particles. The mixture was hand-mixed for several minutes and the catalyst was added to start the polymerization. To remove any trapped gas, the mixture was placed in a vacuum chamber. The viscosity highly increases during the polymerization reaction and particles were checked to be randomly dispersed in the matrix at the end of the curing step.

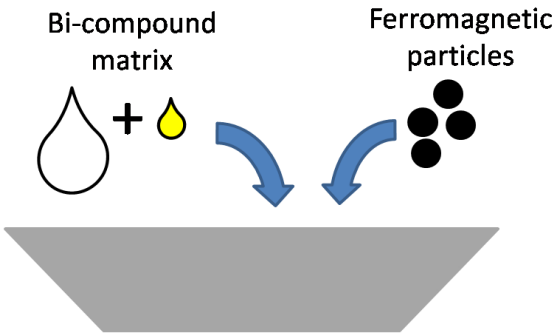

Fig.II.1 Mixture preparation

The demagnetizing factor effect on the magnetization (cf. Chapter 4) and on the magnetostriction (cf. Chapter 5) is investigated further in this thesis. This factor, for an ellipsoidal/cylindrical shaped sample, is a function of the aspect ratio c/a (cf. Chapter 4). Easiest shape to produce with tunable aspect ratio is the cylinder. Cylindrical samples were made for those experiments and also for mechanical tests. Cylindrical moulds were coated with vacuum grease in order to facilitate the

extraction of the sample from the mould. Such samples are shown in Fig.II.2a&b. Fig.II.2a shows a pure silicone elastomer and the Fig.II.2b shows a composite filled with iron particles.

Fig.II.2a Pure silicone elastomers

Fig.II.2b Particle-filled elastomer

Different examples of filled samples are presented in Fig.II.3a&b, where the cylindrical samples were cut in half along an axis-symmetric plan. An example of non-homogenous sample is shown in Fig.II.3b, where it can be seen that such composite presents many macroscopic air bubbles and also some aggregates unlike to the homogeneous sample, shown in Fig.II.3a.

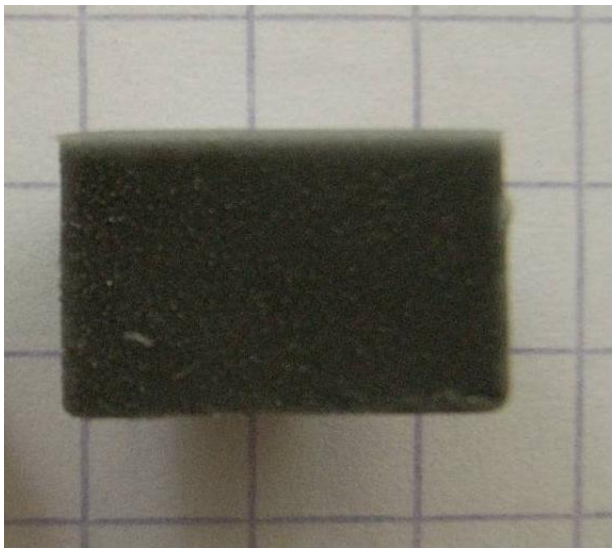

Fig.II.3a Homogeneous particle-filled elastomer

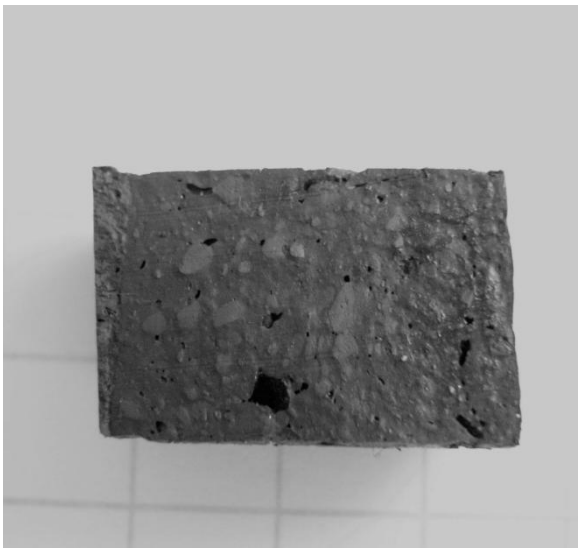

Fig.II.3b Heterogeneous particle-filled elastomer

Most of the measurements were made on cylindrical samples, but we sometimes changed the sample shape. The magnetic sphere produces a homogenous demagnetizing field; thus, it was interesting to make some spherical samples. This was achieved using a spherical mould and proceeding as described in Fig.II.4. The mould consists of a spherical cavity inside 2 blocks screwed together. As it was done with the cylinder moulds, the spherical mould is also coated with vacuum grease to facilitate the extraction of the sphere.

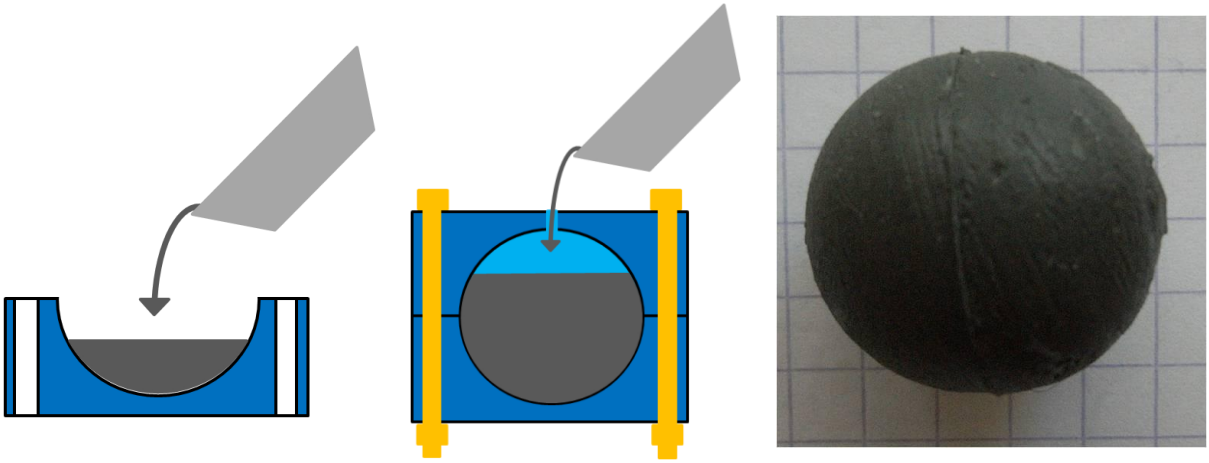

Fig.II.4 Spherical-shape sample synthesis

II. Magnetization measurement

II.1. Faraday balance

The Faraday balance is a device designed in 1855 for magnetic properties measurements. This device induces a magnetization on the sample and a field gradient; thereby a magnetic force is applied on a sample. Magnetization is extracts from the force measurement.

II.1.1. Principle

Fig.II.5. Superconducting coil(Oxford)

Magnetization curves of composites were measured with such device. The sample was exposed to a magnetic field inside a superconducting coil (Oxford), as shown in Fig.II.5, with a maximum magnetic induction up to 7 Tesla. The force acting on the sample (see Fig.II.6) is then read

as the weight, m_{read}, on the balance. The expression of that magnetic force, induced on the magnetized sample by the gradient is given as (eq.II.1):

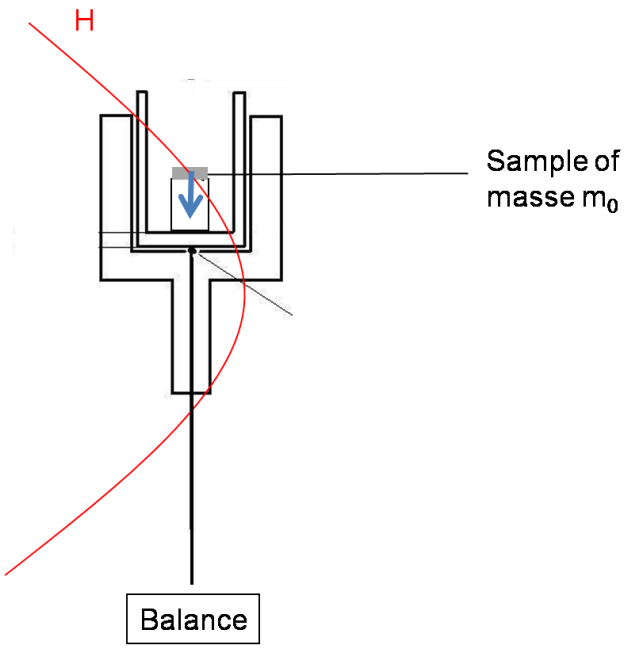

Fig.II.6. Faraday balance 's Principle

$$F_{mag} = \mu_0 m_0 M(H) \frac{dH}{dz} \qquad \text{eq.II.1}$$

Which in turn balances the weight;

$$m_{read} g = F_{mag} \qquad \text{eq.II.2}$$

Thus, we obtain the magnetization:

$$M(H) = \frac{g \cdot m_{read}}{\mu_0 m_0 \frac{dH}{dz}} \qquad \text{eq.II.3}$$

Experimental values were measured using the CGS units:

- m_0 [g] is the mass of the sample, without external magnetic field (H=0).
- m_{read} [g] is the mass of the sample read with the balance.

- $\mu_0 = 1$ is the vacuum permeability.
- $\frac{dH}{dz}$ [Oe/cm] is the local magnetic field gradient.
- g = 981 [cm/s^{-2}] is the gravitational acceleration constant.
- M [emu/g] is the magnetic moment of the sample per unit of mass.

Magnetization is converted into the S.I. units through the relation:

1 emu/g = 1 Am²/Kg

M [A/m] =ρ_{sample}* M [emu/g]

where ρ_{sample} [Kg/m^3] is the mass density of the sample.

Sometimes the magnetic polarization is used; it is extracted from the magnetization as follow:

J [T] = μ_0* M [A/m]

The S.I. value of μ_0 (See eq.I.1) is used in this relation.

II.1.2. Experimental data

Sample is put at 16 cm from the highest maximum magnetic field, just above the inflection point of magnetic curve, which is located at x=14.5cm (Fig.II.7) where the magnetic field gradient is maximal, for a given field, in order to maximize the magnetic force and to get benefit of centripetal radial forces that held the sample along the coil axis. The sensibility of the balance is 0.05g with a maximal load of 600g.

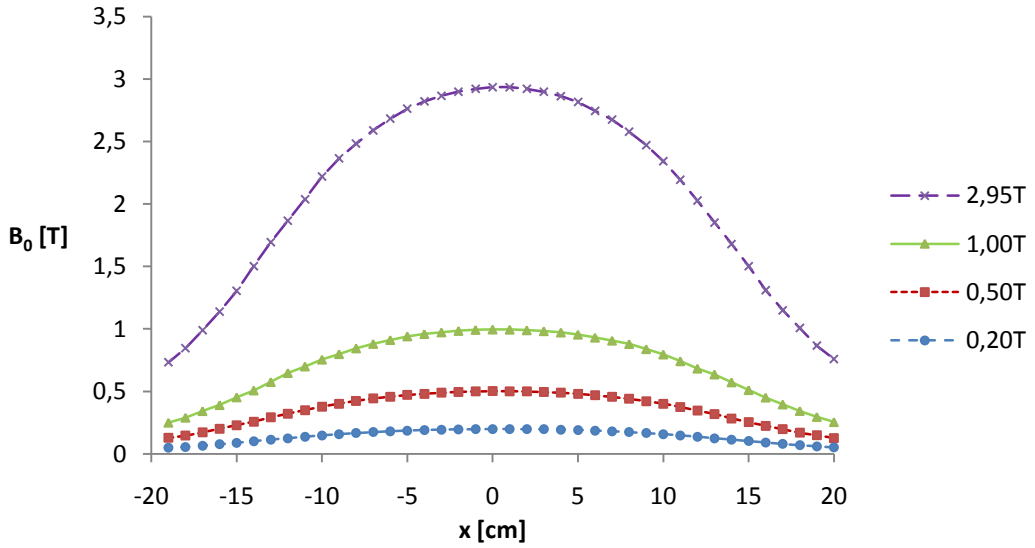

Fig.II.7.measurement of the axial component of the magnetic induction inside the superconducting coil versus the position along the coil axis

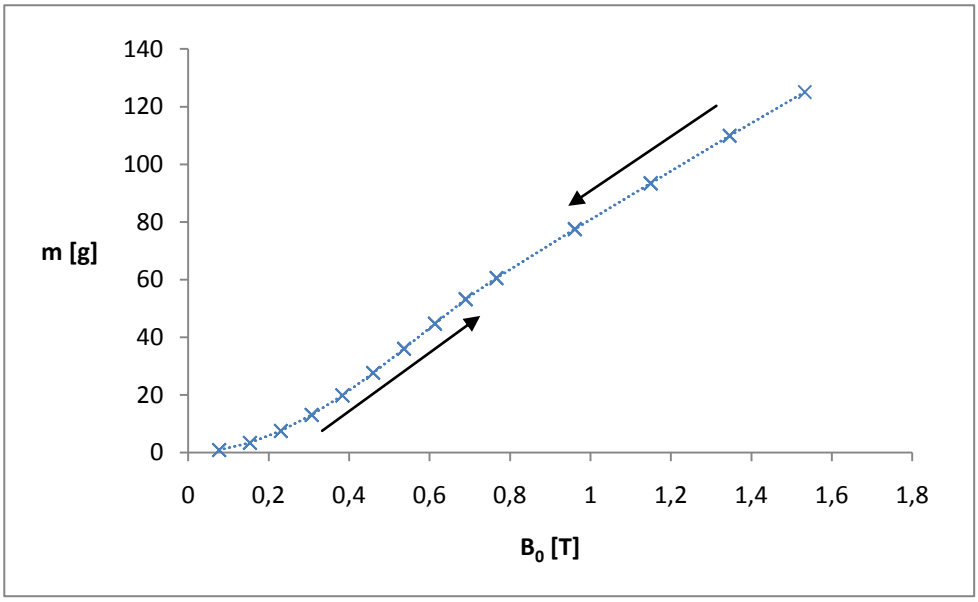

Fig.II.8. Mass (weight) measured on the balance versus the applied magnetic field on a spherical sample randomly filled with 3% (vol.) iron particles

Fig.II.8 presents an example of a mass measurement as a function of the applied magnetic field on the sample. This curve can be split into two parts: at low field, the mass is a quadratic function of the applied field; at larger field, it becomes linear. The mass is proportional to the magnetic force, which is the product of the magnetization and the field gradient (eq.II.1 and eq.II.2); at low magnetic field,

both are linear to the applied field, yielding to that quadratic behavior. Increasing the applied field saturates the sample, i.e. the magnetization becomes a constant, and the only contribution to the force is the field gradient. In order to determine the limit between these two regimes, experimental data were obtained up to the saturation of the sample.

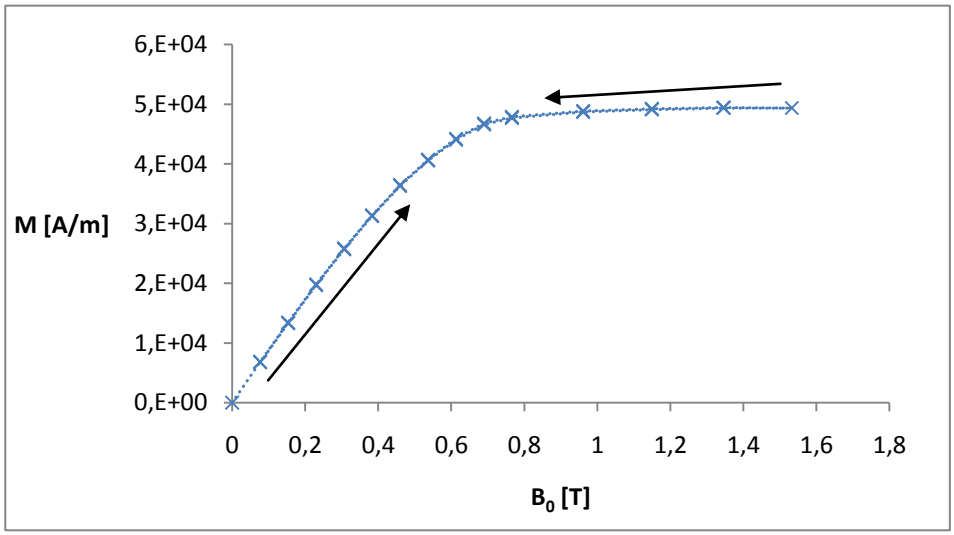

Fig.II.9. Magnetization versus the applied magnetic field on a spherical sample randomly filled with 3% (vol.) iron particles

Magnetic measurement is a non-destructive technique (unlike thermo-gravimetric analysis). The filling factor of a sample can be easily deduced from the knowledge of both the saturation of the ferromagnetic material and of the sample. In this example, the sample saturated at 49 kA/m whereas the Iron saturation is 1735 kA/m; thus the filling factor of this sample is checked to be 3%.

III. Mechanical

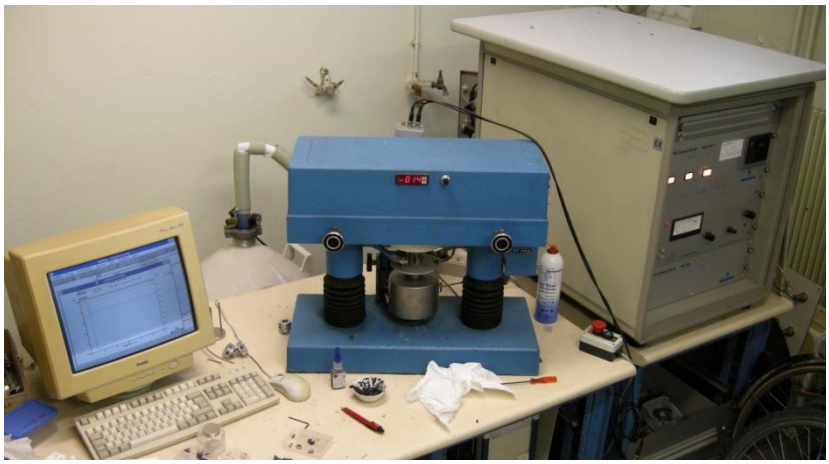

Fig.II.10. Dynamic Mechanical Thermal Analyser VA 2000 (Metravib R.D.S.)

The Dynamic Mechanical Thermal Analyser (DMTA) VA 2000 (Metravib R.D.S.) (Fig.II.10) is a versatile instrument dedicated to the measurement of viscoelastic properties of materials, and their dependence on temperature. The dynamic elastic modulus and damping coefficient are parameters usually studied in polymer science. Those parameters are characterized as a function of temperature and/or frequency. In this work, these measurements can be used to determine the stiffness reinforcement of soft matrices filled by hard particles and can lead to information on the interaction between matrix and fillers.

III.1. Principle

The DMTA applies a dynamic stress on the sample:

$$\sigma(t) = \sigma_{\max} \cos(\omega \cdot t) \qquad \text{eq.II.4}$$

where $\sigma(t)$ is the stress characterized by it maximal amplitude σ_{max} and the pulsation ω in radian/s. As far as mechanical behavior is linear, this applied stress results in sine wave strain, shifted by the angle δ, relatively to the applied stress:

$$\varepsilon(t) = \varepsilon_{\max} \cos(\omega \cdot t - \delta)$$ eq.II.5

In the same way, the strain signal *ε(t)* is defined by it maximum amplitude ε_{max} and the pulsation *ω*, as seen in Fig.II.11.

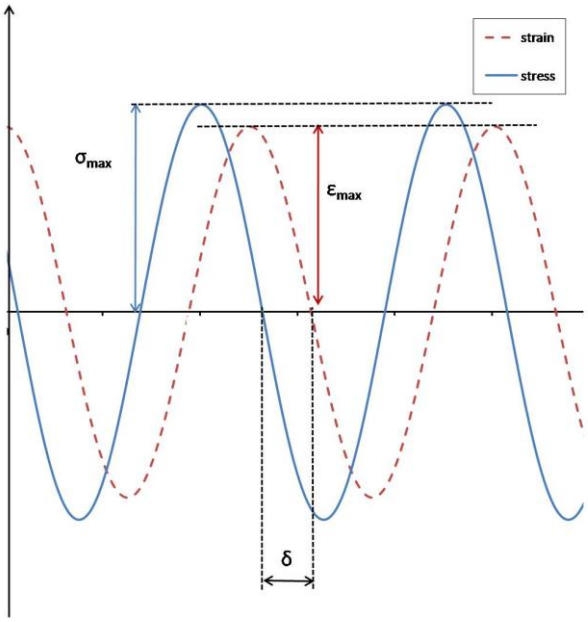

Fig.II.11. Dynamic mechanical test

For small deformation, a complex dynamic modulus, defined as the ratio of the stress to the strain, can be expressed by a complex value:

$$G^*(i\omega) = \frac{\sigma^*(i\omega)}{\varepsilon^*(i\omega)} = Ge^{i\delta} = G'(\omega) + iG''(\omega)$$ eq.II.6

The real part *G'* stands for the polymer elastic modulus or storage modulus and the imaginary part *G''* out of phase with the displacement, is called the viscous modulus or loss modulus. The phase shift (*δ*) between the force and the displacement is called the loss angle of the material and the tangent of the loss angle (with *tan(δ)=G''/G'*) is called the loss factor for internal friction coefficient and corresponds to the damping of the material.

III.2. Sample measurement

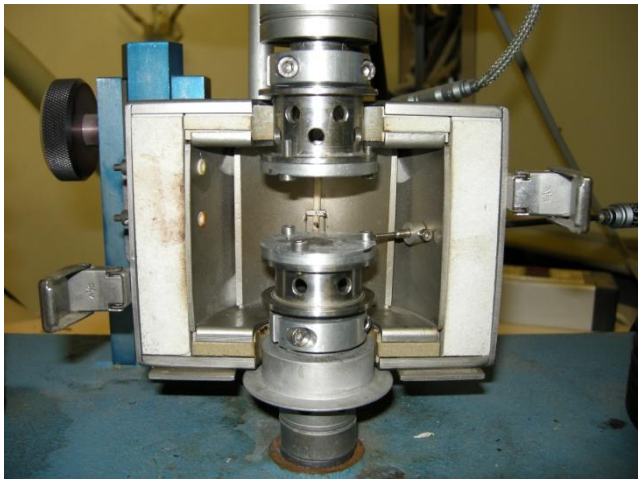

Fig.II.12. Thermal chamber

Sample is pasted between a static plate and a moving plate in the thermal chamber (Fig.II.12). The moving plate applies an oscillating force and the resulting displacement of the sample is measured. Data are converted into real part and imaginary part of Young modulus

IV. Scanning Electron Microscope

Magnetic particles shapes were characterized via a Scanning Electron Microscope (S.E.M.). A Princeton Gamma-Tech EDX also allowed a X-ray analysis to investigated the composition/purity of the ferromagnetic particles.

Fig.II.13a. S.E.M.

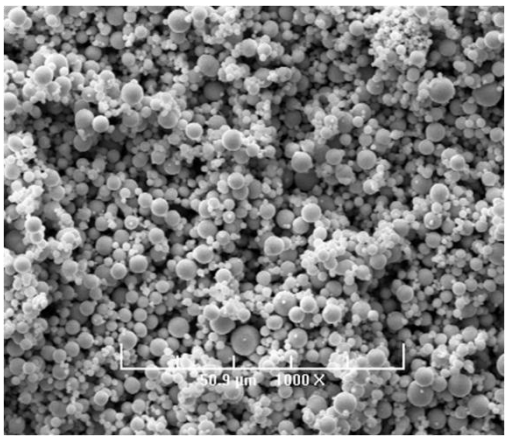

Fig.II.13b. Iron particles picture

V. Magnetostriction measurement

V.1. Device

Magnetic field viewed by the sample is generated by an electromagnet TE 200A (TEK Elec), which is made of a couple of coils and an iron core to enhance and canalize the magnetic field into an air gap. This air gap is about 4 cm wide (to be compared with the cross section of the core, of roughly 12 cm). The electromagnet is connected to a Hewlett Packard power supply providing a maximal current of 170 A yielding to a maximal magnetic induction of 1.2 Tesla. For the magnetostriction measurement, the sample is put inside the air gap, via a sliding piece on a rail.

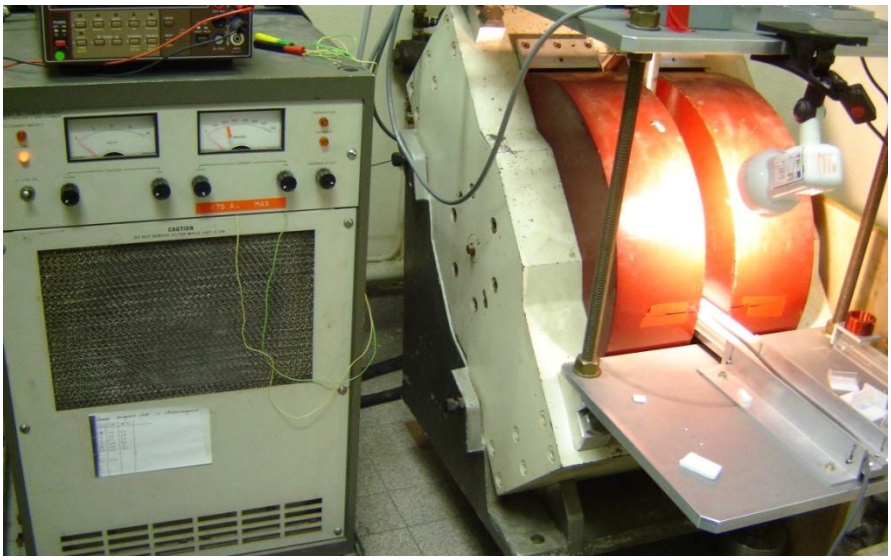

Fig.II.14 Electromagnet

A video camera (ELMO) is attached behind the sample holder on the sliding piece, to visualize directly the strain on the sample exposed to the magnetic field. Thus, pictures have been shot for different values of magnetic field. A light spot is added to improve the contrast. Black & white pictures have 768x512 pixels resolution. The strain is determined by image analysis.

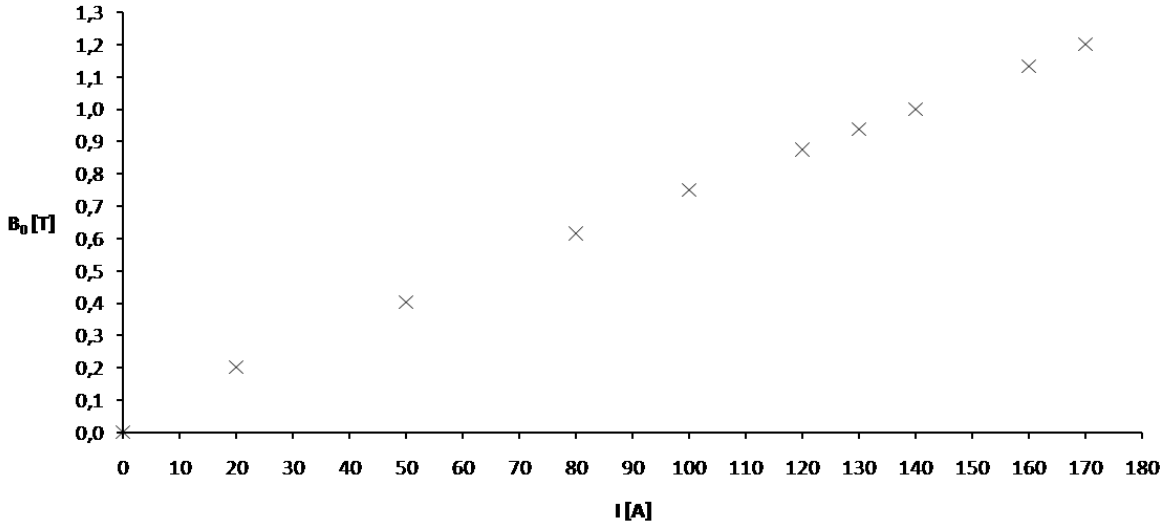

Fig.II.15. Magnetic field versus the current inside the coils

V.2. Data extraction

The video camera is shooting pictures of the sample at different amplitude of the applied magnetic field. Experiment data is thus a stack of picture which has to be processed.

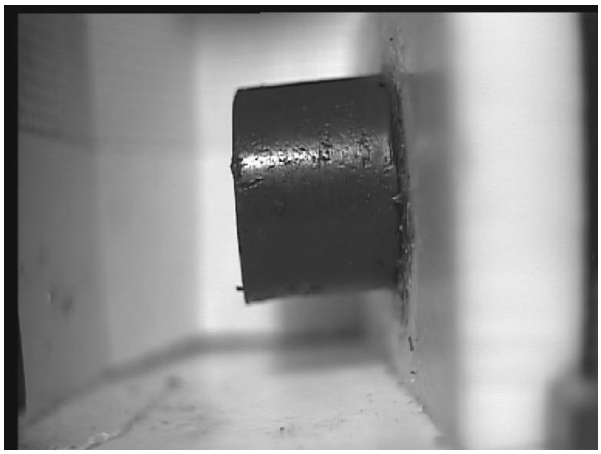

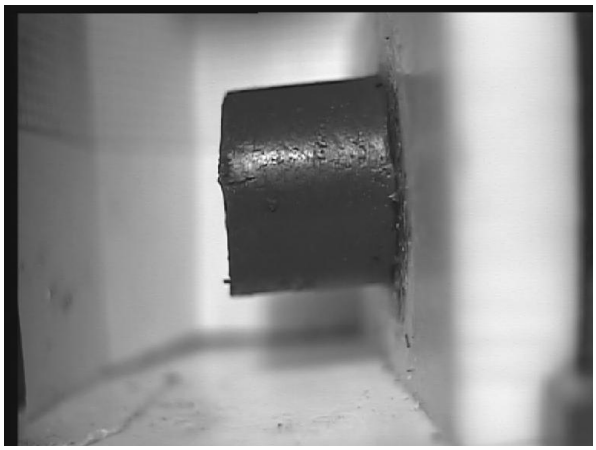

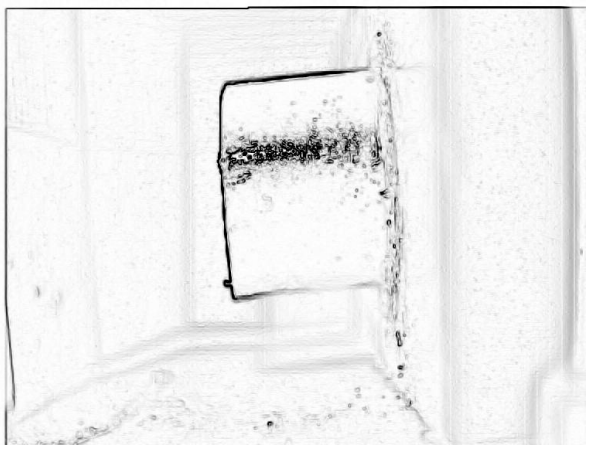

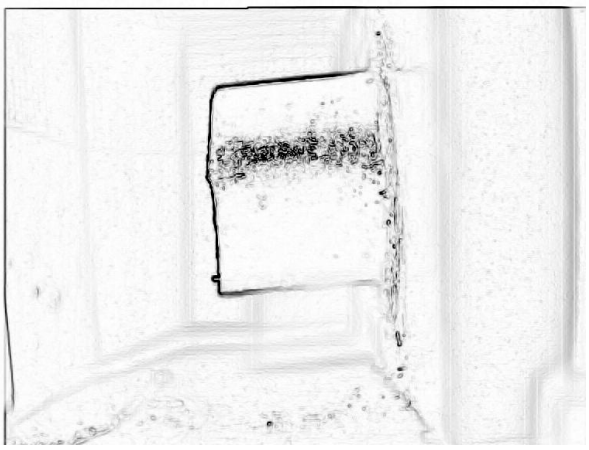

Fig.II.16a Sample at rest (H=0)

Fig.II.16b Sample exposed to an external magnetic field (H≠0)

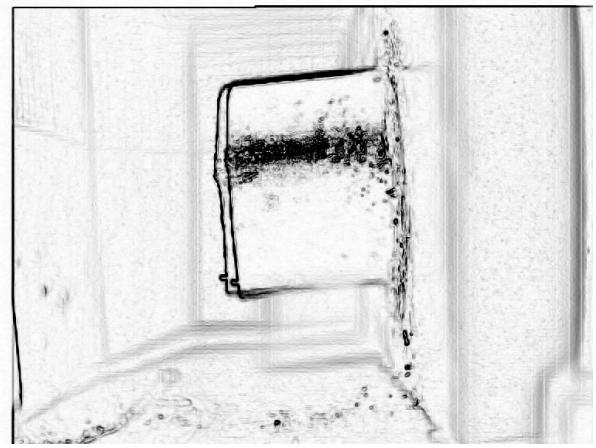

Fig.II.17 Superposition of the 2 images (H=0) and (H≠0)

The image processing is effected using the software «ImageJ». This treatment has been written in Java language and executes the following procedure on the stack of recorded pictures;

→The first step consists in choosing a reference picture, usually the one taken without any external magnetic field. Any changes in the further pictures would be calculated relatively to that reference picture.

→The entire picture will be transformed in a way that highlights sharp changes in intensity. Because of its dark color, due to the particle reinforcement of the matrix, the composite stands out of the white background (Fig.II.16a&b). Hence, the boundaries can be easily tracked. Moreover, light reflection on the sample also brings other possible targets to track, in order to get more local strain data.

→ At first, the reference picture is processed. An area is chosen for a tracking mark of which the coordinates will be saved. Then, the other pictures are successively analyzed in the same area and the mark coordinates are compared to those of the reference. Displacements of the marks are obtained. Finally, the whole stack is processed and displacements for different values of the magnetic field are calculated (Fig.II.17).

→ Finally, displacements are converted into strain via the knowledge of the initial length of the sample (accounting for the low strain).

$$\varepsilon(H) = \frac{L(H \neq 0) - L(H = 0)}{L(H = 0)} \qquad \text{eq.II.7}$$

Maximum resolution is estimated around 0.1%.

Chapter 3

Dipolar interactions and magnetostriction

I. Introduction

In this chapter, we give an explanation of the positive magnetostriction of MRE exposed to homogeneous applied magnetic field. Bednarek [Bed1] and Guan [Gua1] have both postulated that the MRE magnetostriction is a result of rotation of irregular-shaped particles. But a measurement made on MRE filled with spherical ferromagnetic particles, provided below in this chapter, also presents a positive magnetostrictive behavior. Because of the shape of these particles, the strain is the consequence of force acting on particles and does not result from couple as proposed in their model. Because of the homogeneity of the applied field, the experienced force is the outcome of inter-particle interactions. Therefore, the complete force is calculated through the inter-particle forces.

The magnetic field created by a magnetized sphere is the same as the dipolar field. Thus, the model used to perform this calculation is based on the dipolar interaction of magnetic moments. The effective force between spherical soft ferromagnetic particles, which are in the saturation state will be first described and discussed. Then, this force (between two particles) will be calculated for all the particles, randomly distributed in the volume, as is our composite.

These forces are projected on a cylinder axi-symmetric plan to extract a map of the local forces, inside the volume. This map is implemented in a Finite Element Modeling software to determine the macroscopic deformation. In order to compare theory and experimental data, the strain calculation is performed using the same parameters, i.e. filling factor, sample shape, mechanical and magnetic properties.

II. Experimental

A magnetostriction experiment is firstly performed in order to be compared with calculation. This calculation will also need data like the magnetic saturation of the particles and the effective composite Young modulus.

II.1. Composite characterization

II.1.1. Magnetic particles

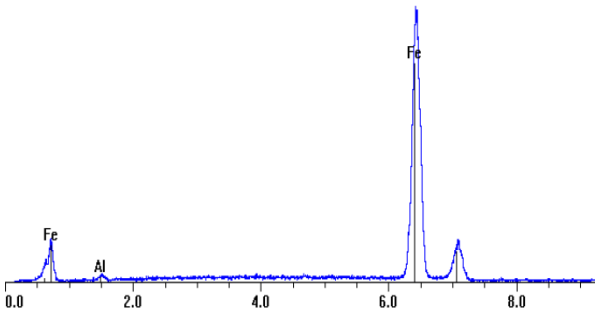

Fig.III.1: X-ray analysis of the magnetic particles (EDX)

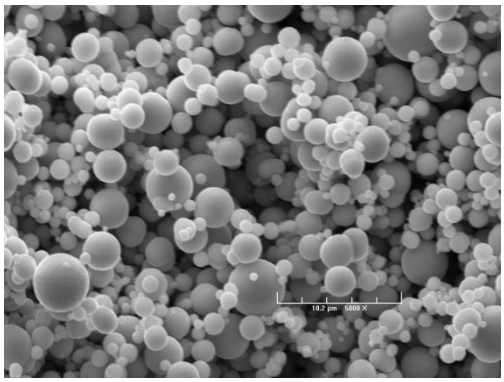

Fig.III.2: SEM picture of the magnetic particles (bar is 10µm)

Chemical composition of the magnetic particles, provided by SPETELEC, has been measured using a X-ray micro-analyzer with a Princeton Gamma-Tech. System Spirit. From the spectral curve shown in Fig.III.1, we determined that magnetic particles are mainly made of iron (98.7%). Fig.III.2 shows a SEM picture of these particles. We can observe that particles are spherical with a diameter close to 5 µm. In Fig.III.3 the iron magnetization curve using a Vibrating Sample Magnetometer is presented, the magnetization was measured under an external magnetic field increasing from -1 T to 1 T and decreasing back to -1T in order to determine the hysteresis. The iron powder has a low magnetic remanence and a high saturation magnetization. We measured the powder saturation magnetization $\mu_0 Ms = 2.08T$.

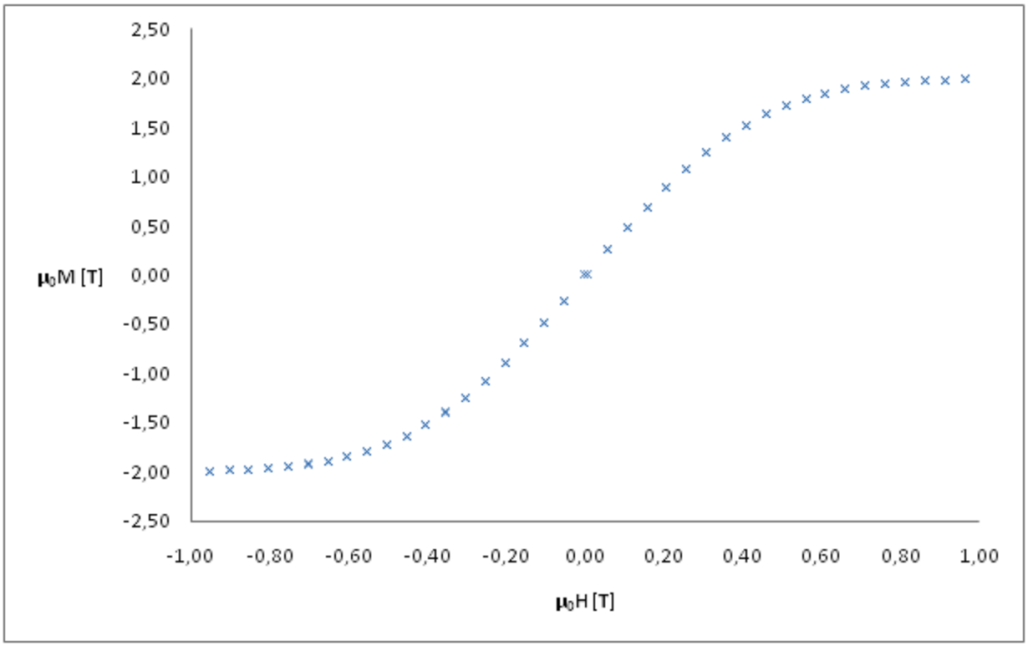

Fig.III.3: Magnetization loop of the magnetic particles

II.1.2. Matrix

An isotropic composite was prepared by hand-mixing 30% vol. of iron particles in a silicone macro monomer (liquid) from DALBE. Then the silicone was polymerized by the addition of a catalyst. The choice of that specific monomer has been made for its low glass transition temperature (Tg) after polymerization, which led to an elastomeric behavior at room temperature. Before polymerization, a procedure of degassing step was applied to remove bubbles; the mixture was placed in a vacuum chamber at 1 mbar for 5 min. The mixture was finally molded into a cylindrical mould (height 14 mm, diameter 11.7 mm) and kept at room temperature for 1 day.

The dynamic Young modulus was measured with a Visco analyzer VA 2000 (Metravib R.D.S.) with solicitations ranging from 5 to 50 Hz. At 5 Hz, a 7.10^5 Pa modulus was measured at room temperature (fig.III.4).

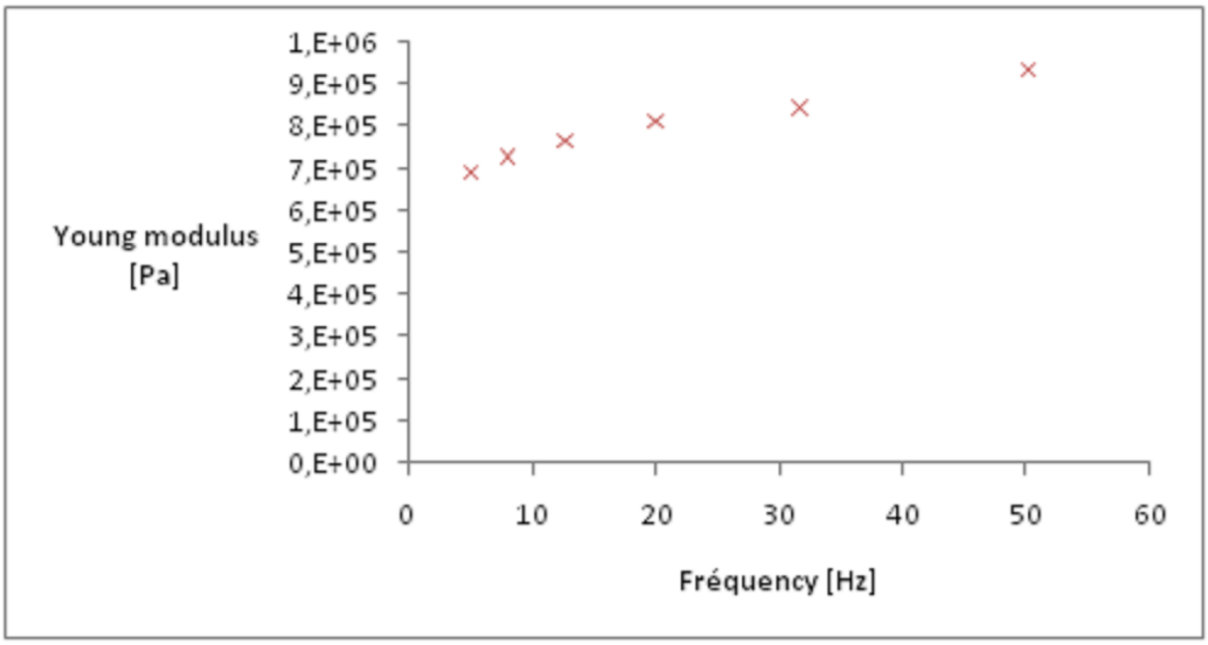

Fig. III.4: Young modulus at different frequency of the composite filled with 30% (vol.) iron particles

II.2. Strain measurement

II.2.1. Principle

Sample dilatation has been obtained using an electromagnet to generate a uniform magnetic field within the sample. This electromagnet is made of a couple of coils which have been placed around a magnetic circuit (fig.III.5). The magnetic circuit has a small gap providing a uniform magnetic field on the sample. The electrical current ranged from 0 to 160 A yielding a magnetic field up to 1.2 T. The sample was placed inside this device and was observed with the CCD camera from ELMO. Pictures were recorded every 0.14 Tesla, at both increasing and decreasing field. Displacement between each step was determined by images analysis (See Chap.II).

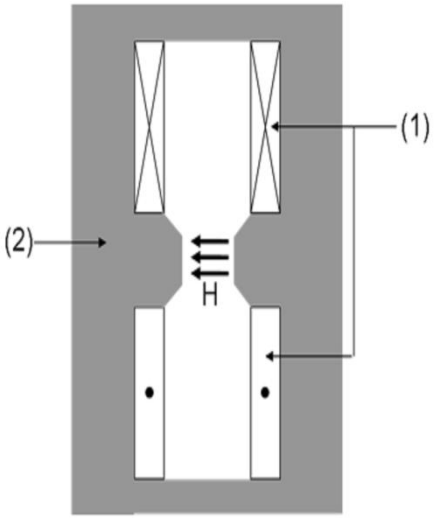

Fig.III.5: Electromagnet generating a uniform magnetic field. (1) Helmholtz coil; (2) Magnetic core

II.2.2. Magnetostriction curve

Longitudinal magnetostriction curve is presented in Fig.III.6. As the magnetic field increased, the interaction between magnetized particles increased too. The sample starts to enlarge its longitudinal size. When the magnetic field is large enough, all the particles reach their magnetic saturation, which in turn, leads to the maximum magnetostriction. Thus, a saturated magnetostriction of 4.3 % was

measured. This result is close to the value measured by Bednarek [Bed1] but, in our case, the applied magnetic field is only 1.2 Tesla, whereas he used 8 Tesla to achieve this result.

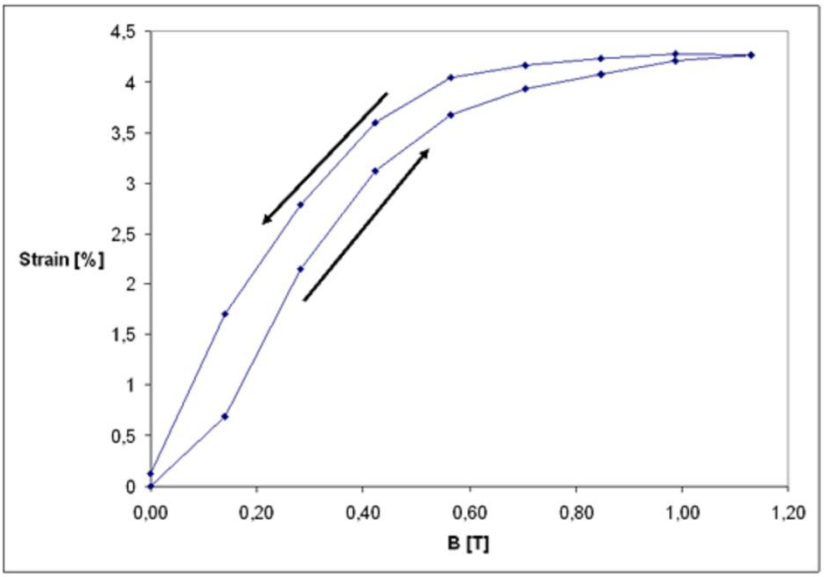

Fig.III.6: Relative longitudinal strain as a function of the magnetic field

Reduction in magnetic field leads to a decrease of particles interaction and of the magnetostriction. When the magnetic field is turned off, interaction is assumed to disappear because of the low magnetic remanence (Fig.III.3) of iron. However, a 0.12% residual strain was measured. This hysteresis probably results from damage at the particle-polymer interface, comparable to what happens for the Payne's effect [Pay1] and for higher strain, for the Mullin's effects [Mul1]. Stretching the composite may create decohesion between matrix and particles or cavitations inside the matrix [Coq1]. Those phenomena are irreversible. So the strain, when the magnetic field goes back to zero, is not zero.

III. Magnetic calculation

III.1. Dipolar interaction of a couple of particles

In order to understand the physical mechanisms at the origin of the above observed magnetostriction, a simple model has been developed. Let a set of N spherical magnetic particles be distributed in a cylinder shape. All magnetic moments are supposed to have equal magnitude which

corresponds to the saturated state of all the particles and are all directed parallel to the cylinder Z-axis, i.e. to the applied magnetic field direction.

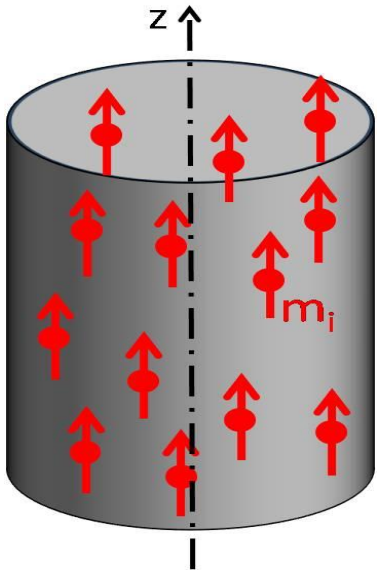

Fig.III.7: System of saturated particles in a cylinder

Magnetic induction field created by a magnetic moment $\vec{m}$ is calculated using the dipolar magnetic field expression [Mag1].

$$\vec{B} = \frac{\mu_0}{4\pi}\left[\frac{3(\vec{m}\cdot\vec{r})\vec{r}}{r^5} - \frac{\vec{m}}{r^3}\right] \qquad \text{eq.III.1}$$

Where μ_0 is the vacuum permeability, $\vec{r}$ is defined as the vector from the particle centre to a given position in the cylinder. This dipolar expression of the magnetic field is the exact expression of the magnetic field created by a spherical particle, assuming that the testing point is at a distance larger than the sphere radius, r>R. Gathering magnetic moments will enhance the interaction energy. The dipolar energy E_{12} between two magnetic moments may be expressed by the interaction of one moment with the dipolar field created by the second one:

$$E_{12} = -\vec{m}_2 \cdot \vec{B}_{12} = -\frac{\mu_0}{4\pi}\left[\frac{3(\vec{m}_2\cdot\vec{r}_{12})(\vec{m}_1\cdot\vec{r}_{12})}{r_{12}^5} - \frac{\vec{m}_2\cdot\vec{m}_1}{r_{12}^3}\right] \qquad \text{eq.III.2}$$

The force created by a moment m_1 on the moment m_2 at a distance r_{12} is then deduced by:

$$\vec{F}_{1\to 2} = -\vec{\nabla}(E_{12}) \qquad \text{eq.III.3}$$

$$\vec{F}_{12} = \frac{\mu_0}{4\pi}\left[\frac{3(\vec{m}_2\cdot\vec{r}_{12})\vec{m}_1 + 3(\vec{m}_1\cdot\vec{r}_{12})\vec{m}_2 + 3(\vec{m}_1\cdot\vec{m}_2)\vec{r}_{12}}{r_{12}^5} - \frac{15(\vec{m}_2\cdot\vec{r}_{12})(\vec{m}_1\cdot\vec{r}_{12})\vec{r}_{12}}{r_{12}^7}\right] \qquad \text{eq.III.4}$$

With all moments parallel to the Z-axis and having the same value, the force expression is simplified and is given within the polar coordinates system by:

$$\vec{F}_{1\to 2} = \frac{3m^2\mu_0}{4\pi}\left[\frac{\sin(2\theta)\vec{u}_\theta + (1-3\cos^2(\theta))\vec{u}_r}{r_{12}^4}\right] \qquad \text{eq.III.5}$$

where the distance between the 2 particles is r_{12}, θ is the angle between the Z-axis and the inter-particle vector. The dependence of the radial and the angular components of the forces are plotted in Fig.III.8a, whereas the corresponding vectors are represented in Fig.III.8b. Particles inside FSE, being all aligned, should attract the 2 closest particles and then the whole chain-like should contract leading to a contraction of the composite.

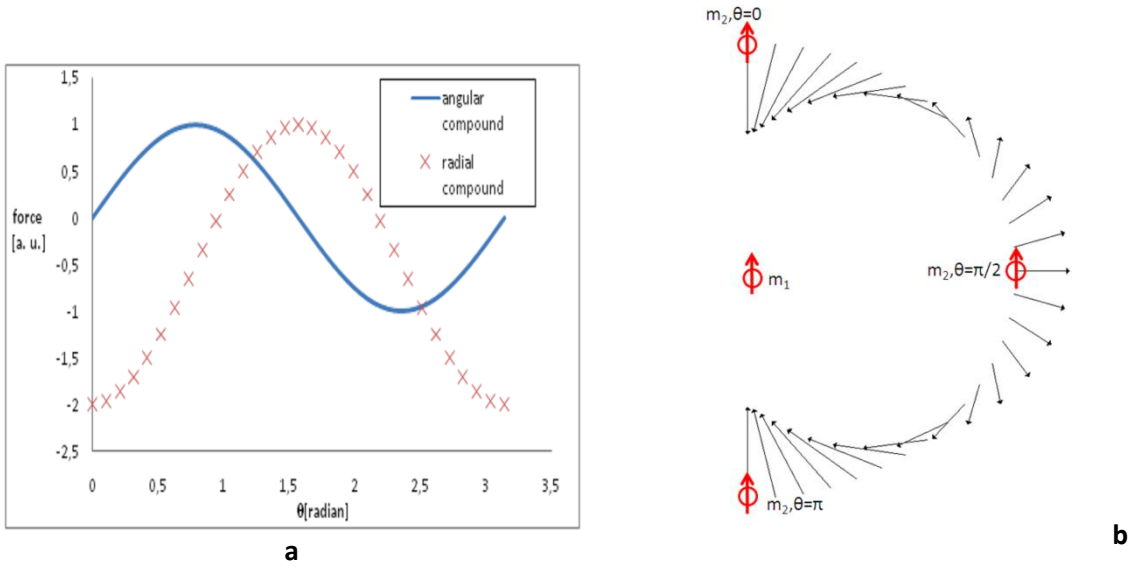

Fig.III.8: Angular dependence of dipole-dipole force. Fig.III.8a: The dot line represents the radial component and the dash line represents the angular one. Fig III.8b: The force is represented for different positions of the second particle.

Unlike the head-to-tail particles which attract themselves, face-to-face particles repel. Particles on the top of the cylinder would be attracted towards the core of the cylinders in a first approximation. In the same way, particles on the lateral edges would be repelled out of the cylinder.

The only solution, in the case of randomly filled composite, is to take into account the interaction over all the particles on every single particle.

III.2. Forces map within a cylinder shaped volume

A cylindrical-symmetric mesh (Fig.III.9) has been performed for our sample. Forces are calculated on all the nodes of an axi-symmetric plane of this mesh to probe their amplitudes and directions inside the sample.

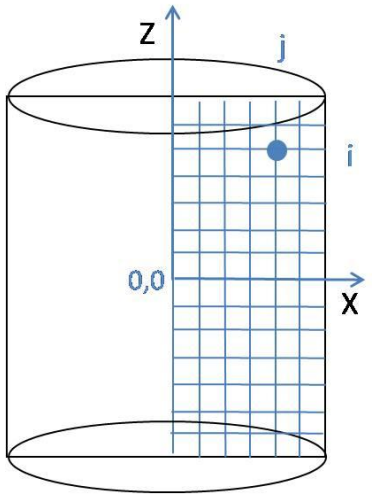

Fig. III.9: cylindrical-symmetric mesh

Force given by Eq.3 can be written into Cartesian coordinates, to get the resultant created by all the dipoles on a given point of the cylinder. Thus:

$$\vec{F}_{1\to 2} = F_{z1\to 2}\vec{u}_z + F_{x1\to 2}\vec{u}_x \qquad \text{eq.III.6}$$

where:

$$F_{z1\to 2} = \vec{F}_{1\to 2}\cdot\vec{u}_z = \frac{3m^2\mu_0}{4\pi r_{12}^4}\cos(\theta)(3-5\cos^2(\theta)) \qquad \text{eq.III.7}$$

$$F_{x1\to 2} = \vec{F}_{1\to 2}\cdot\vec{u}_x = \frac{3m^2\mu_0}{4\pi r_{12}^4}\sin(\theta)(1-5\cos^2(\theta)) \qquad \text{eq.III.8}$$

The resultant force on a point (i, j) inside the cylinder is calculated by summing the forces created by the N particles randomly distributed in the cylinder. In order to determine the average force map, this calculation was repeated for K distributions and we averaged the result s as shown below:

$$\vec{F}(i,j) = \frac{\sum_{K}\sum_{p=1}^{N}\vec{F}_{p\to(i,j)}}{K} \qquad \text{eq.III.9}$$

Fig.III.10a and Fig.III.10b presents the distribution inside the cylinder of average axial (a) and radial (b) forces components.

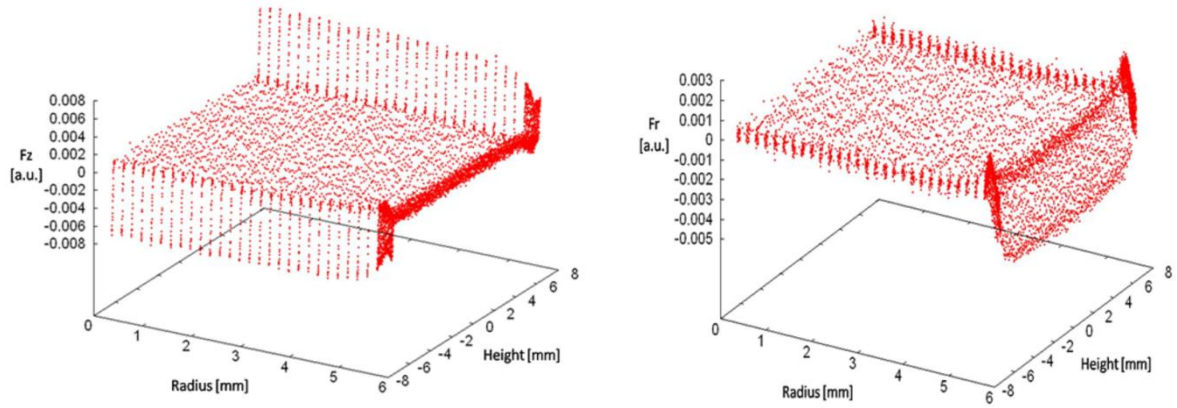

a b

Fig. III.10a & III.10b: Forces distribution inside the cylinder; (a) the axial component and (b) the radial component

In Fig.III.10a, the axial forces are plotted against the position on the considered plan. These axial forces are almost null in the volume and non-null close to the maximal and minimal axial position, i.e. the top basis and the bottom basis. On the top and bottom of the cylinder, axial forces are directed from inside toward outside, acting as a tensile stress, leading to the cylinder dilatation.

In fig.III.10b, the radial forces are plotted versus the position on the same plan. These radial forces are also almost null in the volume and non-null at the maximal radial position, i.e. the lateral surface of the cylinder. The radial forces are negative close to that lateral edge leading to an additional pressure for the overall magnetostriction.

Magnetic force is created by the product of magnetization and the variation of the inner magnetic field. This magnetic field is the sum of the applied field and the field created by the distribution of particles. The applied field is homogenous, so the forces are mainly due to the

variation of the particles field. The average forces inside the core of the composite are zero, the particles field is then assumed to be homogenous in this part of the composite. On the edges of the cylinder, where the field created by all the particles is inhomogeneous, the magnetic forces are not null.

IV. Mechanical analysis

In order to compare our experimental data with our simulation, we calculated the forces distribution inside a cylinder with the same size as for our experiments. The strain was then calculated using commercial Finite Element software, namely ABAQUS. The radial and axial forces fields as determined above were injected in the software as pressure: positive for radial forces and negative for the axial ones.

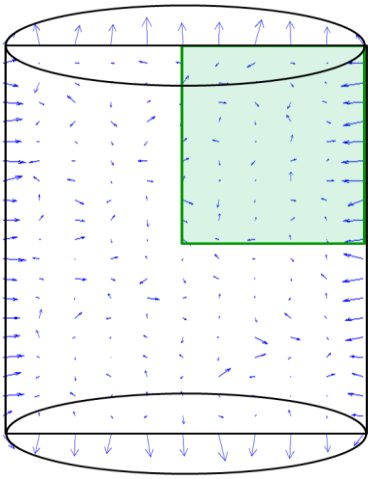

Fig. III.11 Tested part of the cylinder

Because of the cylindrical symmetry of the considered system and because of the symmetry of the axial forces, upper and lower disks are submitted to tensile forces, the strain calculation was done on the upper half part of an axi-symmetric plane (Fig.III.11). The measured deformation was roughly 5%, which is small enough to use linear mechanical properties of the composite. The Poisson ratio was set as 0.49, to avoid numerical divergence, but is still close to the ideal elastomer value of 0.5; and the Young modulus was set as 0.7 MPa (Fig.III.4).

Continuum mechanics laws are linear, so the strains generated by the axial and radial forces were treated apart and summed afterward. The axial and radial forces effects on the cylinder shape are respectively plotted in Fig.III.12a & III.12b.

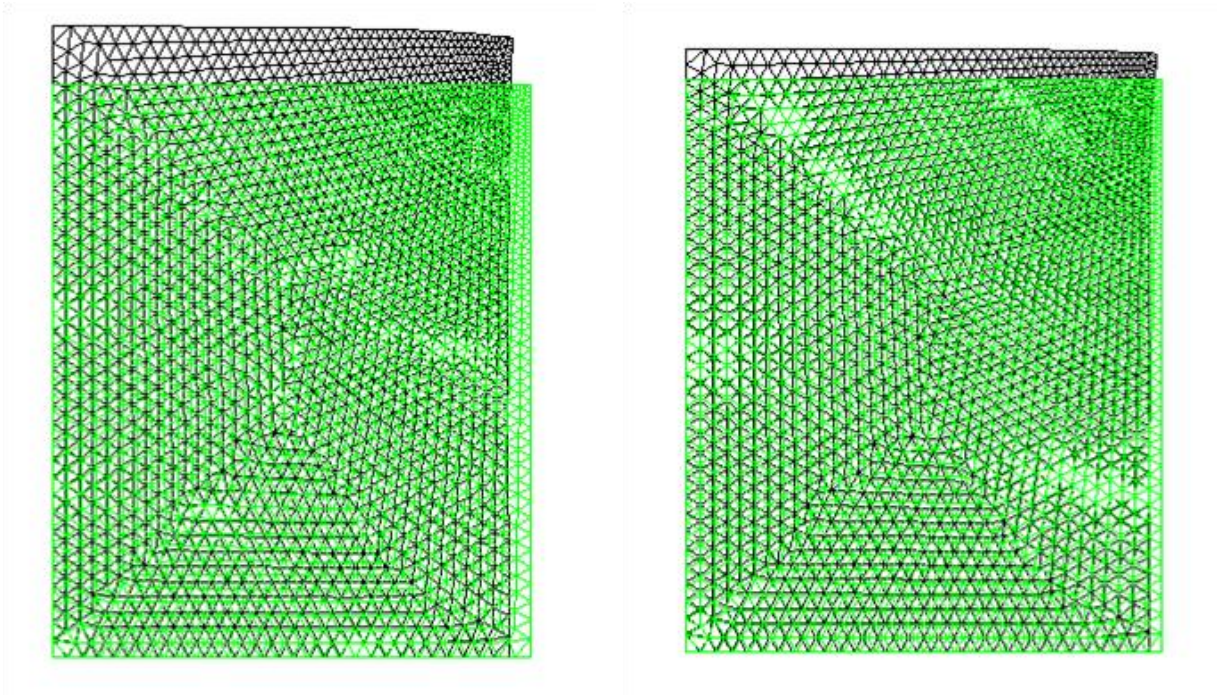

a b

Fig. III.12a & III.12b: Deformation distribution inside the cylinder due to (a) the axial forces and (b) the radial forces. The black-meshed part represents the deformed sample where the green-meshed part set for the initial sample shape

An axial strain of 3.08% was obtained due to the axial forces whereas a 1.59 % with the radial forces, which is a consequence of the hypothesis of almost constant volume (Poisson ratio close to 0.5). The whole sample calculated deformation is presented in Fig.III.13; the axial deformation is larger than the radial one as expected and the longitudinal strain was of 4.7 %. This value is very close to the experimental one, i.e. 4.3%, which confirms the interest in the modeling method, as it can be applied for all kind of sample shape.

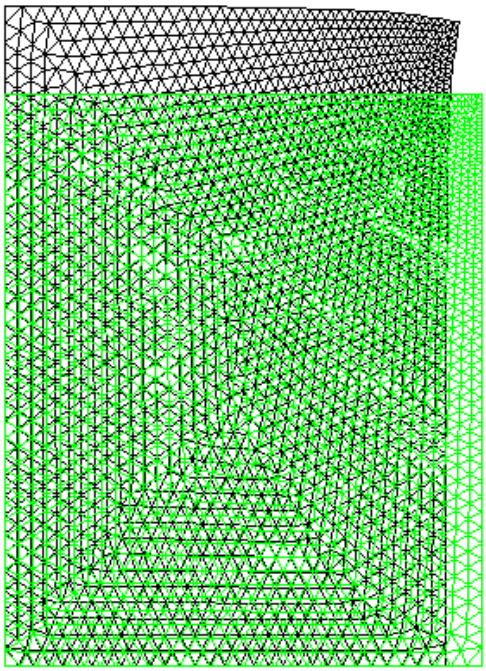

Fig. III.13: The addition of the 2 deformations. The black-meshed part represents the deformed sample where the green-meshed part set for the initial sample shape

V. Discussion on the dipolar interaction

V.1. Boundaries forces

As described above, we have proved that the dipolar interaction is responsible for the observed strain of a MRE placed in a uniform magnetic field. These dipolar forces are localized on each boundaries of the cylinder unlike to the inner part of the sample where no force is acting. We can figure out these forces with geometrical assumptions. Considering a magnetic moment surrounded entirely or partially by an elementary spherical shell, it will provide the same kind of force.

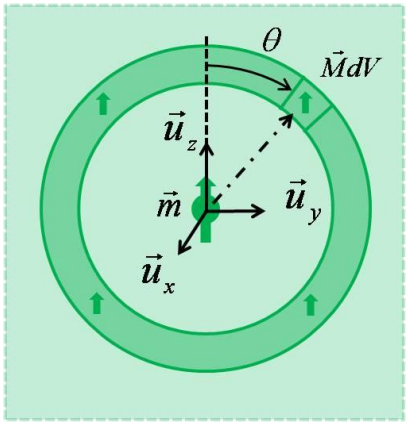

Fig. III.14: Magnetic moment in a magnetic medium

The expression of the dipolar force represented by eq.III.5 shows that such force is acting at very short distance. Hence, considering a distance *d* for which an increment *Δd* will slightly increase the force, we calculate the resultant force, acting on a single moment $\vec{m}$, by the other magnetic moments placed below that distance *d*. The mathematical way to get this result is to integrate the force created by all the magnetic moments placed on a spherical shell on that moment. To ease the calculation, by using the spherical symmetry, we use the reciprocal force, i.e. the force created by the moment on the shell:

$$\vec{f}_{shell \to moment} = -\vec{f}_{moment \to shell} \qquad \text{eq.III.10}$$

The force acting on the shell is evaluated by summing all forces created by the moment on an elementary magnetized volume set i.e $\vec{m} = \vec{M}dV = Mr^2 dr d\varphi \sin(\theta) d\theta$ as seen in Fig.III.14. This force *df* (eq.III.5) can be written in spherical coordinates as:

$$d\vec{f} = C \cdot A_r(r) \begin{bmatrix} f_x(\theta,\varphi) \\ f_y(\theta,\varphi) \\ f_z(\theta,\varphi) \end{bmatrix} r^2 dr d\varphi \sin(\theta) d\theta \qquad \text{eq. III.11}$$

where *C* is a constant equal to $-3mM\mu_0/4\pi$, $A_r(r)$ is the radial amplitude function due to radial distance *r* and the *fx*, *fy* and *fz* are angular functions of the spherical angles θ and φ. The direction of the force depends on only these 2 angles; the distance r modulates the amplitude of the force. The amplitude function is:

$$A_r = \left[\frac{1}{r^4}\right] \qquad \text{eq.III.12}$$

And the components of the force due to the angular term:

$$f_x(\theta,\varphi) = \cos(\varphi)\sin(\theta)[1-5\cos^2(\theta)] \qquad \text{eq.III.13}$$

$$f_y(\theta,\varphi) = \sin(\varphi)\sin(\theta)[1-5\cos^2(\theta)] \qquad \text{eq.III.14}$$

$$f_z(\theta,\varphi) = \cos(\theta)[1-5\cos^2(\theta)] \qquad \text{eq.III.15}$$

In this case, when the summation is made over all space directions, θ is ranging from 0 to π and φ from 0 to 2π, yielding to the same result: no force. So that, the dipolar force inside a magnetic medium is always zero as found on the two figures Fig.III10a&b. This result is easily understood because of the symmetry of the system. This is not the case for a magnetic moment placed on the edge of the material. We can check the above presented results: for the upper basis and for the lateral surface of the cylinder as seen on the Fig.III.15a&b.

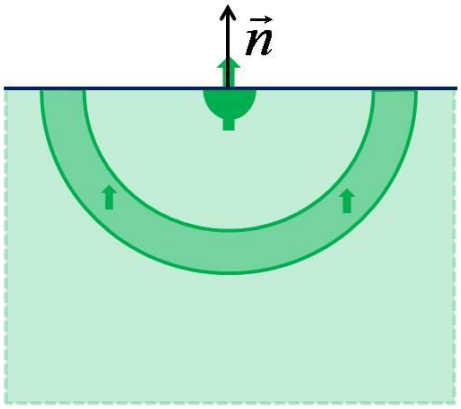

Fig. III.15a: Magnetic moment on the upper edge of a magnetic medium

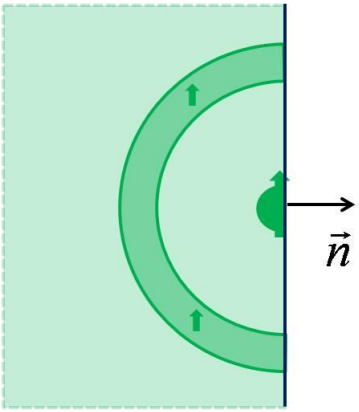

Fig. III.15b: Magnetic moment on the lateral edge of a magnetic medium

The radial amplitude force created on the magnetic moment by a half spherical shell is the same in the two cases represented by Fig.III.15a&b. It can be estimated as follows; the distance between the shell and the moment is *d*. But the volume of the moment itself has to be excluded because it does not create a force on itself. If the excluded length (corresponding to the excluded volume) is *e*, the amplitude of the force due to the distance between the moment and the shell is:

$$\int_e^d A_r r^2 dr = \frac{1}{e} - \frac{1}{d} \qquad \text{eq.III.16}$$

Because *e* is smaller than *d*, this integral is positive.

Now we have to consider the modulation of the force due to the angular component.

First case: an upper boundary. Here, all the other magnetic moments are placed on a half spherical shell below the considered moment as seen in Fig.III.15a. Due to symmetry, the *fx* and *fy* components are null (integral of cosinus and sinus over 2π). With this geometry, only axial force arises. Thus, *fz* component is evaluated with the angle θ ranging from π/2 to π:

$$\int_0^{2\pi}\int_{\pi/2}^{\pi} f_z(\theta)\sin(\theta)d\theta d\varphi = 2\pi\int_{\pi/2}^{\pi}\sin(\theta)\cos(\theta)[3-5\cos^2(\theta)]d\theta = -\frac{\pi}{2} \qquad \text{eq.III.17}$$

The angular component is negative. The force created by the shell on the moment is the product of the radial component (positive), the angular component (negative) and the constant C which is negative resulting finally in the positive force. Top surface experiences an outward force.

Since the whole force, experienced by an entirely surrounded moment is zero and the upper boundary moment experiences a positive force (in the same of the applied field), the lower boundary moment will consequently experience a negative force. Top and bottom face of the cylinder are under tensile stress.

The second case is a lateral boundary. Here, all the other magnetic moments are placed on a half spherical shell aside the considered moment as seen in Fig.III.15b. Because of symmetry, *fz* component is null. The same result can be found for θ ranging from 0 to π. If we restrict the normal vector to be collinear with the unit vector $\vec{u}_y$ (general case is treated in annex), the integral of the respective component *fy*, for the angle φ ranging from π to 2π and θ from 0 to π is:

$$\int_{\pi}^{2\pi}\int_{0}^{\pi} f_y(\theta)\sin(\theta)d\theta d\varphi = \int_{\pi}^{2\pi}\int_{0}^{\pi}\sin^2(\theta)[1-5\cos^2(\theta)]d\theta\sin(\varphi)d\varphi = \frac{\pi}{4} \qquad \text{eq.III.18}$$

The angular component is positive. The force created by the shell on the moment is the product of the radial component (positive) and the angular component (positive) and the negative constant giving a force that is negative. Lateral boundary is under compressive stress.

This calculation concludes to macroscopic positive (resp. negative) force on the top (resp. bottom) of the cylinder and negative force on the lateral surface of the cylinder. In fact, the sign of the forces is a consequence of the exclude volume as shown in eq.III.15; therefore those forces are located in a thin layer just under the surface of the sample. Dipolar forces are created in the neighborhood of the edges of the sample and also due to the volume of the moment. This is a force created on a volume; a body force with a non-null value close to edges and null inside the core.

These results are like those found through the complete dipolar calculation. A limit in this calculation arises from the fact that all other magnetic moments in the composite are not placed on a spherical shell, but in the entire volume of the sample. So despite it provides the same behavior, the full calculation is more rigorous.

V.2. Introduction to shape effect on the forces

It is proved above that the dipolar interaction is responsible for the observed strain of a MRE placed in a uniform magnetic field. This dipolar interaction is highly dependent on the way particles are distributed. For example, two magnetic moments, with a radius *R* and distant of *r*, can be placed with different relative angle θ (from *m* to *r*) as seen in Fig.III.16a & b:

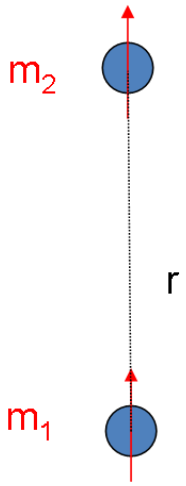

Fig.III.16a. Magnetic moments placed with a relative angle of 0 rad.

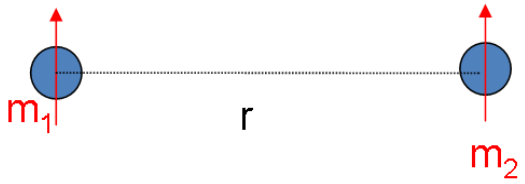

Fig.III.16b Magnetic moments placed with a relative angle of π/2 rad.

The interacting energies (eq.III.2), of these two cases are different. In the case of magnetic moments placed in a head-to-tail configuration (Fig.III.16a), energy is written as:

$$E_{12}(\theta = 0) = -\frac{\mu_0 m^2}{2\pi r^3} \qquad \text{eq.III.19}$$

whereas the energy of the magnetic moments placed in a face-to-face configuration (Fig.III.16b) is written as:

$$E_{12}(\theta = \pi/2) = \frac{\mu_0 m^2}{4\pi r^3} \qquad \text{eq.III.20}$$

So, the interacting energy for given distance is lower, when particles are in a head-to-tail configuration compare to the face–to-face configuration. This consideration, made on 2 particles separated by the same distance can be expanded for a larger set of particles inside a given volume. Summing all the energies of interacting pairs being expressed as:

$$E_D = -\frac{1}{2}\sum_i m_i B_i \qquad \text{eq.III.21}$$

B_i is the induction created on the site *i* by all the other moments. The reduced dipolar energy $E_D/\{\mu 0/2[m/R^3]^2\}$ is a density of energy per volume. For volume characterized by a cylindrical symmetry, as ellipsoid, this reduced energy exhibits a shape effect. The shape effect appears with the definition of the aspect ratio c/a with *c* as the length of the sample parallel to the moments direction and *a* as the transversal length. Considering 2 cases: the ellipsoid is an oblate, the ratio is low, particles see the others particles with a relative angles θ tending toward π/2, and in contrary, if the ellipsoid is a prolate, the aspect ratio is large, the relative angles θ are tending toward 0; the oblate has a higher energy per unit of volume than the prolate. This available larger energy of low ratio shaped sample is then converted into a force that strains the sample.

Following this idea, we have performed the force calculation over several shapes. The testing parameter was the aspect ratio. This aspect ratio was ranging from 0.33 to 1.2. The summation of all pair-forces inside the volume, due to the summation of reciprocal forces would lead to zero. Forces were therefore summed over the top half cylinder like in Fig.III.11 and normalized by the chosen volume.

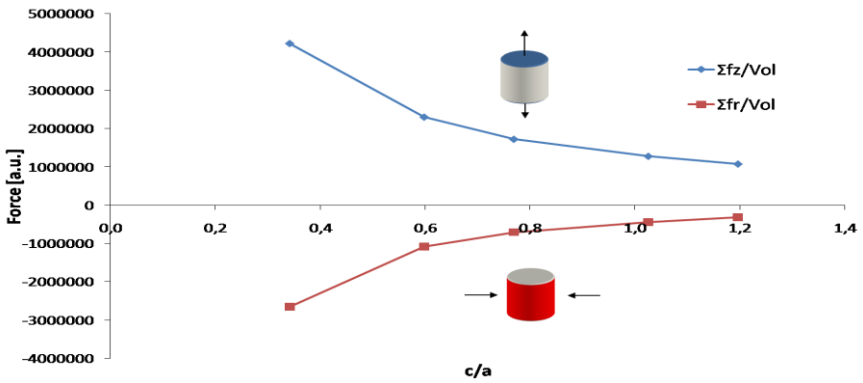

Fig.III.17 Shape effect on the forces

The increment of both, the axial dipolar force and radial dipolar forces when the cylinder is tending to a flat disk, c/a →0 can be seen in Fig.III.17; in the same way, these forces are decreasing when the shape tends to a long rod, c/a→∞. Hence, we have introduced a shape effect; flatter shape creates a larger force compared to needle-like shape. Those calculations are in agreement to measurements made on 30% (vol.) filled sample with different aspect ratio, as seen in Fig.III.18.

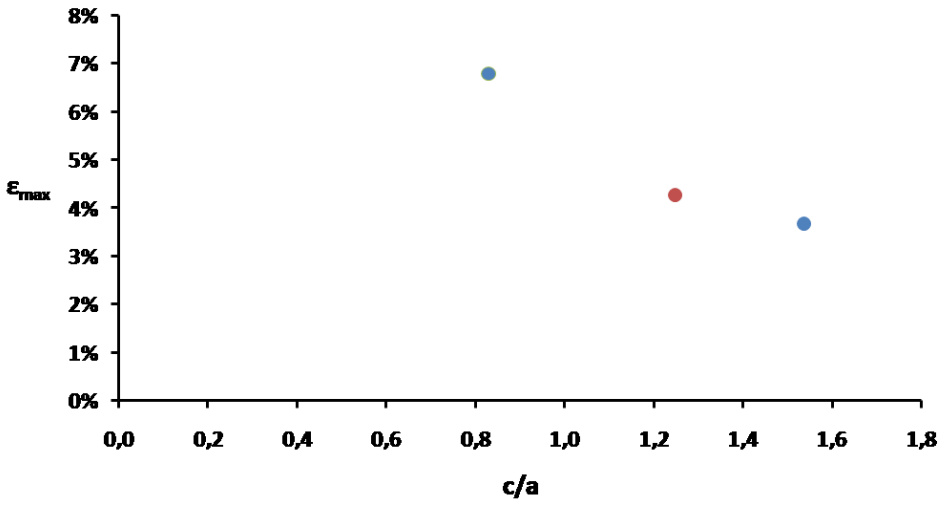

Fig.III.18 Shape effect on the saturation of the magnetostriction. Red point stands for the sample considered above.

The smaller the ratio, the larger the strain. This effect will be discussed in detail in the 5th Chapter.

For sample with same aspect ratio but with different sizes, forces have the same amplitude and are located in the same thin layer near the surface (whose thickness is about the particle size) as shown in Fig.III.19. The resulting force per surface unit i.e. stress is the same for samples with same geometry. Same stresses yield to same strains.

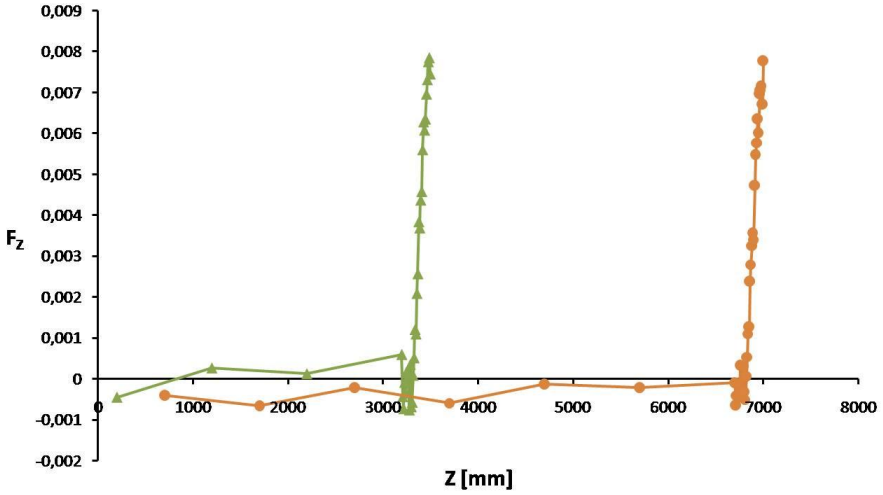

Fig.III.19 Force distribution as the function of the highness, for 2 samples with different size, keeping the same aspect ratio

VI. Conclusion

We have studied the measurement of the positive magnetostriction of a composite, made of spherical ferromagnetic particles embedded in an elastic matrix, under a homogenous magnetic field. Experimental data were compared to a theoretical calculation. The force calculation is only based on the dipole-dipole interaction of saturated spherical particles randomly embedded in a cylindrical volume. This force field, coupled with a strain calculation (using FEM software) on an effective elastic material, provides a positive axial deformation 4.7 % very close to the one measured i.e. 4.3 %. Inter-particle forces successfully provided the explanation to the apparent magnetostriction of the composite when placed in the applied field. The calculation of interaction between magnetized particles has proved the dependence the force on the square magnetization, eq.III.5. The applied magnetic field does not play a key-role in the phenomenon; it just induces a magnetization in all the particles which in turn interact together.

Forces are located in the neighborhood of the edges; top and bottom faces of the cylinder are under a negative pressure while the lateral face is under a positive pressure. These forces were result in an extension of the cylinder. Dipolar forces act on the cylinder in such way that the demagnetizing energy of that cylinder decreases.

The calculation has also proved a shape effect showing that as the cylinder becomes longer, axial and radial forces per unit of volume decrease as seen in Fig.III.17. This is also a characteristic of the demagnetizing field. The following chapter deals with the demagnetizing field and coefficient of a composite made of ferromagnetic spherical particles inside a non-magnetic matrix.

References:

[Bed1]: The Giant linear magnetostriction in elastic ferromagnetic composites within a porous matrix, S. Bednarek, *Journal of Magnetism and Magnetic Materials* 301 (2006) 200

[Gua1]: Magnetostrictive effect of magnetorheological elastomer, Xinchun Guan, Xufeng Dong, Jinping Ou, *Journal of Magnetism and Magnetic Materials* 320 (2008) 158

[Pay1]: The dynamic properties of carbon black-loaded natural rubber vulcanizates, A.R. Payne, *Journal of Applied Polymer Science* 6 (1962) 368

[Mul1]: Theoretical model for the elastic behavior of filler-reinforced vulcanized rubbers, L. Mullins, N. R. Tobin, *Rubber Chemistry Technology* 30 (1957) 355

[Mag1]: Magnetism I-Fundamentals, E. du Tremolet de Lacheisserie, D. Gignoux, M. Schlenker, Springer-Verlag New York Inc. (2004), #ISBN-10: 0387229671, #ISBN-13**:** 978-0387229676

[Coq1] Propriétés élastiques et viscoélastiques de matériaux composites adaptatifs, E. Coquelle, PhD Thesis (2004) Nice

Chapter 4

Magnetization of a ferromagnetic composite

I. Introduction

In the previous chapter, we have calculated the magnetic force induced on a particle by all the other magnetic moments, except itself. The force was calculated from the field which is created by the magnetized particles. Inside a bulk magnetic material, this field is in fact the demagnetizing field which depends on the sample shape: it decreases with increasing aspect ratio c/a for a cylinder (length/diameter). We have also shown that the magnetostriction effect is also reduced for high aspect ratio cylinders. Both effects might be correlated and suggest a better understanding of the demagnetizing field effect in a composite.

In this chapter, we will bring back to mind the concept of demagnetizing field and demagnetizing factor and its effect on the magnetization curve of a ferromagnetic material. Then, we will present some basis on the effective demagnetizing factor of a composite made of ferromagnetic particles embedded in a non-magnetic matrix. Experiments will be provided for the discussion on this effective demagnetizing factor for the shape of the sample and for the filling factor (volume fraction of fillers). A model taking into account the distribution of the particle will be then presented and discussed.

II. Magnetization of a ferromagnetic material

II.1. Pure ferromagnetic material

For a pure ferromagnetic material, the magnetization is related to the local magnetic field via susceptibility χ of the ferromagnetic material:

$$M = \chi H_{\text{int}} \qquad \text{eq.IV.1}$$

When a magnetic sample is exposed to an external magnetic field (experimentally, the applied field), the material is magnetized and hence creates a magnetic field outside and inside the material, changing the viewed field H_{int}. This inner magnetic field is the superposition of the external magnetic field and the magnetic field created by the material itself, known as demagnetizing field:

$$H_{\text{int}} = H_D + H_{ext} \qquad \text{eq.IV.2}$$

where H_{ext}, H_{int} and H_D are respectively the external, the internal and the demagnetizing magnetic field. The magnetic field generated by the magnetized body, is inside the material, is opposite to the magnetization, so that it is called demagnetizing field. In many cases, this field is expressed as a linear function of the magnetization:

$$H_D = -NM \qquad \text{eq.IV.3}$$

In the case of an ellipsoid of revolution, H_D is homogenous and N is a function of aspect ratio, length to diameter of the sample. N is then called the demagnetizing factor (or sometimes demagnetizing coefficient). The effective or apparent susceptibility is then defined with the external magnetic field:

$$M = \chi_{eff} H_{ext} \qquad \text{eq.IV.4}$$

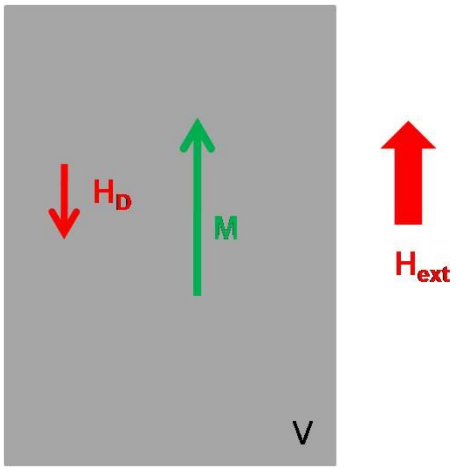

Fig.IV.1. Magnetization within the sample volume with the external and demagnetizing field

Using equations eq.IV.1, eq.IV.2 and eq.IV.3 in equation eq.IV.4, the effective susceptibility can be expressed as:

$$\chi_{eff} = \frac{\chi}{1 + N\chi} \qquad \text{eq.IV.5}$$

For a pure ferromagnetic material, the susceptibility is large enough to use the following approximation, $\chi >> 1$, providing the result:

$$M = \frac{1}{\frac{1}{\chi} + N} H_{ext} \approx \frac{1}{N} H_{ext} \qquad \text{eq.IV.6}$$

This expression shows that the magnetization at low magnetic field (far from the saturation), in the case of a soft ferromagnetic material, is controlled by the shape of the sample via the demagnetizing factor. The general expression of the magnetization sample, below and above saturation of the ferromagnetic material is:

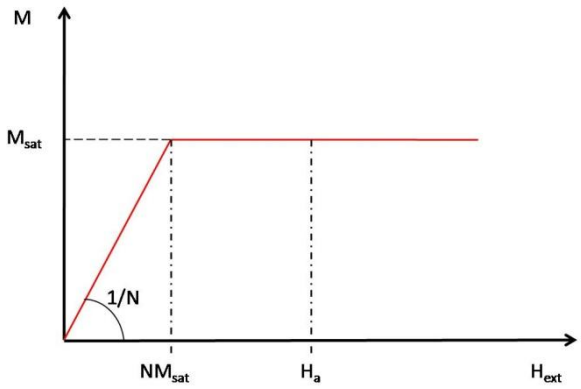

Fig.IV.2a. Magnetization curve of a ferromagnetic material

$$M = \frac{1}{N} H_a \quad if \; H_a < NM_{sat}$$
$$M = M_{sat} \quad if \; H_a \geq NM_{sat}$$

Fig.IV.2b. Equivalent equation

On fig.IV.2a and 2b, it can be seen that the saturation is reached for a critical applied field equal to the product of the demagnetizing factor and the saturated magnetization.

Calculation of the effective demagnetizing factor is known analytically for an ellipsoid. Hence, for an oblate sample with the dimension ratio γ= diameter /length, the formula is [Chi1]:

$$\bullet \; N = \frac{1}{2}\left[\frac{\gamma^2}{(\gamma^2-1)^{3/2}} Arc\sin\frac{\sqrt{\gamma^2-1}}{\gamma} - \frac{1}{\gamma^2-1}\right] \qquad \text{eq.IV.7}$$

The case of a sphere leads to the factor [Chi1]:

$$\bullet \; N = \frac{1}{3} \qquad \text{eq.IV.8}$$

In the case of a prolate sample with the dimension ratio γ=length/diameter, the formula is [Chi1]:

$$\bullet \; N = \frac{1}{\gamma^2-1}\left[\left(\frac{\gamma}{\sqrt{\gamma^2-1}} \ln(\gamma + \sqrt{\gamma^2-1})\right) - 1\right] \qquad \text{eq.IV.9}$$

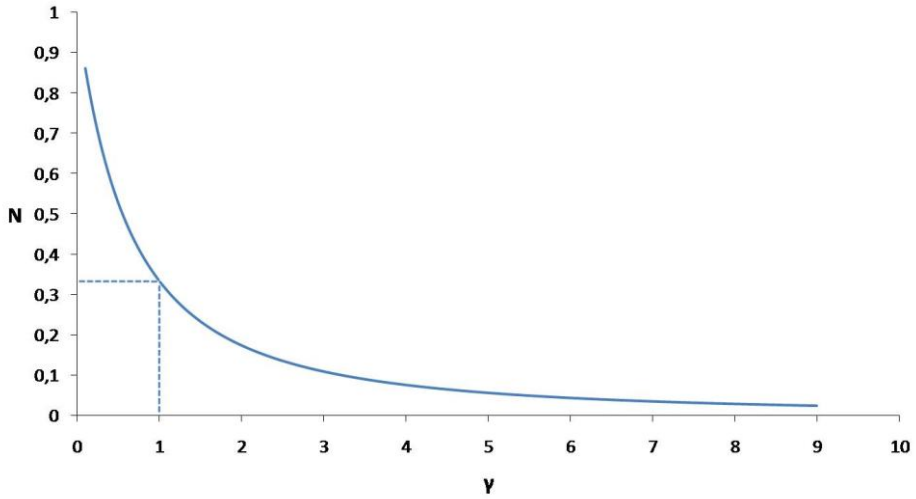

Fig.IV.3. Demagnetizing factor of ellipsoid sample versus the aspect ratio γ=length/diameter

In one hand, when the aspect ratio is large, γ>>1, the demagnetizing factor tends toward 0, the magnetization slope is infinite; the sample is easily magnetized. On the other hand, when the aspect ratio is small, γ<<1, the demagnetizing factor tends toward 1 and the sample is hardly magnetized.

For non-ellipsoidal geometries, the inner magnetic field created by the magnetic material is no more homogeneous. The demagnetizing factor is replaced by a demagnetizing tensor [Jos1, Zhe, and Lu]. The amplitude and the direction of the magnetization are functions of the local demagnetizing tensor:

$$H_i = N_{ij} M_j \qquad \text{eq.IV.10}$$

where *i,j*={x,y,z}. Hence, considering a cylinder of length *L* and diameter 2*a*, a complex calculation [Jos1] yields to the non-homogeneous demagnetizing field which depends on the tested point inside the cylinder:

$$N_{rz}(r,z) = \frac{1}{\pi}\sqrt{\frac{a}{r}}\left[\frac{1}{k_1}\left(\left(1-\frac{1}{2}k_1^2\right)K(k_1)-E(k_1)\right)-\frac{1}{k_2}\left(\left(1-\frac{1}{2}k_2^2\right)K(k_2)-E(k_2)\right)\right] \qquad \text{eq.IV.11}$$

$$N_{zz}(r,z) = 1-\frac{zk_1K(k_1)}{4\pi\sqrt{ar}}-\frac{\Lambda_0(\alpha_1,\beta_1)}{4}-\frac{(L-z)k_2K(k_2)}{4\pi\sqrt{ar}}-\frac{\Lambda_0(\alpha_2,\beta_2)}{4} \qquad \text{eq.IV.12}$$

The origin of the coordinates coincides with the center of the cylinder on lower basis. *K(k)*, *E(k)* and $\Lambda_0(\alpha, \beta)$ are respectively the complex elliptic integral of the first, second and third kind and *k, α, β* are defined as :

$$\begin{cases} k_1^2 = \dfrac{4ar}{z^2 + (a+r)^2} \\ \sin(\alpha_1) = k_1 \\ \sin(\beta_1) = \dfrac{z}{z^2 + (a-r)^2} \end{cases} \quad and \quad \begin{cases} k_2^2 = \dfrac{4ar}{(L-z)^2 + (a+r)^2} \\ \sin(\alpha_2) = k_2 \\ \sin(\beta_2) = \dfrac{(L-z)}{(L-z)^2 + (a-r)^2} \end{cases} \qquad \text{eq.IV.13}$$

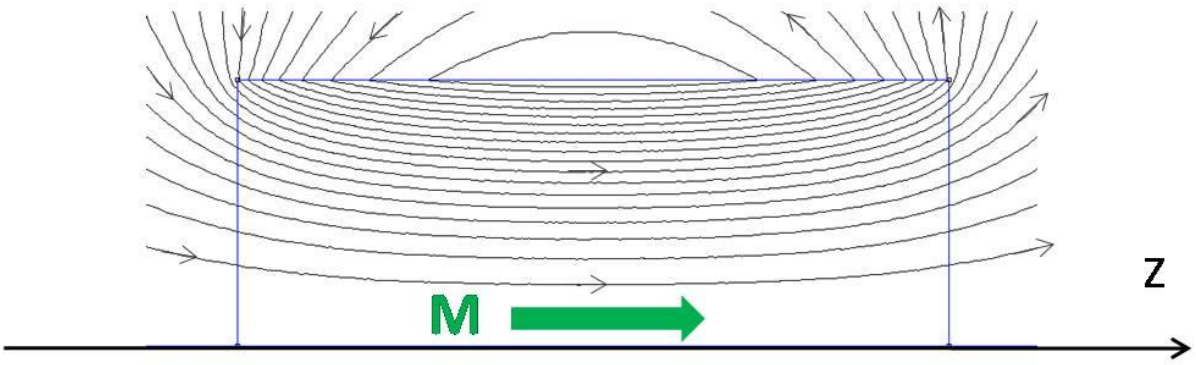

Fig.IV.4. Magnetic induction inside an uniform magnetized cylinder

The effective demagnetizing factor or magnetometric demagnetizing factor, of a non-ellipsoidal sample, is defined by the volume average of all local value of the demagnetizing tensor [Jos2]:

$$\overline{N} = \frac{1}{V} \int_V N(r,z) dV \qquad \text{eq.IV.14}$$

A simple formula has been given by Sato & Ishii [Sat] providing the averaged geometrical demagnetizing factor of a cylinder with a maximum error of 3 % for a ratio γ ranging from 0.1 to 10.

$$\overline{N} = \frac{1}{2\left(\dfrac{2\gamma}{\sqrt{\pi}}\right)+1} \qquad \text{eq.IV.15}$$

The magnetic energy density of a magnetized body depends on the external field and on the magnetization. The magnetization in turn depends on the inner field which is the sum of the external field and of the demagnetizing field, so that, the energy, per unit of volume is written as:

$$E_d = -\mu_0 \int_0^{H_a} MdH = -\mu_0 MH_a + \frac{1}{2}\mu_0 NM^2 \qquad \text{eq.IV.16}$$

From eq.IV.16, this energy can be seen as the opposite of the area under the magnetization in a MH curve as seen in Fig.IV.2a. The first term stands for the interaction of the sample placed in the external magnetic field, the Zeeman energy, whereas the second one represents the interaction of the sample in its own magnetic field, the demagnetizing energy. Demagnetizing density of energy is defined as the energy paid to gathered magnetized moment inside the considered volume. This demagnetizing energy is proportional to the demagnetizing factor, so that, a flat sample has a larger energy than a needle-like one.

II.2. Ferromagnetic composite

Considering a non-magnetic matrix filled by ferromagnetic particles, the magnetization of such sample is controlled by demagnetizing factor n_{sample} of the sample, the fraction ϕ of volume occupied by the particles, the demagnetizing factor $n_{particle}$ of particles and the distribution of the particles within the sample. The way the particle inside the matrix magnetizes depends highly on the particles distribution in the volume of the sample. We will first consider a randomly filled composite.

II.2.1. Randomly filled composite

As the ferromagnetic particles are soft, without any remnant magnetization, the magnetization of a randomly filled composite is carried through both its saturation and demagnetizing factor parameters.

II.2.1.1. Effective magnetic saturation

The magnetic saturation of a composite is the density of magnetic moment of all the compounds inside, i.e. the particles and the matrix:

$$M_{composite}^{sat} = \frac{\sum_{p} M_{particle}^{sat} V_p + \sum_{m} M_{matrix}^{sat} V_m}{Vtot} \qquad \text{eq.IV.17}$$

V_p, V_m and V_{tot} are the volume of the particles, the matrix and the sample (composite) respectively. The magnetization $M_{particle}^{sat}$, M_{matrix}^{sat} and $M_{composite}^{sat}$ are the saturate magnetization of the particles, the matrix and the sample (composite) respectively. An important parameter for such composite is the filling factor which is defined as the volume of all the particles inside the sample:

$$\phi = \frac{\sum_{p} V_p}{Vtot} \qquad \text{eq.IV.18}$$

Assuming that the matrix magnetization is null and using eq.IV.17 and eq.IV.18, the magnetic saturation of randomly-filled composite is interrelated to the filling factor and the magnetic saturation of the ferromagnetic particles by the following equation:

$$M_{composite}^{sat} = \phi M_{particle}^{sat} \qquad \text{eq.IV.19}$$

II.2.1.2. Effective demagnetizing factor

II.2.1.2.1. Kneller model

This effective demagnetizing factor for a random dispersion was calculated by Kneller [Kne] through the point of view of a single particle inside the composite. The effective demagnetizing field of a ferromagnetic particle, inside a non-magnetic volume, is the summation of both the geometrical (shape) demagnetizing factor of the volume and that of the particles, and a term which takes into account the interaction of particles.

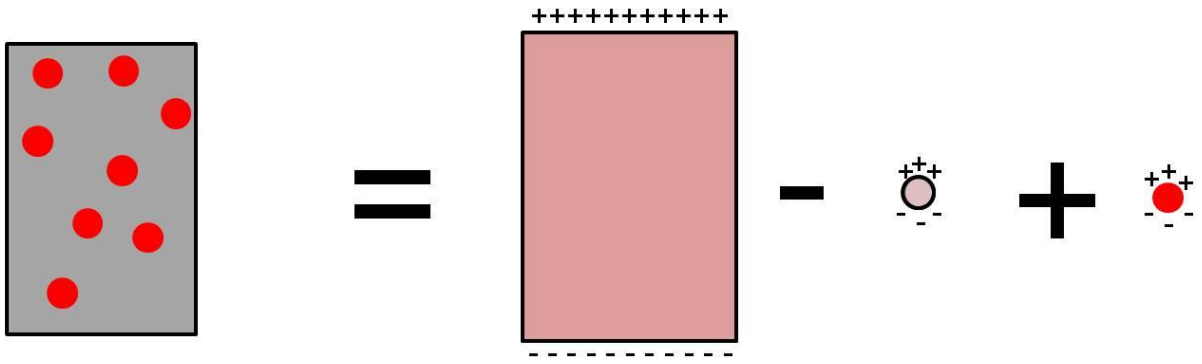

Fig. IV.6. Model of the demagnetizing coefficient of a composite

This particle sees a geometrical demagnetizing field with the factor n_{sample} due to the sample shape, a vicinity field due to the particles magnetic field and the inner demagnetizing field of that particle with the factor $n_{particle}$. Calculation of that vicinity field is complicated because of its dependence on the distribution of particle, on the filling factor and of course on the particle shape. Increasing the filling factor leads to high increase of the particles interaction. Kneller converts this vicinity field as a field created by the cavity surrounding the particle; it is set as a hole, with the particle shape, into the homogenized matrix.

$$H_{d/p} = -n \cdot M_{particle} = -(n_{sample}\phi M_{particle} - n_{particle}\phi M_{particle} + n_{particle} M_{particle}) \qquad \text{eq.IV.20}$$

$$n = n_{sample}\phi + n_{particle}(1-\phi) \qquad \text{eq.IV.21}$$

In the extreme case, where ϕ=1, the volume is completely filled by particles and $n = n_{sample}$, that particle will be affected only by the geometrical demagnetizing field. In the case ϕ→0, $n = n_{particle}$, the isolated particle will be affected by its own demagnetizing field. This demagnetizing factor viewed by a particle is ranging between $n_{particle}$ and n_{sample}.

The final expression of the composite demagnetizing factor is found considering that there is only one magnetic field within the volume, but the magnetization is different for the particle and for the sample, thereby, an extra operation is needed to extract the sample demagnetizing factor. Equaling those factors will provide N_{eff}: the demagnetizing factor of the composite.

$$N_{eff}\phi M_{particle} = nM_{particle} \qquad \text{eq.IV.22}$$

$$\Rightarrow N_{eff} = n_{sample} + n_{particle}\left(\frac{1}{\phi} - 1\right) \qquad \text{eq.IV.23}$$

This composite demagnetizing factor does not range between 0 and 1 unlike the pure ferromagnetic one. Nevertheless, this property is still true for high concentration of particle, when $\phi \to 1$, the effective factor N_{eff} tends toward n_{sample}. For lower concentration, values are greater than 1 and a divergence of that effective factor for the lowest concentration can be seen. In this case, when the concentration is very low, $\phi \to 0$, the effective demagnetizing factor tends to infinity, so that the magnetization slope is null. Physically, the fewer the particles inside the composite, the harder the magnetization of the composite, still assuming the matrix is non-magnetic. Also, the magnetization is null for low concentrations. Considering the demagnetizing energy, we will find:

$$E_d = \frac{1}{2}\mu_0 N_{eff} M^2_{composite} \qquad \text{eq.IV.24}$$

$$E_d = \frac{1}{2}\mu_0\left(n_{sample} + n_{particle}\left(\frac{1}{\phi} - 1\right)\right)M^2_{composite} = \frac{1}{2}\mu_0(\phi n_{sample} + n_{particle}(1-\phi))\phi M^2_{particle} \qquad \text{eq.IV.25}$$

The demagnetizing energy would not diverge regardless of the concentration. This energy, as viewed by the sample is the same as the one viewed by the previously considered particle. The magnetic energy is concentrated locally inside the ferromagnetic particles, but it can be homogeneously distributed over the whole sample volume.

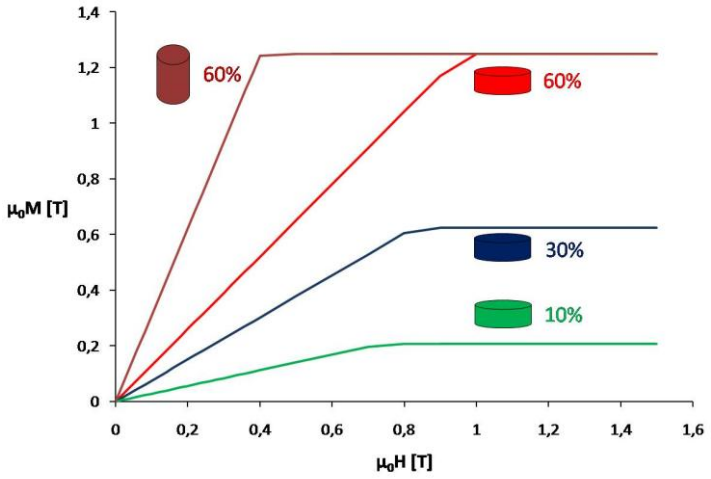

Fig. IV.7. model of the magnetization of a Iron composite

Fig.IV.7. summarizes the behavior of a ferromagnetic composite for different filling factor and composite shape.

II.2.1.2.2. Composite demagnetizing factor and composite susceptibility

The effective composite demagnetizing factor can be generalized in a way as for a pure ferromagnetic material. The difference arises from the localization of the magnetization in the material. Only particles are magnetized.

$$M_{composite} = \phi M_{particle} \qquad \text{eq.IV.26}$$

$$M_{composite} = \phi \chi_p H_{\text{int}} \qquad \text{eq.IV.27}$$

The internal magnetic field here is the applied field and the effective demagnetizing field in the composite:

$$M_{composite} = \phi \chi_p (H_{ext} - N_{eff} M_{composite}) \qquad \text{eq.IV.28}$$

$$M_{composite} = \frac{\phi \chi_p}{1 + \phi \chi_p N_{eff}} H_{ext} \qquad \text{eq.IV.29}$$

$$M_{composite} = \frac{1}{\frac{1}{\phi \chi_p} + n_{sample} + n_{particle}\left(\frac{1}{\phi} - 1\right)} H_{ext} \qquad \text{eq.IV.30}$$

The above equation (eq. IV.28) relates the magnetization to the external field. It can be rewritten as it was done for the pure ferromagnetic material (eq. IV.6) with a composite susceptibility:

$$\chi_{eff} = \frac{1}{\frac{1}{\chi_c} + n_{sample}} \qquad \text{eq.IV.31}$$

Where χ_c is the susceptibility of the composite. Identifying those expressions, eq.IV.30 and eq.IV.31, the effective susceptibility is:

$$\frac{1}{\chi_c} = \frac{1}{\phi \chi_p} + n_{particle}\left(\frac{1}{\phi} - 1\right) \qquad \text{eq.IV.32}$$

$$\chi_c = \frac{\phi\chi_p}{1+\phi\chi_p n_{particle}\left(\frac{1}{\phi}-1\right)} \qquad \text{eq.IV.33}$$

We can notice that this formula, in the special case, $n_{particle}$ = 1/3 for a spherical-shape particle, yields to the Maxwell-Garnett formula.

$$\chi_c = \frac{3\phi\chi_p}{3+\chi_p(1-\phi)} \qquad \text{eq.IV.34}$$

This relation gives the following expression of the susceptibility of such composite for low filling factor, considering this medium as randomly-filled by spherical particles. This has proved the validity of the Kneller model at low concentration of particles, in the range of validity of the Maxwell-Garnett expression.

The effective demagnetizing factor for a composite is the summation of the geometrical demagnetizing factor, n_{sample}, and a term including the effective composite susceptibility. Many expressions of composite susceptibility are available for any filling factor, any orientation of non-spherical inclusions [Jyl] or for larger inter-particles interaction [Yin].

II.2.1.3. Experimental

The aim of such measurements is the characterization of both the saturation and the slope of the magnetization of the isotropic composites. Previously, it was shown that this magnetization slope was shape dependent in the case of ferromagnetic materials. Non-deformable composites were therefore used for the following experiments. These composites were prepared by mixing iron particles with a bi-compound Araldite provided from Bostik Findley. The particles and matrix were mixed together. The mixture was then degassed in a vacuum chamber at 1 mbar for 5 minutes to remove bubbles, molded into different shapes and finally kept at room temperature for 1 day to

harden the composite. The shapes of those samples were cylinder, ellipsoidal or spherical, Fig IV.9. Demagnetizing factor's dependence on the filling factor was also investigated.

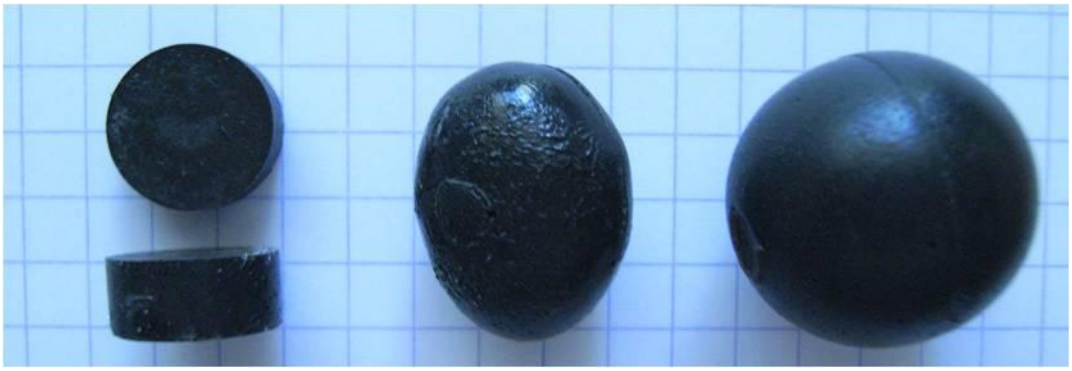

Fig. IV.9. Sample shape : cylinder, ellipsoid and sphere

The magnetization curve is presented on Fig.IV.10 for different filling factors. As expected, the ferromagnetic composite magnetization curves are like pure ferromagnetic ones, linear until they reach saturation. That saturation is limited by the amount of ferromagnetic particles in the composite.

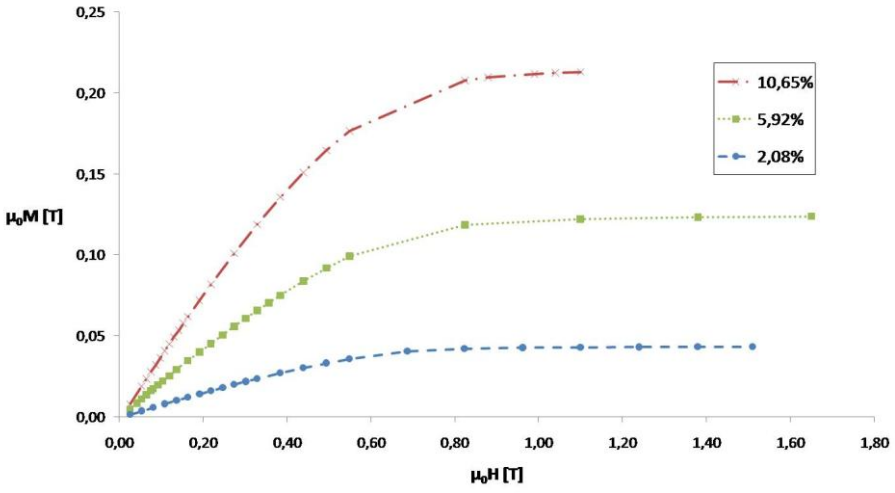

Fig. IV.10. Magnetization versus the applied magnetic field for cylinder-shaped composite, c/a= 0.3, for different concentrations

Magnetic saturation of randomly-filled composite is plotted as a function of the filling factor. This saturation is linearly dependent on the filling factor (Fig.IV.11*)* as expected from eq.IV.19:

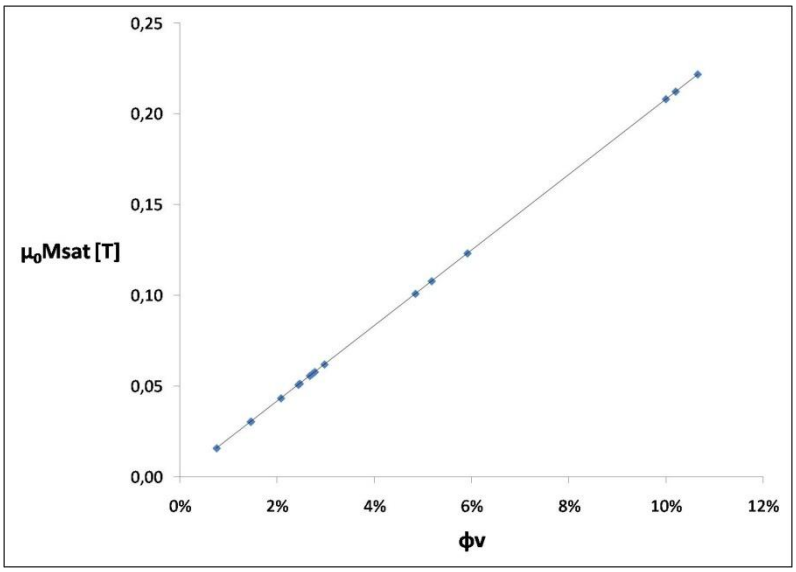

Fig. IV.11. Magnetic saturation of randomly-filled composite versus the filling factor

The experimental filling factor is thus extracted from the magnetization curve when the saturation is reached. In the table fig.IV.12 the different tested sample with their respective shape, with aspect ratio and the corresponding geometrical demagnetizing factor are presented. The measured saturated magnetization and filling factor are then provided and finally the effective demagnetizing factor of the composite is shown with both theoretical and experimental values.

shape	G	N_{shape}	Msat[T]	ϕ_v	N_{Theory}	$N_{experimental}$
cylinder	0,37	0,55	0,0567	2,73%	12,42	9,90
cylinder	0,68	0,39	0,0557	2,68%	12,51	10,21
cylinder	0,87	0,34	0,0513	2,47%	13,51	10,57
cylinder	0,37	0,55	0,0507	2,44%	13,87	11,01
cylinder	0,37	0,55	0,0433	2,08%	16,21	13,10
cylinder	0,37	0,55	0,0158	0,76%	44,01	32,38
cylinder	0,37	0,55	0,1230	5,92%	5,85	4,40
cylinder	0,34	0,56	0,2215	10,65%	3,36	2,82
cylinder	0,46	0,49	0,2121	10,20%	3,43	2,48
cylinder	0,60	0,42	0,2079	10,00%	3,43	2,48
Sphere	1,00	0,33	0,1008	4,85%	6,87	5,49
Sphere	1,00	0,33	0,1077	5,18%	6,43	5,31
Sphere	1,00	0,33	0,0619	2,98%	11,19	9,45
Sphere	1,00	0,33	0,0303	1,46%	22,82	19,25
Ellipsoid	1,34	0,26	0,0578	2,78%	11,92	9,99
Ellipsoid	1,34	0,26	0,0305	1,47%	22,65	19,18
Ellipsoid	1,34	0,26	0,4112	19,77%	2,61	1,41

Fig.IV.12. Effective Demagnetizing factor of randomly-filled composites

As expected, for low filling factor, the effective demagnetizing factor is larger than 1; the maximum value measured was 32 (44 expected) for a sample with a filling factor of nearly 0.8 % and a geometrical demagnetizing factor n_{sample} = 0.55.

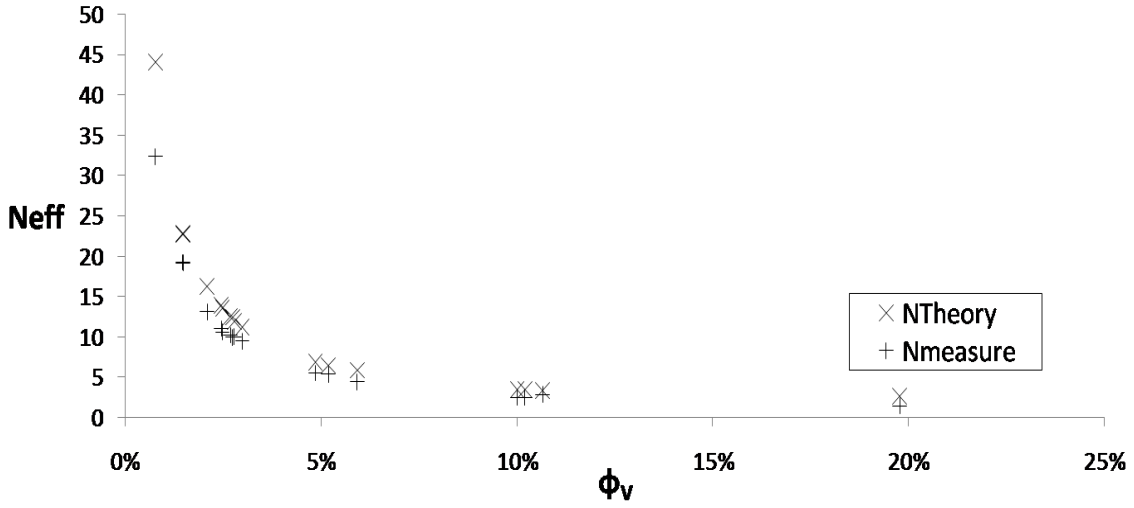

Fig. IV.13. demagnetizing coefficient of a composite versus the filling factor

Theoretical and experimental values follow the same curve, but experimental values are lower than theoretical values for cylinders similar to ellipsoids or spheres. The effective demagnetizing factors of randomly-filled cylinders and ellipsoids are plotted on fig.IV.14 and fig.IV.15 respectively:

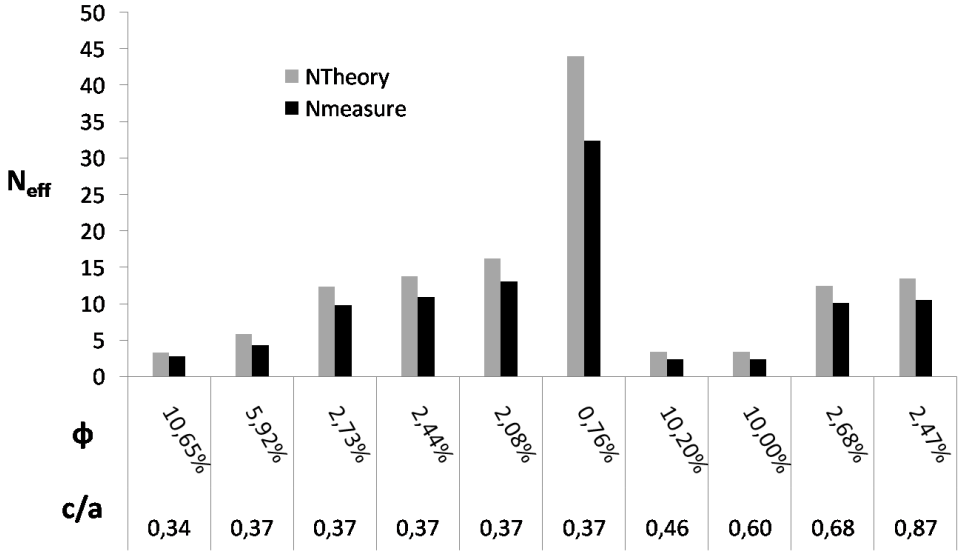

Fig.IV.14. Effective demagnetizing factor of cylinder randomly-filled composites

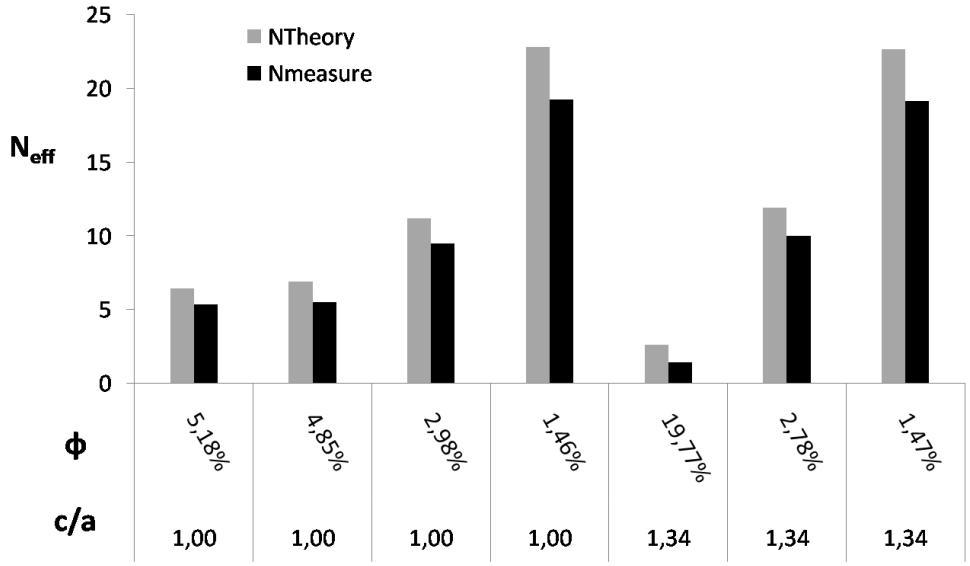

Fig.IV.15. Effective demagnetizing factor of ellipsoid randomly-filled composites

Fig.IV.14 and Fig.IV.15 show that the gap between theoretical and experimental values is not linked to the sample shape. The experimental value is always lower than the expected value. Experimental data are corrected as follow. The particles may have gathered into clusters. The composite can be seen as a dispersion of such clusters (Fig.IV.16). Moreover, a cluster is a local dispersion of particles. Because of this agglomeration of particles, the effective demagnetizing factor will be modified.

If the clusters are well-dispersed in the matrix, we can use the Kneller model (eq.IV.23) with a volume fraction of clusters, ϕ_c, inside the matrix:

$$N_{eff}^{*} = \left(n_{sample} + N_{eff\_cluster}\left(\frac{1}{\phi_c} - 1\right)\right) \qquad \text{eq.IV.35}$$

$N_{eff\_cluster}$ is the effective cluster demagnetizing factor which is calculated as the effective demagnetizing factor of particles.

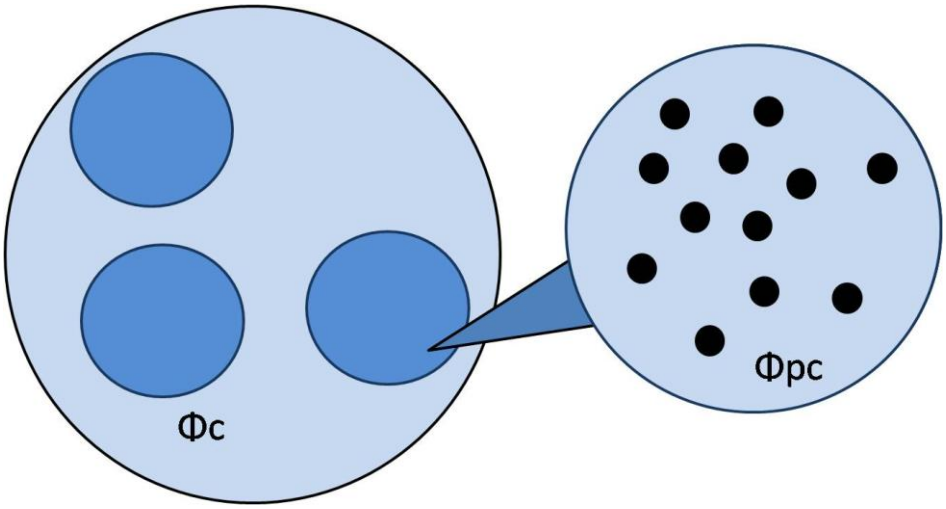

Fig.IV.16. model of the composite with clusters of particles

We once more applied the Kneller model to have the expression of the demagnetizing factor of the cluster, assuming that particles are also well-dispersed inside a cluster, with a fraction of particles per cluster of ϕ_{pc} and having its own demagnetizing factor $n_{cluster\_shape}$:

$$N_{eff\_cluster} = \left(n_{cluster\_shape} + n_p \left(\frac{1}{\phi_{pc}} - 1 \right) \right) \qquad \text{eq.IV.36}$$

The fraction of clusters in the composite and the fraction of particles per cluster are linked by:

$$\phi = \phi_c \phi_{pc} \qquad \text{eq.IV.37}$$

In the case of filled clusters, ϕ_{pc} =1, the eq.IV.36 is reduced as $N_{eff\_cluster} = n_{cluster\_shape}$, the eq.IV.35 is alike the eq.IV.23 ($\phi_c = \phi$); clusters have the role of filler of the matrix. The case of the composite filled by cluster cannot be treated with this formula. Having ϕc =1 means the cluster occupies the whole volume of the sample, so that, the demagnetizing factor of the cluster, $n_{cluster\_shape}$, must be the equal to the sample one. However, such composite can be treated by using directly the eq.IV.23 and switching ϕ_c by ϕ and $n_{cluster\_shape}$ by n_{sample}.

If the clusters are spherical, $n_{cluster\_shape}$ = 1/3, the expression of the effective demagnetizing factor N_{eff}^{*} of a composite with local cluster of particles is:

$$N_{eff}^{*} = \left(n_{sample} + \frac{1}{3}\left(\frac{1}{\phi} - \frac{1}{\phi_{pc}} \right) \right)$$ eq.IV.38

Comparison of the expression N_{eff}^{*} and the theoretical Kneller model demagnetizing factor N_{eff} yields to:

$$N_{eff}^{*} - N_{eff} = \frac{1}{3}\left(1 - \frac{1}{\phi_{pc}} \right) \leq 0$$ eq.IV.39

As shown with the eq.IV.39, a composite with spherical cluster of particles, presents a smaller effective demagnetizing factor N_{eff}^{*} than the well-dispersed given by the Kneller model N_{eff}. This difference means that experimental samples are not randomly filled. Clusters are present in the tested composite.

II.2.2. Field structured composite

In the expression of the effective demagnetizing factor, Kneller assumed that particles were affected by a vicinity field, which was set as the field created by the surrounding cavity in a homogenized medium. It has been proved that this model can be seen as the summation of the sample demagnetizing factor and the invert composite susceptibility (eq.IV.31). The above expression of the Kneller (eq.IV.23) provides The Maxwell-Garnett susceptibility (eq.IV.34). We are now interested in the case of a structured composite. Invert calculation, based on the susceptibility of such material, will provide an expression of the effective demagnetizing factor of the structured composite. Martin & al. give the following expression of the anisotropic susceptibility [Mar2] for spherical particles structured composites:

$$\chi_w = \frac{3\phi\chi_p}{3 + \chi_p(1 - \phi + \delta_w\psi_z)}$$ eq.IV.40

Where χ_w is the susceptibility of the anisotropic composite along the axis w of measurement and χ_p is the ferromagnetic particle susceptibility. ψ_z is a parameter depending on the structure (chain-like, sheet-like or random). In the case of a random distribution, this parameter is null, leading to the Maxwell-Garnett expression. Fig.IV.17a presents the different values, numerically evaluated for this parameter, in the case of column-like structure of the particles, for different filling factor. δ_w is an

anisotropic constant linking the direction of measurement and the direction of the particle structure in the way that δ_w=-2 if the two directions are the same and δ_w=1 otherwise. This susceptibility depends therefore on the axis of measurement of the magnetization.

ϕ	ψ_z (chain)
0%	-0.301
5%	-0.263
10%	-0.246
15%	-0.232
20%	-0.211
25%	-0.187
30%	-0.162
40%	-0.115
50%	-0.07

Fig. IV.17a. Table of calculated values of ψ_z [Mar2]

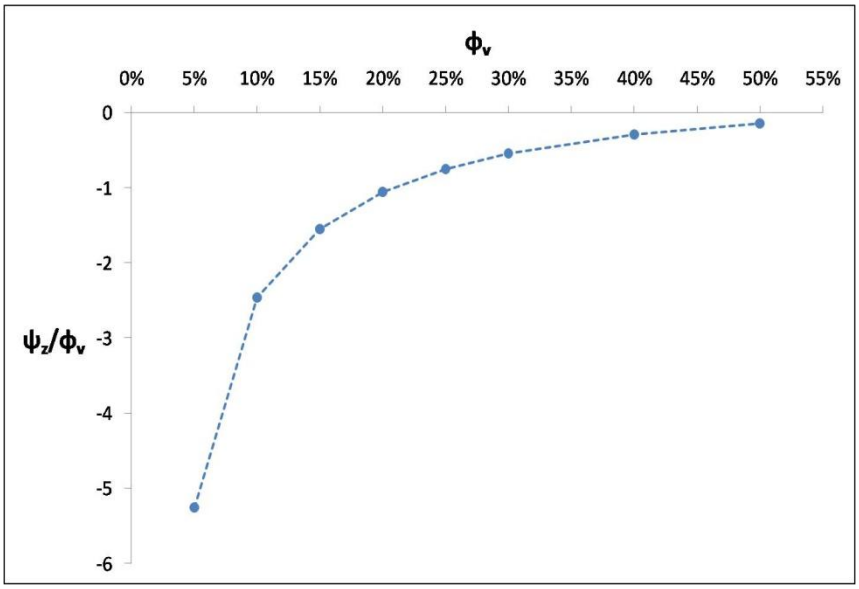

Fig. IV.17b. Filling factor behaviour of ψ_z/ϕ.

Since the ferromagnetic particles' susceptibility in eq.IV.40 is larger than 1, this equation, hence injected in eq.IV.31 provides the effective demagnetizing factor for the anisotropic composite:

$$N_{eff} = n_{sample} + \frac{1}{3}\left(\frac{1-\delta_w\psi_z}{\phi} - 1\right) \qquad \text{eq.IV.41}$$

This expression is roughly the same as in the case of the MRE. In this case with a random structure, the parameter ψ_z is null, leading to the expression of MRE factor. The effective factor is the summation of the geometrical factor and the composite term as for the MRE, but an anisotropic term is added here. Assuming that the direction of the particle is chain-like and the measurement direction are the same, δ_w=-2, this expression could be written to ease the comparison of the structured and randomly-filled composite demagnetizing factor:

$$N_{eff\_struct} = N_{eff\_random} + n_{particle}\frac{2\psi_z}{\phi} \qquad \text{eq.IV.42}$$

Eq.IV.42 shows that the effective demagnetizing factor of a structured-composite can be split in two components. The first term is the factor of the randomly-filled composite whereas the second term provides the behavior of the composite's inner structure which behaves as shown in Fig.IV.17b. Two samples were made to check this shift of the effective demagnetizing factor when the composite is structured. The shift is large for low filling factor. For these samples, the filling factor was then chosen at 3% to enhance this effect. One has hardened without a magnetic field, yielding to a randomly filled composite, whereas the second one has hardened with an external induction.

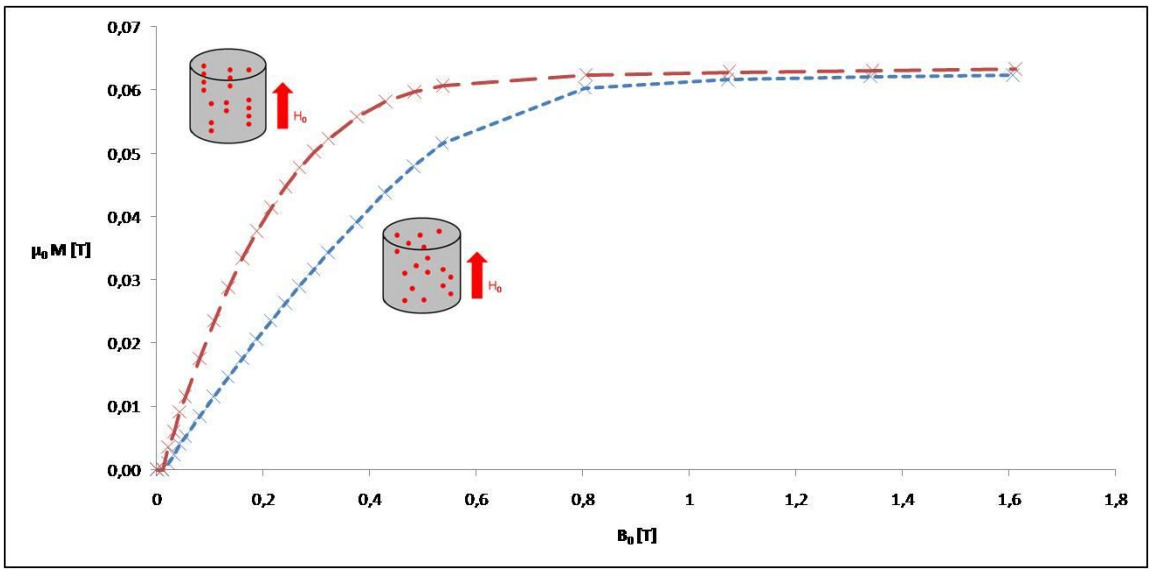

Fig.IV.18. Magnetization curve of a randomly-filled (dot-line) and a chain-like structured (strait-line) composite

Magnetization curve of a chain-like distribution of the particles is presented above in fig.IV.18. The magnetization is measured in the applied field so that the directional parameter δ_w=-2 and the filling factor is low enough to enhance the structure parameter ψ_z. Such composites are easier to magnetize than randomly-filled composite; a lower magnetic field will saturate it but the same state of magnetic saturation is reached. As seen in Fig.IV.11 and in the Fig.IV.18, the effective magnetization in the saturated state is proportional to the total amount of magnetic material in the composite volume, no matter how the distribution of the particles is.

III. Conclusion

In this chapter, the magnetization of a non-magnetic matrix filled by ferromagnetic particles has been studied through the knowledge of two important parameters: the saturation at high magnetic field and the magnetization slope at low magnetic field. The saturated magnetization of the composite is simply the saturated magnetization of the ferromagnetic particle times the filling factor. It does not depend on the distribution of the ferromagnetic particles. The magnetization of the composite at low applied magnetic field is ruled by the demagnetizing field. Composite being made of non-magnetic materials, the effective demagnetizing factor can be larger than 1 (which is the larger value in a case of a pure ferromagnetic material). This effective demagnetizing field of a composite includes a term, n_{sample}, which is a function of the aspect ratio of the sample. The second term is determined by the filling factor and the distribution of the particles inside the composite. This second term can be evaluated by the measurement of the composite susceptibility.

References:

[Chi1]: Physics of Magnetisms, Chikazumi, John Wiley and Sons (1984)

[Jos1]: Demagnetizing field in nonellipsoidal bodies, R. I. Joseph, E. Schlomann, *Journal Applied Physics* 36 (1965)1579

[Jos2]: Ballistic demagnetizing factor in uniformly magnetized cylinders, R. I. Joseph, *Journal of Applied Physics* 37 (1966) 4639

[Zhe]: Guobao Zheng, M. Pardavi-Horvath, Xiaohua Huang, B. Keszei, J. Vandlik, *Journal Applied Physics* 79 (1996) 5742

[Lu]: On the computation of local-demagnetization tensor for nonellipsoidal ferrites, Mai Lu, Zheng Yang, Fu-Lin Wei, *International Journal of Infrared and millimeters waves* 19 (1998) 1027

[Sat]: Simple and approximate expressions of demagnetizing factors of uniformly magnetized rectangular rod and cylinder, M. Sato, Y. Ishii, *Journal of Applied Physics* 66 (1989) 983

[Kne]: Ferromagnetismus, Kneller, Springer, Berlin (1962)

[Jyl]: Equation for the effective permittivity of particle-filled composites for material design applications, L. Jylhä, A. Sihvola, *Journal of Physics D: Applied Physics* 40 (2007) 4966

[Yin]: Magnetic properties of randomly dispersed magnetic properties particulate composites: A theoretical study, H. M. Yin and L. Z. Sun, *Physical Review B* 72 (2005) 054409

[Mar2]: Anisotropic magnetism in field-structured composites, J. E. Martin, E. Venturi, J. Odinek, R. A. Anderson, *Physical Review E* 61(2000) 2818

Chapter 5

Shape effect on the magnetostriction

I. Introduction

In this chapter, we present another way to model the magnetostriction, based on energetic calculations. The magnetostriction is a phenomenon which is the combination of two factors, the magnetic stress and the mechanical strain. The stress is caused by the apparition of forces within the magnetic material, submitted to a magnetic field. In the following section, we will focus on the magnetic stress induced in a uniform magnetic field. Forces are self-generated by the material unlike to those generated by an external gradient of field, called magnetophoretic force [Zri2]. In the previous Chapter (3), calculation of dipolar forces on the particles has led to several conclusions:

- The force is due to interactions between ferromagnetic particles dispersed within the matrix; thus, applied uniform magnetic field has no effect in the force calculation.
- The macroscopic force is shape dependent. The flatter the disk, the larger the force.
- The force results from the pair interactions between particles with magnetic moment m. It is then dependent on the square of m.

Effective magnetic stress will be presented but also the effective elastic response of the composite. Magnetic and mechanical properties depend on the filling factor. The filling factor of a randomly filled composite will also be discussed for its effect on the magnetostriction behavior.

II. Experimental

II.1. Composite characterization

To test the shape effect, cylindrical samples with different aspect ratios defined by length divided by the diameter were prepared. Aspect ratio ranged from 0.33 to 1.46. These samples have a filling factor set as 30% vol. to allow a large deformation. A sphere (with diameter 196 mm and the filling factor 28% vol.) was also prepared to test another shape.

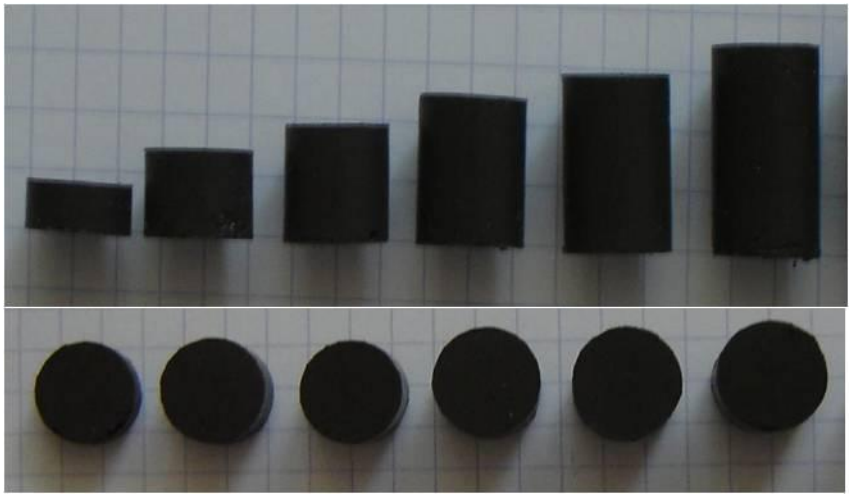

Fig. V.1. Cylinder-shaped samples with different aspect ratio

Another set of samples were prepared in order to have the filling factor effect. Magnetostriction measurements as well as Young modulus were recorded for samples with different filling factors. These samples had an aspect ratio set at 0.62. The experimental filling factor ranged from 5 % to 35 % (vol.).

II.2. Results

Magnetostriction versus the applied magnetic field of samples with different aspect ratio is presented in Fig.V.2. The dilatation of the composite increased with the increment in applied magnetic field. Then, magnetization of those composite is saturated, resulting in a saturated state of magnetostriction. Hysteresis is thought to be the consequence of decohesion between the particles and the silicone matrix.

Dependence on the aspect ratio effect of the saturated state of magnetostriction of 30% vol. filled composites is plotted in Fig.V.3. The largest strain appears for the smallest aspect ratio. The strain at saturation for the smallest aspect ratio (0.33) is 2.6 times larger than for the largest (1.46). Thus, we can reach a strain of 9.2% for an aspect ratio of 0.33. The difference is the same for the demagnetizing factor of the cylinder. For a ratio of 0.33, the demagnetizing factor is 2.5 times larger than for the demagnetizing factor of the 1.46 ratio sample. This curve is presented in Fig.V.8b, showing the linear relationship between strain and samples demagnetizing factor.

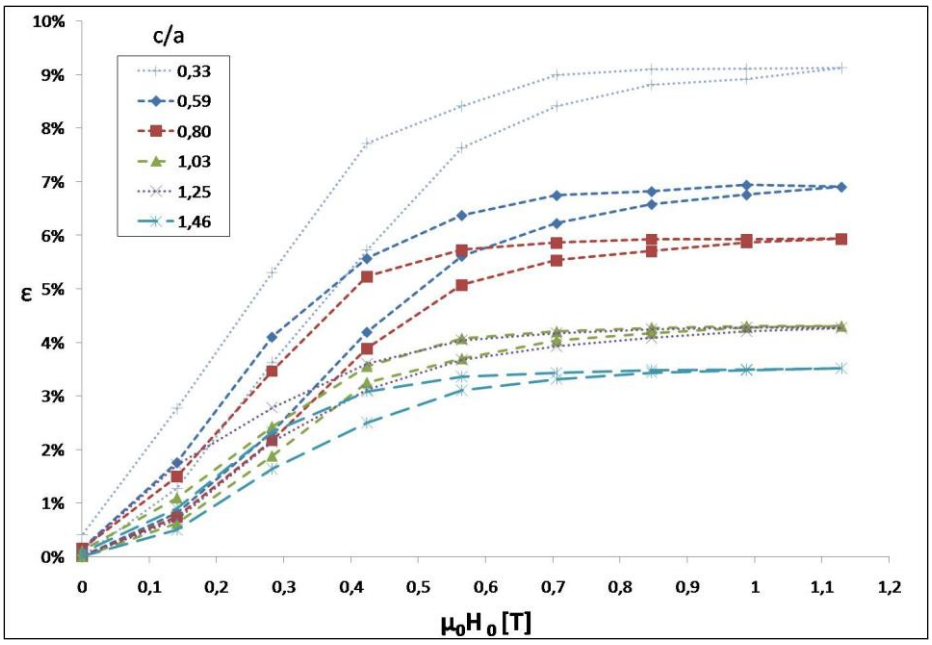

Fig.V.2: magnetostriction versus the applied magnetic field for different aspect ratios

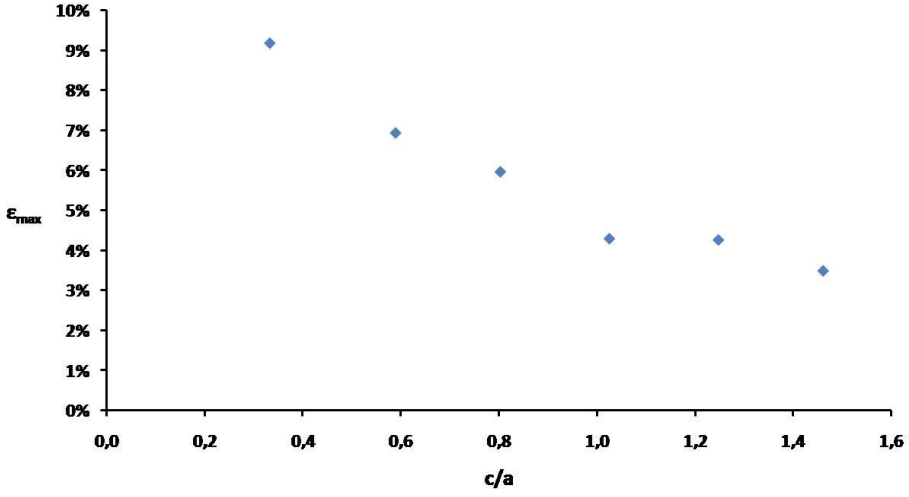

Fig.V.3: Saturation magnetostriction versus the aspect ratio

III. Model

III.1. Magnetic energy

Calculation of magnetic force on the composite is made by the knowledge of the interacting particles energy in the composite. It has been shown that dipolar interaction between particles explains the positive magnetostriction of a randomly filled composite [Dig].

The energy E of interaction of a magnetic particle, with a magnetic moment *m*, in a magnetic induction *B* is given by:

$$E = -\vec{m} \cdot \vec{B} \qquad \text{eq.V.1}$$

In the third Chapter, inter-particles forces were calculated using this interaction energy and was further derived into a force expression. Calculation was made from the point of view of a particle. Now we will expand the calculation on the whole set of magnetic particles and consider this set as an equivalent magnetic body with effective parameter. Thus, the energy E_D of interaction of a set of n magnetic particles is:

$$E_D = -\frac{1}{2}\sum_{i=1}^{n}\sum_{j=1, j\neq i}^{n}\vec{m}_i \cdot \vec{B}_{ij} \qquad \text{eq.V.2}$$

where B_{ij} is the magnetic induction on the moment m_i created by all the other moments m_j (See eq.III.1). This dipolar energy is the work for gathering isolated magnetic moments into the volume. The ½ factor is added to avoid the double summation of reciprocal terms. In this energy, a shape-dependent term can be extracted; the demagnetizing energy.

In the case of the MRE composite, which is described as a set of magnetic moment randomly dispersed in the volume, we can write demagnetizing energy seen in Chapter 4 as:

$$E_d = \frac{1}{2}\mu_0 N_{eff} M^2_{composite} V_{composite} \qquad \text{eq.V.3}$$

This energy is then converted into mechanical energy through the strain. Change of size therefore leads to a reduction of the demagnetizing energy of the composite [Lan2]:

$$\Delta E_d = \frac{1}{2}\mu_0 M^2_{composite} \Delta N_{eff} V_{composite} \qquad \text{eq.V.4}$$

But, looking carefully on the expression of the composite demagnetizing factor,

$$N_{eff} = n_{sample} + n_{particle}\left(1 - \frac{1}{\phi}\right) \qquad \text{eq.V.5}$$

only the demagnetizing factor of the sample is shape-dependent shape. Moreover, the fact that the particles are magnetically soft and spherical induces no changes in their own demagnetizing energies (on the contrary, a flake particle would rotate during the strain due to the conservation of the volume of the elastomer and then its demagnetizing field would change).

Thus, in our case, only the demagnetizing factor of the sample plays a role. When magnetized, the composite has energy linked to its shape, which is available for the strain. As the sample is flat and the energy is large, the only possibility to reduce that energy is to increase the aspect ratio. That means as the sample elongates and the strain is positive as seen in Fig.V.4 below:

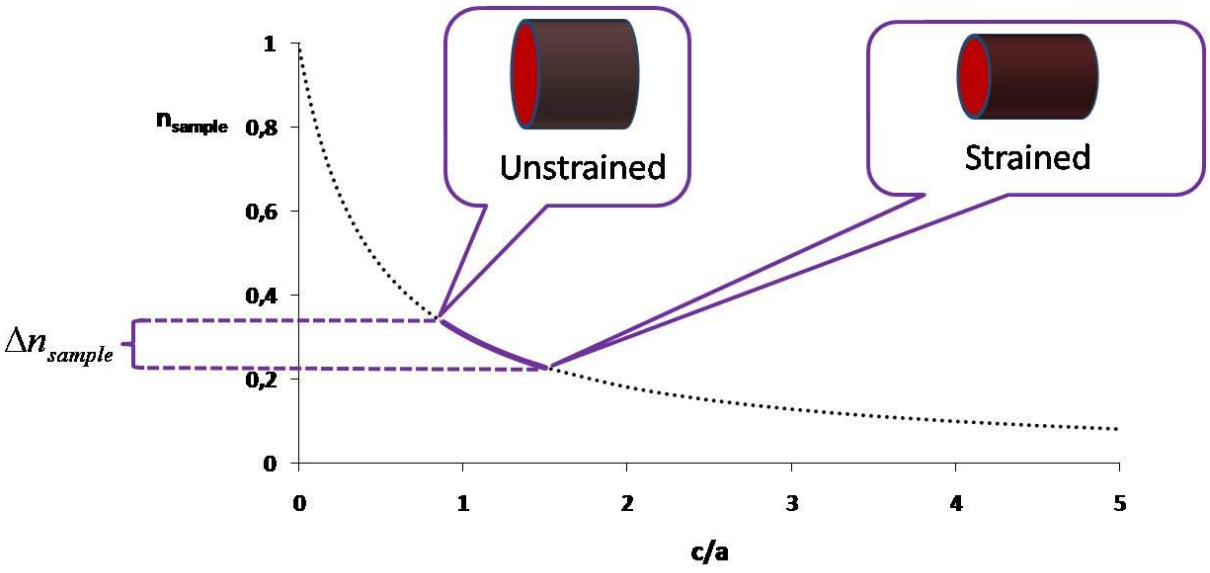

Fig.V.4: Demagnetizing factor decreasing as the sample elongates

Now that the qualitative description is made, we can provide a quantitative evaluation of the strain. This change of demagnetizing energy dE_d can be evaluated as a function of the strain by the variation of the sample demagnetizing factor dn_{sample}.

$$dN_{eff} = dn_{sample} \qquad \text{eq.V.6}$$

Considering a cylinder with length *c* and diameter *a,* with all the surface of that cylinder free to move; submitted to the magnetic field, the reduction of the demagnetizing energy results in a change of length *dc* and also a change of diameter *da* as seen in Fig.V.5; the sample experiences a strain:

$$dn_{sample} = \frac{dn_{sample}}{d\left(\frac{c}{a}\right)} d\left(\frac{c}{a}\right) = n'_{sample} d\left(\frac{c}{a}\right) \qquad \text{eq.V.7}$$

The derivative form of the demagnetizing factor with respect to the aspect ratio is introduced. During the transformation, the differential of the aspect ratio is calculated using the elongation defined by ε and the Poisson ratio ν, as:

$$d\left(\frac{c}{a}\right) = \frac{c}{a}\left(\frac{dc}{c} - \frac{da}{a}\right) = \frac{c}{a}\varepsilon(1+\upsilon) \qquad \text{eq.V.8}$$

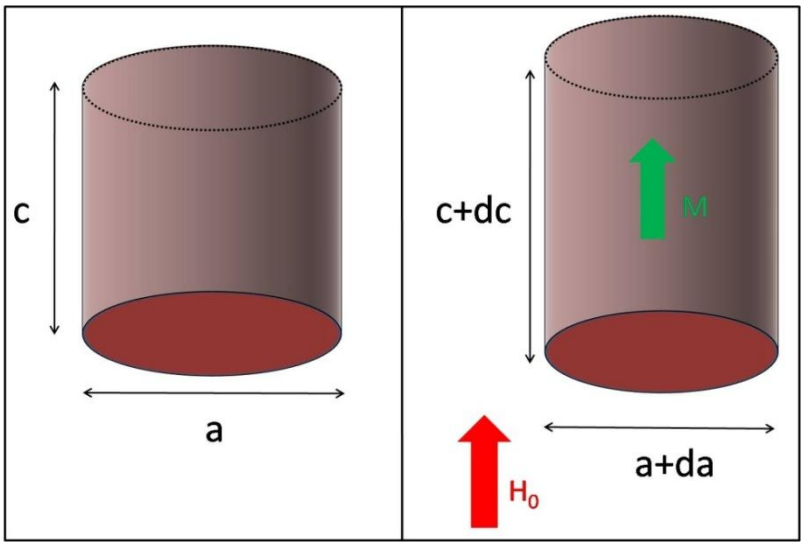

Fig.V.5: Dimensions changes of the cylinder

During the transformation, the change of the demagnetizing factor of the composite is set as:

$$dN_{eff} = n'_{sample} \frac{c}{a} \varepsilon(1+\upsilon) \qquad \text{eq.V.9}$$

III.2. Elastic response of the composite

Elastomers are known to exhibit visco-elastic behavior under external solicitation. The response can be written as the response is the sum of viscous and elastic force. The Voigt model, consisting of a spring and a damper in parallel, has been widely used as a first approximation to evaluate the damping or stiffness of viscoelastic materials.

Viscoelastic stress can be split into 2 components: σ_{elas} and σ_{visc} which are the elastic and the viscous stresses respectively.

$$\vec{\sigma}_{visc} = -\eta\dot{\vec{\varepsilon}} \qquad \text{eq.V.10}$$

where the viscous stress is time-dependent, and η is a viscous constant. This viscous stress accounts for the relaxation behavior of the magnetostriction of the composite when the magnetic field is switched off [bed]. In our case, we are interested in the magnetostriction at the saturate state, where the composite reaches a steady state ($\dot{\vec{\varepsilon}} = 0$). The remaining visco-elastic term is the elastic force which is written as:

$$\vec{\sigma}_{elas} = E\vec{\varepsilon} \qquad \text{eq.V.11}$$

The general form of the elastic energy is defined as:

$$E_{elas} = \frac{1}{2}\varepsilon_{ij}\sigma_{ij}V_{composite} \qquad \text{eq.V.12}$$

Considering a change of shape at constant volume, this elastic energy can be written as [Lan]:

$$E_{elas} = \frac{1}{2}E_{composite}\varepsilon^2 V_{composite} \qquad \text{eq.V.13}$$

with $E_{composite}$ is the effective Young modulus of the composite.

III.3. Strain of the magnetized composite

The total change energy involved in the transformation is then written as the sum of the change of demagnetizing energy and the elastic energy:

$$E_{tot}(\varepsilon) = \frac{1}{2}\mu_0 M^2_{composite}\Delta n_{sample} V_{composite} + \frac{1}{2} E_{composite}\varepsilon^2 V_{composite} \qquad \text{eq.V.14}$$

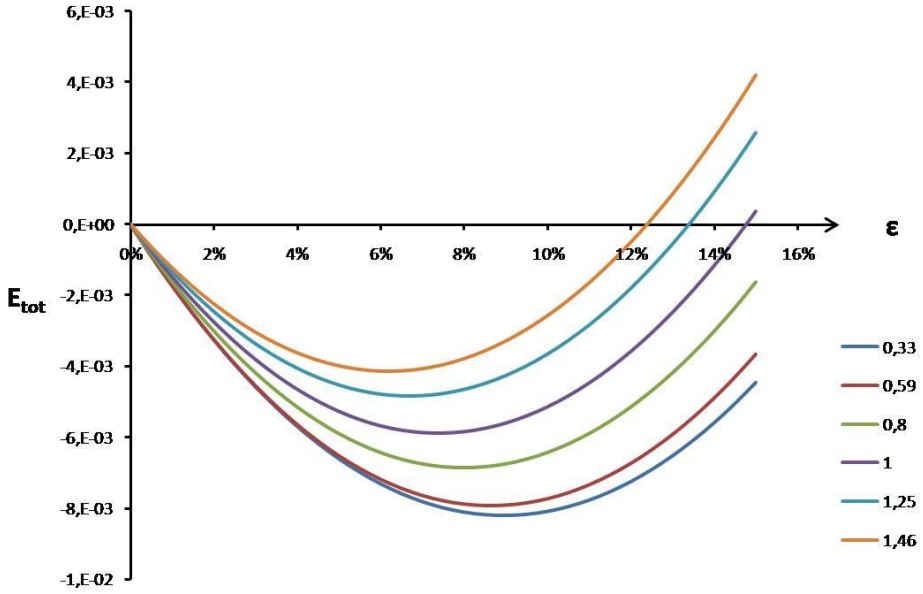

Fig.V.6 Variation of the total energy versus the strain for different aspect ratio

The whole energy plotted as a function of elongation is presented in Fig.V.6. This curve shows the conversion of the demagnetizing energy into elastic energy. For small strain, the energy decreases, which means the demagnetizing energy is dominant. Then the total energy reaches a minimum and increases for larger strain. From this minimum, the elastic energy is the dominant component of the total energy. The effective elongation ε is calculated via minimizing this energy with respect to the elongation:

$$\frac{dE_{tot}(\varepsilon)}{d\varepsilon} = 0 \qquad \text{eq.V.15}$$

which is rewritten as:

$$\frac{1}{2}\mu_0 M_{composite}^2 V_{composite}\frac{dn_{sample}}{d\varepsilon}+\frac{1}{2}V_{composite}E_{composite}\frac{d\varepsilon^2}{d\varepsilon}=0 \qquad \text{eq.V.16}$$

$$\frac{1}{2}\mu_0 M_{composite}^2 n'_{sample}\frac{c}{a}(1+\upsilon)+E_{composite}\varepsilon=0 \qquad \text{eq.V.17}$$

The final expression of the elongation of the M.R.E. when submitted to an external and homogeneous magnetic field is:

$$\varepsilon=-\frac{\mu_0 M_{composite}^2}{2E_{composite}}\frac{c}{a}n'_{sample}(1+\upsilon) \qquad \text{eq.V.18}$$

Due to the negative values of the derivative of the demagnetizing factor and the minus sign and all the others positive parameters M², Young modulus $E_{composite}$, aspect ratio c/a... the elongation is always positive as seen in Fig.V.7

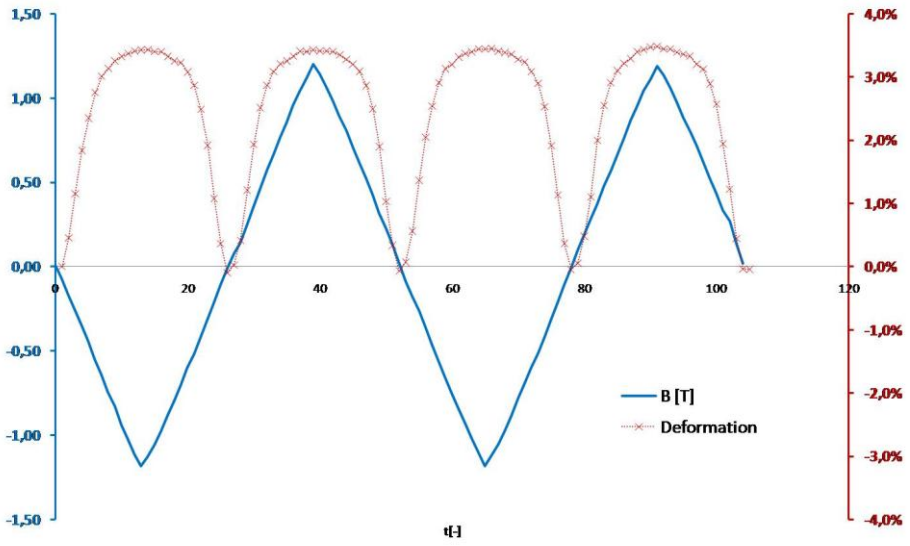

Fig.V.7 Strain and alternative applied field on a time scale

The applied field magnetizes the particles. Interaction of these particles is a pair function of the particle magnetization. Inversing the direction of the field does not change the direction of the strain.

Experimental data and the model are compared in Fig.V.8a as function of the aspect ratio.

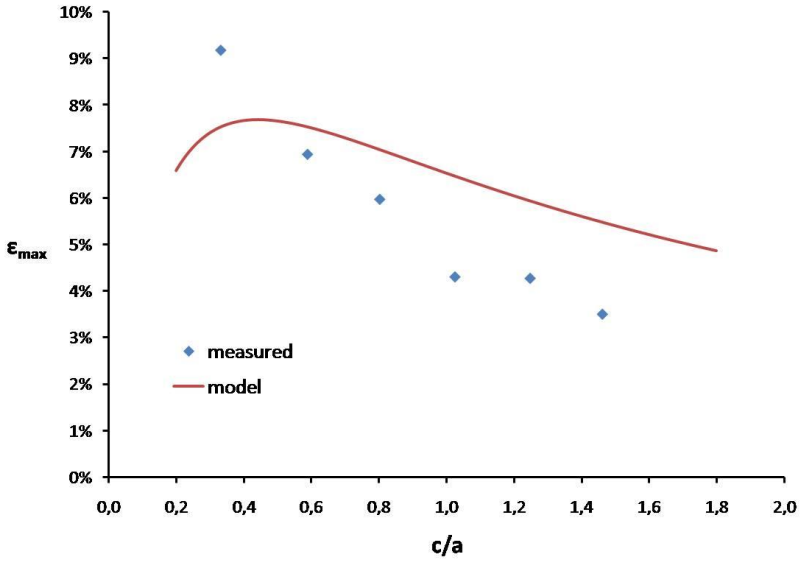

Fig.V.8a Maximal strain as function of the aspect ratio

Calculated strain and experimental data are in similar. However, theoretical values are slightly larger than experimental measurement and exhibit a maximum, which is not the case for experimental data. This might be explained by dissipative mechanisms within the matrix (such as decohesion, damage, etc.) having energy cost which is not taken into account in the model. Measurements were made for 30% vol. particle content, for which such damages are expected. Experimental difficulties prevent us from checking the expected maximum strain.

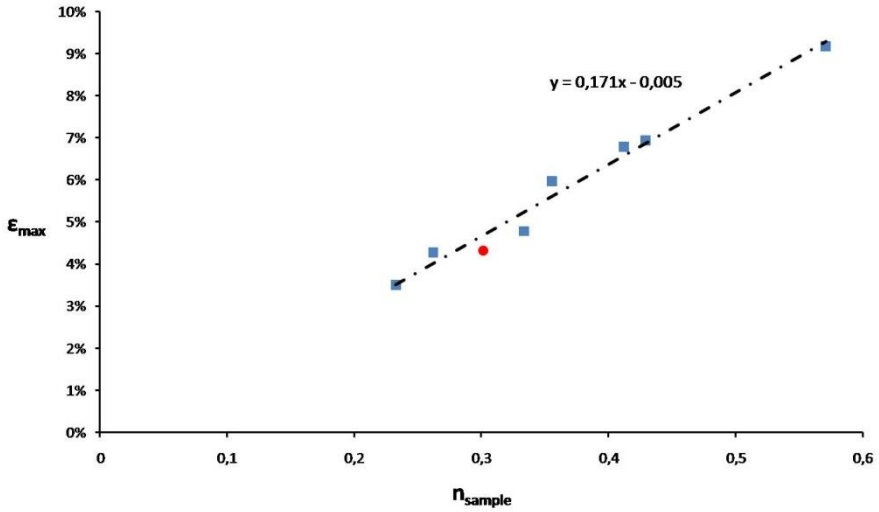

Fig.V.8b: Saturated magnetostriction versus the demagnetizing factor of the sample. Squares represent cylindrical sample and the circle dot corresponds to a spherical sample

III.4. Case of a spherical composite

Experiments were made on cylinders; however, the model presented above was build without any specific shape, so that it has to be valid for another kind of shape. To check this point, a 28 % filled sphere has been made. That M.R.E. sphere is shown unstrained in Fig.V.9a without field and strained in Fig.V.9b, when placed inside a homogenous magnetic field.

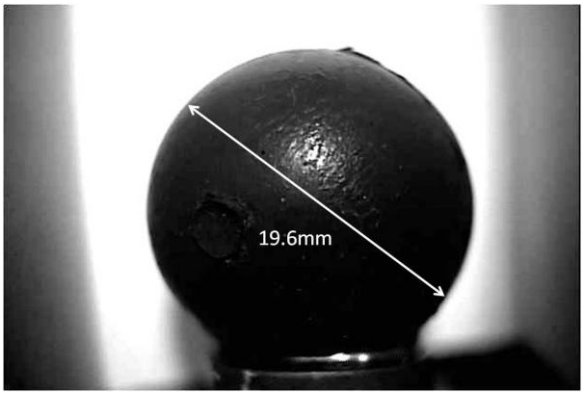

Fig.V.9a Spherical sample(D=19.6mm)without external field (B_0=0T)

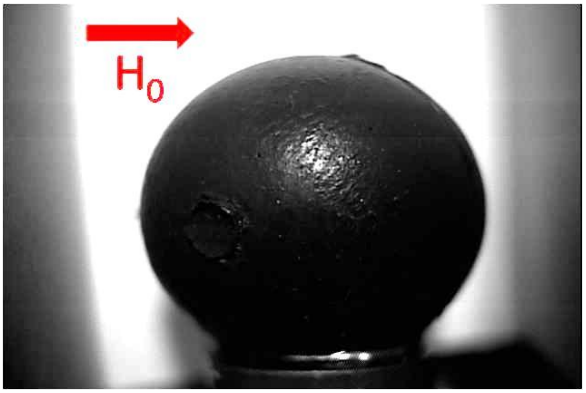

Fig.V.9b Spherical sample with external field (B_0=1.2T)

Applying the maximum magnetic field yields the sphere to its saturate magnetostriction a 4.8%.

The sample demagnetizing factor for a sphere is 1/3, so that when compared with the plot of the strain versus the demagnetizing factor as shown in fig.V.8b, the sphere and the cylindrical samples, are behave in similar ways.

IV. Filling factor effect

The filling factor ϕ is defined as the ratio of the volume of all the particles that fill the matrix over the total volume;

$$\phi = \frac{\sum V_{particle}}{V_{sample}} \qquad \text{eq.V.19}$$

Both elastic constant and magnetization, and so the macroscopic behavior, are function of ϕ.

IV.1. Effect on the magnetic stress

The magnetization of the composite at the saturate state is proportional to this parameter leading to a quadratic dependence of the magnetic stress on this filling factor:

$$M_{composite}^{sat} = \phi M_{particle}^{sat} \qquad \text{eq.V.20}$$

Therefore, the magnetic stress is a quadratic form of the filling factor:

$$\sigma_{mag} \propto \phi^2 \qquad \text{eq.V.21}$$

IV.2. Effect on the elastic constant

The effective Young modulus of the composite depends on the distribution of the particles [Zri1], on the filling factor ϕ and on the Young modulus E_0 of the unfilled composite. For a composite randomly filled by hard particles, various relationships of the Young modulus for such composite have been given versus the particle concentration in the matrix.

- For a dilute composite, the Einstein model, initially developed to express viscosity of dilute suspensions, is a good approximation. It has been used by Zrinyi for a 5% (wt) filled polymer [Zri1]:

$$\frac{E(\phi)}{E_0} = 1 + 2.5\phi \qquad \text{eq.V.22}$$

- For larger filling factor, the Guth & Gold law [Gut1, Gut2], provides the behavior of the modulus of a random and diluted distribution of hard spheres inside an elastomer and is given by:

$$\frac{E(\phi)}{E_0} = 1 + 2.5\phi + 14.1\phi^2 \qquad \text{eq.V.23}$$

- For a filling factor larger than the percolation threshold, the Young's modulus can be expressed using the empirical formula derived from the Maron-Pierce [Mar, Cro, Pab] relation as:

$$\frac{E(\phi)}{E_0} = \left(1 - \frac{\phi}{\phi^*}\right)^{-2} \qquad \text{eq.V.24}$$

where ϕ^* is defined as a maximum packing fraction. When $\phi = \phi^*$, the effective Young's modulus diverges. This maximum packing fraction of isotropic composite can be evaluated from well known values for cubic lattices: 0.52 for "simple cubic" (CS), 0.68 for "body-centered cubic" (BCC), 0.74 for "face-centered cubic" (FCC). Moreover, for a random dispersion of spheres, Jaeger and Nagel (1992) [Jae] have found $\phi^* = 0.64$.

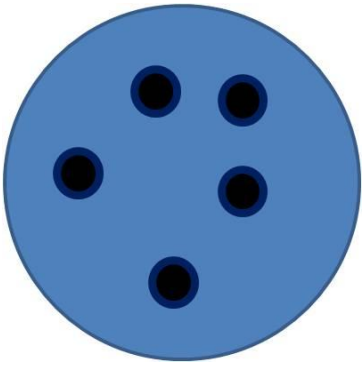

Fig.V.10a Einstein model

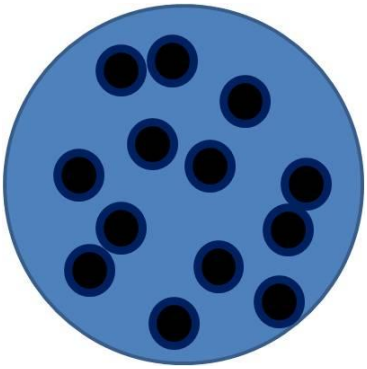

Fig.V.10b Guth & Gold model

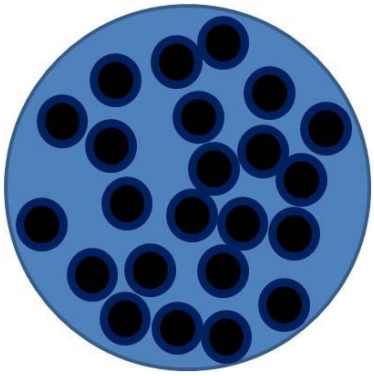

Fig.V.10c Percolation model

Einstein relationship for the relative Young modulus of a suspension of uniform hard sphere is valid only at extremely low value of concentration. At higher concentrations, particle interactions become significant, yielding to the non-linear relation like the Guth & Gold proposed. Larger concentrations induce the formation of aggregates. Bonded polymer does not participate to the whole elasticity, which means that the composite will highly increase its elastic modulus.

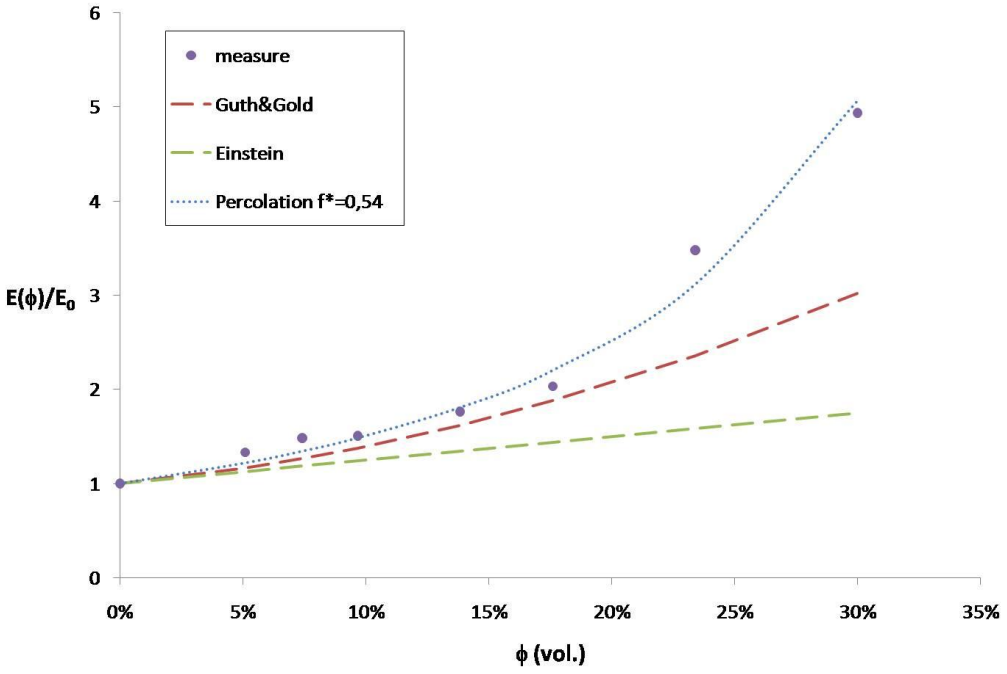

Fig.V.11: Young modulus versus filling factor. E_0=0.14 MPa

Fig.V.11 presents the measured Young modulus of MRE with filling factor ranging from 0 to 35%. On this curve the above mentioned three models of modulus are also plotted. Einstein model and Guth & Gold are not reliable for high filling factor as expected. Measurement data were therefore fitted using an empirical model taking into account the percolation effect; the value of the experimental maximum packing fraction ϕ^* was found as 54%. This fitted curve is also presented on the Fig.V.11. This value of 54% vol. is smaller than the theoretical one (0.64%) maybe because the aggregates are formed during the sample processing

IV.3. Effect on the magnetostriction

Magnetostriction is a competition between the magnetic stress and the ability of the composite to response to that stress. For a large deformation, the ideal would be a large magnetic stress and a low Young modulus. Increasing the magnetic stress without any other source of gradient field would need an increment of the magnetic particle, i.e. an enhancement in the filling factor. Indeed, the magnetization is a quadratic function of that filling factor (eq.V.27). At increasing filling factor the magnetization increases but also the material stiffness. The knowledge of the Young modulus dependence on the filling factor is therefore the important key to determine the filling factor influence on the magnetostriction.

Fig.V.12 presents the measured saturate magnetostriction of MRE with filling factor ranging from 0 to 35%. Theoretical curves of the magnetostriction are plotted using the Maron-Pierce and the Guth & Gold equations for the Young modulus. The curve using the Guth & Gold model does not present a maximum value and increases continuously with the filling factor. The curve using the Maron-Pierce equation presents a maximum for 27%. This optimal ϕ_{op} value, where the saturated magnetostriction amplitude is the largest was experimentally found between 25% and 30%.

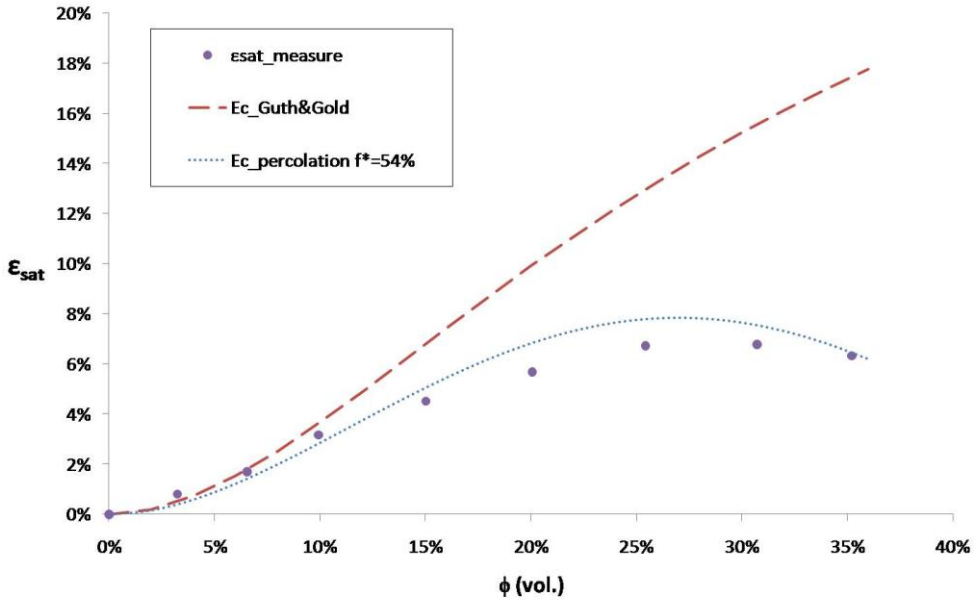

Fig.V.12 Saturated magnetostriction versus filling factor

Between those 3 expressions of the effective Young's modulus, the Maron-Pierce equation, unlike the two other equations, can be used to find an optimal ϕ_{op} value giving the filling factor resulting in a maximum value for the saturated magnetostriction, such as:

$$\frac{d\varepsilon_z}{d\phi} = 0 \Leftrightarrow \phi_{op} = \frac{\phi^*}{2} \qquad \text{eq.V.25}$$

Using the experimental value of ϕ^* of 54%, we have a value for ϕ_{op} of 27%.

V. Conclusion

In this Chapter, we investigated the effect of the sample shape, mainly through the shape factor of cylindrical samples. We compared also our data with data obtained for spherical sample effect; both experimental and theoretical data provided a dependence of the magnetostriction on the sample demagnetizing factor. We have measured a 9.2% saturated strain for a flat sample and 30% filled composite. Dipolar interaction between the particles leads to square dependence of the magnetic stress on the filling factor. However, the elastic response of a composite material depends even more on the filling factor at high concentration (especially close to the percolation threshold). Due to the competition between the increase of magnetic stress and the composite stiffness at increasing the magnetic particles concentration, a maximum strain is obtained for a filling factor of 27%. This is fully consistent with our prediction for which the maximum is reached at half of the maximum packing factor, if we consider that this maximum packing is 54% vol.

References:

[Zri2]: Intelligent polymer gels controlled by magnetic fields, M. Zrinyi, *Colloid Polymer Science* 278 (2000) 98

[Dig]: From dipolar interactions of a random distribution of ferromagnetic particles to magnetostriction, *Journal of Magnetism and Magnetic Materials* 321 (2009) 396–401

[Lan2]: Electrodynamics of Continuous media, L.D. Landau and E. M. Lifshiftz, Pergamon Press, New York (1984), #ISBN-10: 0750626348 #ISBN-13: 978-0750626347

[Zri1]: Deformation of ferrogels induced by nonuniform magnetic field, M. Zrinyi, L. Barsi, A. Büki, *Journal of Chemical Physics* 104 (1996) 8750

[Gut1]: On the hydrodynamics theory of the viscosity of suspension, E. Guth & O. Gold, *Physical Review* 53 (1938) 322

[Gut2]: theory of filler reinforcement, E. Guth, *Journal of Applied Physics* 16 (1945) 20

[Jae]: Physics of Granular States, H.M. Jaeger and S.R. Nagel, *Science* 255 (1992) 1524

[Mar]: Application of ree-eyring generalized flow theory to suspensions of spherical particles, S. H. Maron & P. E. Pierce, *Journal of Colloid Science* 11 (1956) 80

[Cro]: Viscosity-concentration-shear rate relations for suspensions, M.M. Cross, *Rheologica Acta* 14 (1975) 402

[Pab] Fundamental considerations on suspension rheology, W. Pabst, *Ceramics − Silikáty* 48 (2004) 6

Chapter 6

Magnetostriction of composites with hard magnetic particles

Introduction

Bednarek [Bed1] and Guan [Gua1] have experimentally demonstrated the effect of the particle shape on the elongation of the composite in the presence of an applied magnetic field. Their works show how a magnetic torque deformes the composite, but are essentially qualitative. Lanotte [Lao1, Lao2] suggested a mathematical model of this phenomenon linking the rotation of the particle, within the elastic matrix, to the presence of the magnetic field. Rotation of the particles results to a macroscopic strain of the composite. Lanotte has also considered the inverse phenomenon where an applied stress changes orientation of the particles. Here, we focus on the macroscopic strain induced in hard magnetic particles composites placed in a homogeneous applied field. Hard magnetization has a memory effect i.e. it depends not only on the applied field but also on the precedent state unlike soft magnetization which is solely a function of the applied field at a given time. This special effect induces a special behavior on the magnetostriction curve of such composite.

I. Model of Lanotte

The case of the irregular particles embedded in the matrix, submitted to a homogenous magnetic field has been widely studied by Lanotte. Those articles were focused on the change of the composite magnetization, $\Delta M_Z = M_Z^{'} - M_Z$, when stressed or placed in the presence of an external magnetic field. He used soft particles with shape anisotropy [Lao2] magnetic behavior with the aim of designing a sensor [Lao1] device.

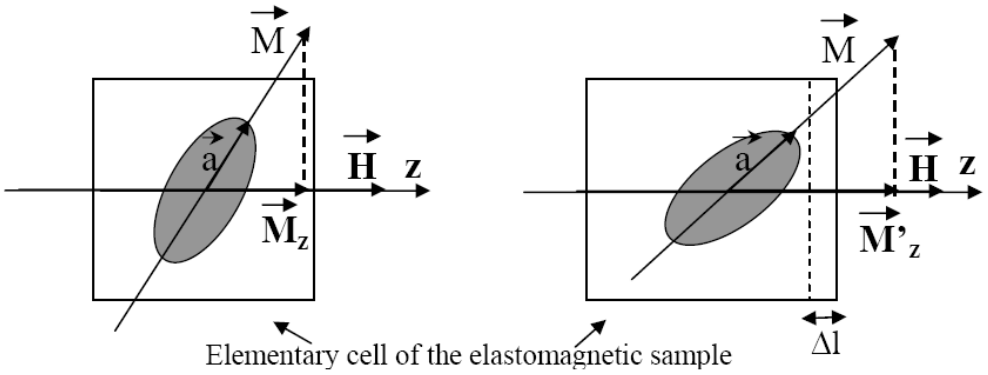

Fig. VI.1: Lanotte model of the rotation of a magnetic moment in an elastic cell when placed in a magnetic field [Lao1]

Two effects are needed for the deformation of an elementary volume: Magnetic torque and the elastic torque (response). The magnetization of the particles is initially characterized by an angle θ*i*, between the applied magnetic field (*H)* and the Z-axis direction. The magneto-elastic torque balance is written as;

$$m\mu_0 H \sin(\theta_i + \theta) = -k\theta \qquad \text{eq.VI.1}$$

Where *k* is the torsional elastic constant. Considering the resulting rotation θ small,

$$\theta = -\frac{m\mu_0 H \sin(\theta_i)}{k} \qquad \text{eq.VI.2}$$

That resulting rotation θ is defining a strain. In this way, he also shows the importance of the initial angle θ*i*. If the average of this angle over all particles is close to 0°, it will provide a minimum effect which is simply explained by the fact that pre-aligned particles won't feel any torque. Best case for the change of the apparent magnetization happens when the particles are directed with an average angle is close to 45 °. A randomly-oriented particles composite is an intermediary state in the effect. In our case, we focus on the strain in composites made of hard ferromagnetic particles; because the particles are hard (keeping a magnetization at zero field), the strain will depends on the sign of the applied field. As an example, the strain observed with a positive applied field (relatively to the first magnetization) is positive (Fig.VI.2a) whereas a negative field results in negative strain (Fig.VI.2b). Of course, this is true only if the viewed field is lower than the coercive field, preventing the magnetization to change its sign.

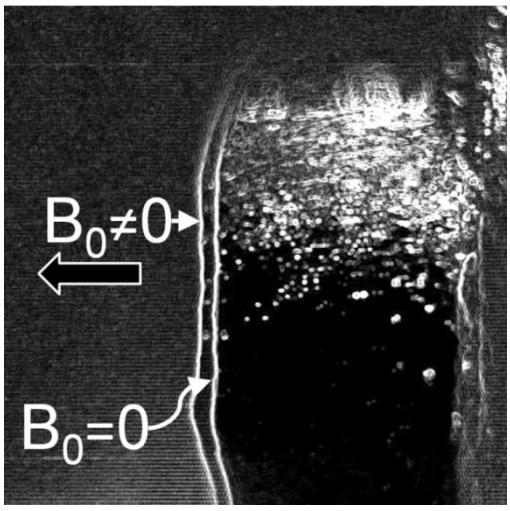

Fig.VI.2a:Composite, with hard particles, exposed to an induction parallel to the magnetization

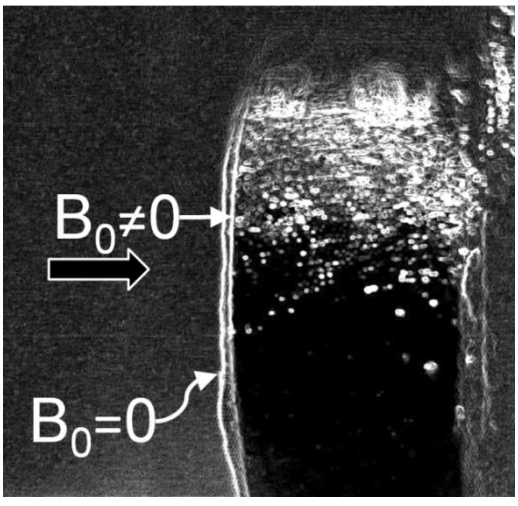

Fig.VI.2b:Composite, with hard particles, exposed to an induction antiparallel to the magnetization

II. Model with the whole internal field

In the model described above, composites were filled by few particles. Thus, particles were assumed to have no interactions with each others; they were in interaction only with the external field. Now, if we consider the composite with larger filling factor, the magnetic field acting on the particle is no more just the applied field but we also have to take into account the magnetic field produced by the other particles.

A single magnetic particle interacts with the composite internal field. This field is therefore expressed as the sum of the external field plus the field created by the particles:

$$\vec{H}_{\text{int}} = \vec{H}_0 + \vec{H}_{composite} \qquad \text{eq.VI.3}$$

with H_0 as the applied field, the one used by Lanotte in his model. The magnetic field produced by the composite is a complex calculation since each particle has its own magnetization. Consequently this magnetic field is estimated though the composite magnetization, which is the volume average of all the ferromagnetic particles magnetization within that volume:

$$\vec{M}_{composite} = \phi < \vec{M}_{particle} > \qquad \text{eq.VI.4}$$

Where ϕ stands for the filling factor and $< \vec{M}_{particle} >$ is the average magnetization of the particles inside the considered volume.

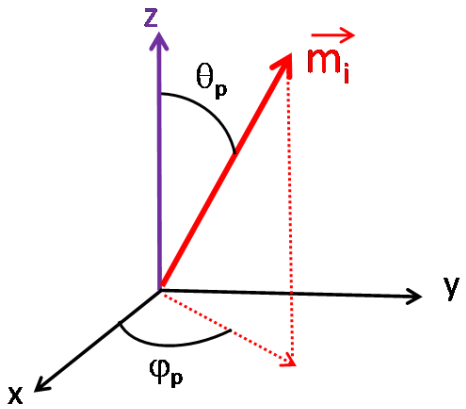

Fig.VI.3a: orientation: Space direction of a moment carried by a magnetic particle

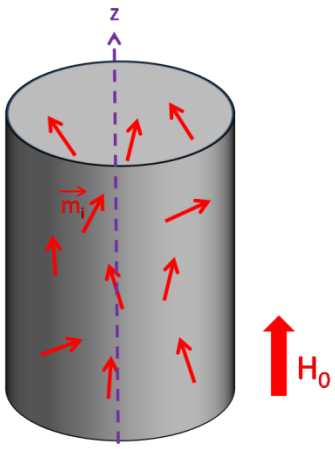

Fig.VI.3b: System of moment with a distribution of orientation

Considering that the applied magnetic field is axial and the strain has an axial and a transverse component, only the θ parameter changes during our experiment. A particle magnetization is expressed in spherical coordinates (Fig. VI.3a) as:

$$\vec{M}_{particle} = M_{particle}[\sin(\theta_p + \theta)\cos(\varphi_p)\vec{u}_x + \sin(\theta_p + \theta)\sin(\varphi_p)\vec{u}_y + \cos(\theta_p + \theta)\vec{u}_z] \qquad \text{eq.VI.5}$$

Where the inclination θ_p and azimuth φ_p are those of the particles without magnetic field or mechanical strain and θ is the resultant rotation of the particle due an applied mechanical or magnetic stress and the elastomer response.

When the particles get magnetized for the first time by an applied magnetic field directed in the z-axis, all particles exhibit a positive axial component to decrease the Zeeman interaction energy. Then, as the applied field sweeps different values, the inclination θ will change. In contrary, nothing set the particles azimuth φ_p. As a result of this, the particle average magnetization of the set of N particles is:

$$<\vec{M}_{particle}>= \frac{1}{N}\sum_{N}\vec{M}_{particle} \qquad \text{eq.VI.6}$$

$$<\vec{M}_{particle}>= M_{particle} <\cos(\theta_p + \theta)> \vec{u}_z \qquad \text{eq.VI.7}$$

We will consider the particles magnetization direction placed on a cone defined by the semi-angle θ_p as seen below in fig.VI.4a and having all the same value.

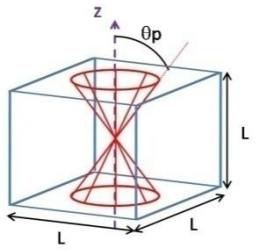

Fig.VI.4a. Magnetization of a unit cell at rest

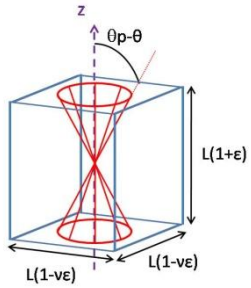

Fig.VI.4b. Magnetization of an elongated unit cell

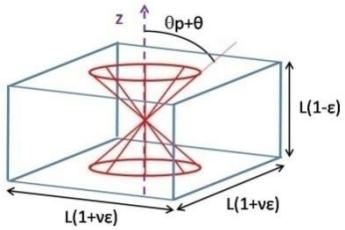

Fig.VI.4c. Magnetization of a contracted unit cell

So that, the composite is using eq.VI.4 and eq.VI.7, expressed as:

$$\vec{M}_{composite} = \phi M_{particle} < \cos(\theta_p + \theta) > \vec{u}_z \qquad \text{eq.VI.8}$$

The average magnetization is expressed as a magnetization along the cylinder axis with its amplitude proportional to the particle magnetization and the filling factor. As seen, in the chapter 4, a uniformly magnetized cylinder generated a demagnetizing field expressed as:

$$\vec{H}_d = -n_{sample}\vec{M}_{composite} \qquad \text{eq.VI.9}$$

Finally, the magnetic field inside the composite is written using eq.VI.9 into eq.VI.6 as:

$$\vec{H}_{\text{int}} = (H_0 - n_{sample} < \cos(\theta_p + \theta)\phi M_{particle} >)\vec{u}_z \qquad \text{eq.VI.10}$$

Using this equation we can define the magnetic torque acting on a magnetic particle; this torque is created by the difference of direction of the magnetization and the local magnetic field:

$$\vec{\Gamma} = \vec{H}_{\text{int}} \times \vec{M}_{particle} \qquad \text{eq.VI.11}$$

The internal field is the combination of the external field and of the demagnetizing field. Torque can be split in 2 components resulting in each of these fields.

$$\vec{\Gamma} = \vec{\Gamma}_0 + \vec{\Gamma}_d \qquad \text{eq.VI.12}$$

With the corresponding definition of these components:

$$\vec{\Gamma}_O = \vec{H}_O \times \vec{M}_{particle} = H_O \cdot M_{particle} \sin(\theta_p + \theta) \qquad \text{eq.VI.13}$$

We have found in eq.VI.13 the magnetic torque as used by Lanotte in eq.VI.1.

$$\vec{\Gamma}_d = \vec{H}_d \times \vec{M}_{particle} = \phi M^2_{particle} \sin(\theta_p + \theta) < \cos(\theta_p + \theta) > \qquad \text{eq.VI.14}$$

Applying a magnetic field will rotate the particle by an angle θ, yielding to the strain in the composite. Fig.VI.4b and fig.VI.5c shows the relation between the strain and the resultant change of direction of a particle's magnetization. Hence, an elongated unit cell decreases that angle unlike the case of a contracted cell which increases it.

III. Experimental

III.1. Hard magnetic particles

MPQ-S-11-9 and MQP-D are hard particles, provided by MAGNETQUENCH with different shapes; MPQ-S-11-9 particles are fine particles with a spherical morphology; median size d_{50} is 35-55µm whereas MQP-D particles present a flake-like shape. These particles are manufactured in such a way that they exhibit an isotropic magnetization; the magnetization is in the same direction as the applied field. Fig.VI.5a and 5b show SEM picture of these particles.

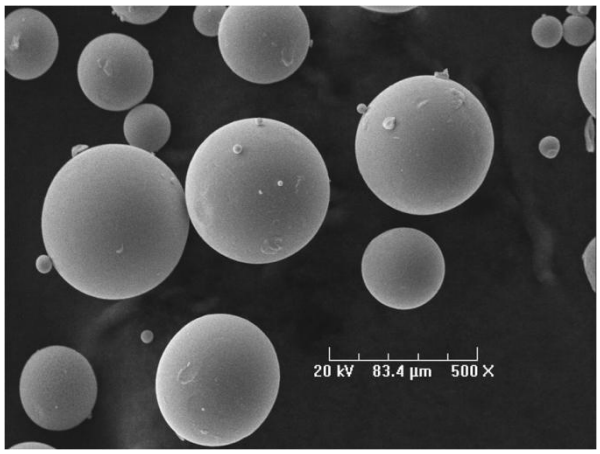

Fig. VI.5a: SEM picture of the magnetic particles MQP-S-11-9

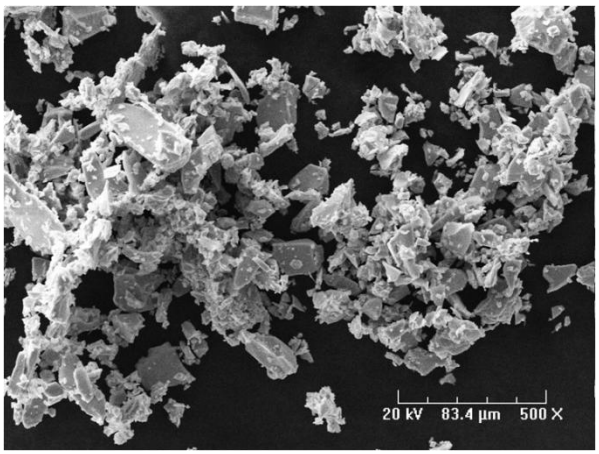

Fig. VI.5b: SEM picture of the magnetic particles MQP-D

Magnetization has been measured as a function of the applied field and is shown in Fig.VI.6 for field ranging from 0 to 7.2 Tesla (to get a first magnetization curve), then looping between -7.2 and 7.2 Tesla. A saturation, $\mu_0 M$=1.34 T is measured for these particles. Important data extracted from this curve are the remnant magnetization and the coercive field measured at $\mu_0 Mr$=0.74 T and $\mu_0 Hc$=0.9 T

respectively. Experimental strain curve were measured in a maximal field of 1.2T, therefore another magnetization measurement was performed to get the pertinent values of magnetization. Magnetization reached for the maximal applied field of 1.2 T is μ_0M=0.80 T, the remnant magnetization is μ_0Mr=0.51 T and the coercive field for this loop is μ_0Hc=0.8 T.

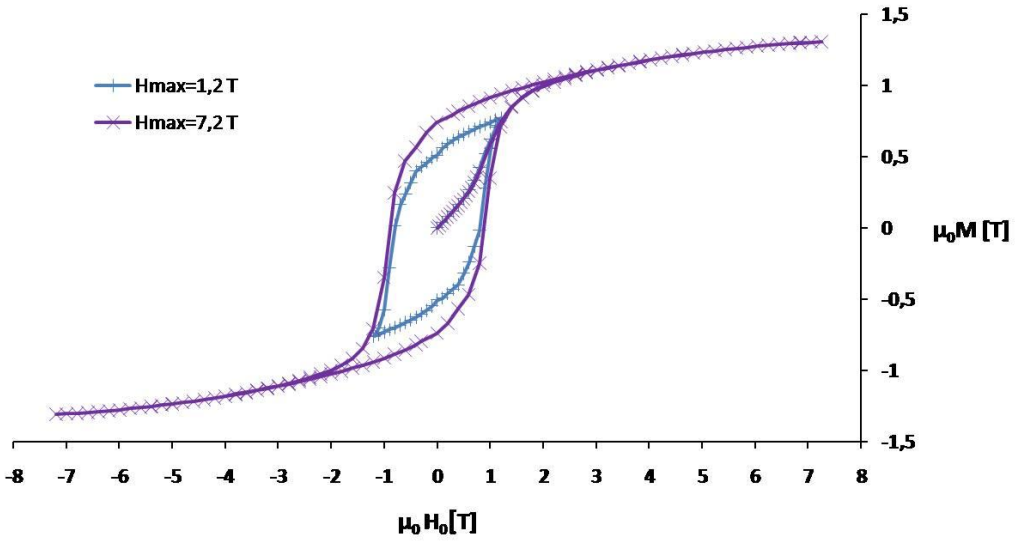

Fig.VI.6 Magnetization curve of MQP-S-9-11 versus applied field. Maximal field applied were 1.2 T in blue and 7.2T in purple.

III.2. Composite strain versus the applied magnetic field

III.2.1. Fist magnetization loop

In the following experiments, we investigated the strain while the sample is exposed to magnetic field for the first time. The samples used were not magnetized before. First, a composite sample, filled by non-spherical particles 20%vol., with an aspect ratio of 0.36 was made. Its strain was recorded for applied field increasing from 0 to 1.2 T, then decreasing to -1.2 T and going back to 0 T.

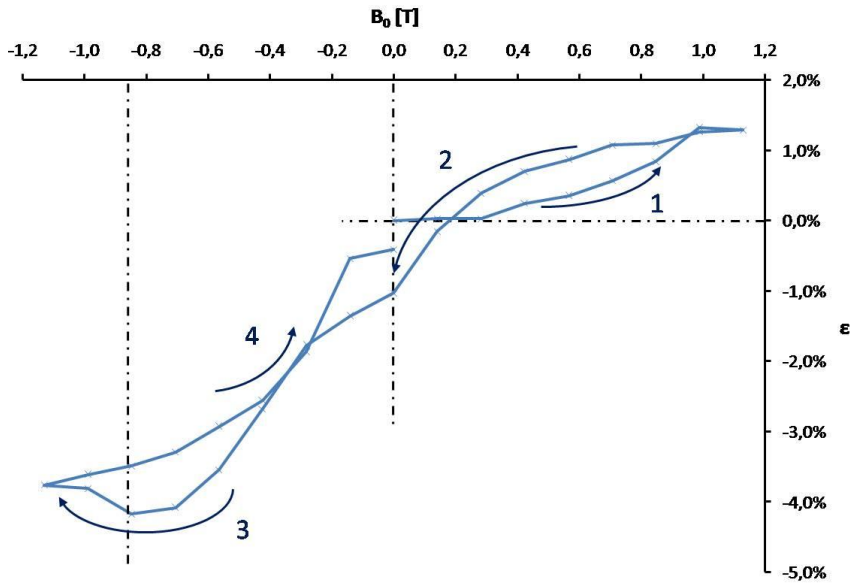

Fig VI.7: First magnetostriction loop

Fig VI.7 presents the measurement of the magnetostriction versus the applied field. Unlike to the case of iron/silicone samples (Fig.V.7) where the magnetostriction was positive for positive or negative applied field, the magnetostriction of composite based on hard magnetic particles is positive for a positive applied field and negative in the other case. The magnetostriction presented in the previous chapter was a quadratic function of the magnetization (M^2); a first consequence of this observation (Fig.VI.7) is the necessity to add the effect of the applied field.

When the applied field becomes zero the remnant strain is negative. In the chapter 3, we have supposed that the remnant state, which was positive, was a consequence of the mechanical damage between particles and the matrix. This cannot explain the observed negative value. At this point, we can say that the particles being magnetized in the first segment keep a remnant value when the applied field goes to zero. Shape effect, i.e. minimizing the average demagnetizing energy as discussed in chapter 5, would produce a positive (M^2) remnant strain. Our experimental results suggest a different mechanism. The average magnetization of the particles is along the cylinder axis and then produces a demagnetizing field along that axis but in the opposite direction. This negative axial field can interact with the positively magnetized particles; this interaction result in a negative strain as discussed in the above model.

To check the effect of the demagnetizing field, 20%vol. samples with different aspect ratio (0.80, 0.64 and 0.36) were made. Those samples were placed in the device to track the

displacements induced by the applied magnetic field. In Fig VI.8, the magnetostriction curves are presented. Data are limited to field values down to -0.4 T: during the experiments, the longest samples were very sensitive to a macroscopic magnetic torque; they started getting bended with high negative field values which is not the effect we are looking at. We are interested in the strain at a zero applied field after a first magnetization which can be seen on this curve.

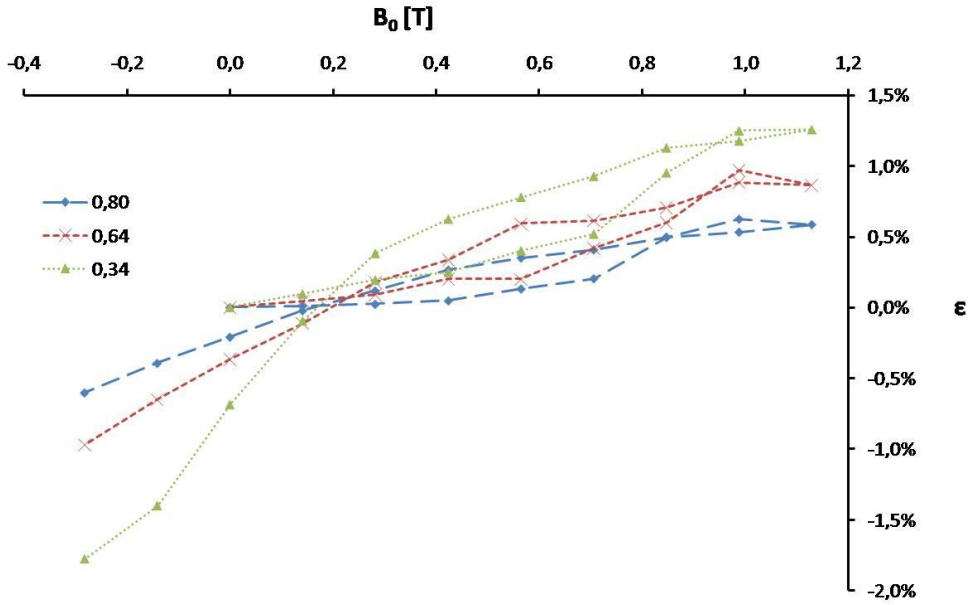

Fig VI.8 : magnetostriction curve as a function of the aspect ratio

In Fig VI.8, the resulting magnetostriction curves are plotted for 3 different aspect ratio parameter c/a (0.36, 0.64 and 0.80). Samples were not magnetized before the experiment. Magnetostriction curves increase in the first segment, when external magnetic field rises from 0 T to 1.2 T with their respective amplitude increasing as the aspect ratio is lower. With the applied field, particles are magnetized which yields to an axial magnetization of the composite and therefore a demagnetizing energy linked to the aspect ratio of the samples. This results in a strain explained by the demagnetizing energy as discussed in the previous chapter. By the way, the applied field also acts on the particles by a magnetic torque, enhancing the resultant rotation of the particles. When the magnetic field decreases, the strain is also decreasing and becomes null before the magnetic field goes to zero. It can be seen that the magnetostriction values are negatives when a zero external field is applied for any aspect ratio. Hard magnetic particles keep their remnant magnetization, so that a demagnetizing field is still present. Besides, in zero external field, this demagnetizing field is larger as

the aspect ratio is lower. This behavior impacts on the magnetostriction value at zero field. The amplitude (in absolute value) is larger when the sample aspect ratio is lower.

For negative applied field, we can see in Fig.VI.7 that the strain is also negative. Moreover, the strain is larger in absolute value than the strain due to the first magnetization. This can be explain by a larger internal field when the applied field is negative (but still does not reach the coercive field) than for the case of a positive applied field. This is discussed below.

III.2.2. Coercive field

The magnetization loop of the hard magnetic powder with a largest field of +/- 1.2 T is presented in Fig.VI.6. Magnetization was found to be null at 0.8 T. Considering that the strain results from interactions like magnetization times magnetic field or magnetization times magnetization, no strain should be measured at this value. However, the experimental curve (Fig.VI.7) shows that the strain is negative (not null) for applied negative field up to the maximal field of 1.2 T. An explanation is provided by the distribution of the orientation of magnetic moment inside the composite.

The internal field on a particle can be expressed as the sum of the applied field and the demagnetizing field (resulting from the magnetized particles):

$$\vec{H}_{\text{int}} = \vec{H}_0 - \vec{H}_d \qquad \text{eq.VI.15}$$

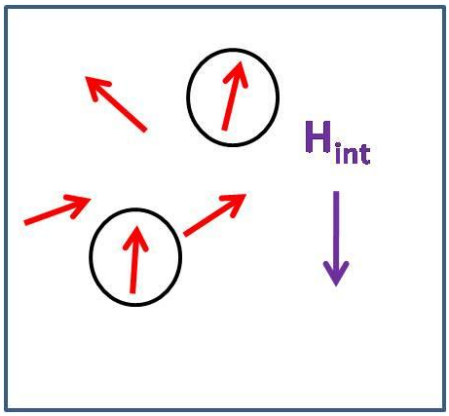

fig.VI.9a: distribution of moments inside the composite placed in the internal field

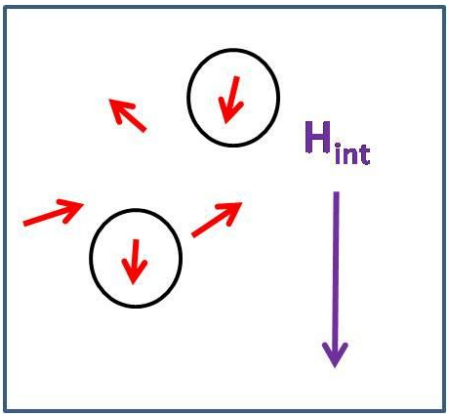

fig.VI.9b: If the internal field increases enough, the moments with low angle can be reversed

Considering than the particles are magnetized (positively), they are creating a demagnetizing negative field. For an applied negative field, but still above the coercive field value, the particles magnetization remains positive. Then, both the applied field and the demagnetizing field are negative; eq.VI.15 shows that the resulting internal field reaches values larger than the solely applied field. Interaction between particles and that internal field is then larger than when the applied field was positive; this results in a larger magnetostriction, in absolute value, when the applied field is negative than when it is positive as seen in Fig.VI.7.

Hard magnetic particles have a large magneto crystalline anisotropy. Any rotation of the magnetic moment inside the particle is avoided by this magneto crystalline anisotropy. Therefore, we assume that the magnetization remains along the anisotropic axis. The amplitude of the magnetization of a particle, which presents an angle relatively to that field, is a function of the field on the particle. A correction of that field has to be taken into account. A particle with a relative angle θ_p for the cylinder axis (field axis) is affected by an effective field, which is the projection of the internal field (relatively to the composite) on that particle expressed as (without strain):

$$H_{see} = H_{\text{int}} \cos(\theta_p) \qquad \text{eq.VI.16}$$

This equation provides the magnetic field that rules the magnetization of a particle. In this way, the field that should reverse the particle magnetization is different from the magnetic field inside the composite and therefore from the applied field. Moreover, the composite being a set of particles with random orientations inside the volume, each particle will experience a different value of magnetic field (eq.VI.15). This equation also shows that particles with a low angle θ_p can easily reach their coercive field, whereas those with larger angle θ_p need a larger applied field to reach their coercive field.

A distribution of orientation of particles results into a distribution of the apparent coercive field. As seen in Fig.VI.9a & Fig.VI.9b, only particles with a low angle θ_p can easily reverse their magnetization as opposed to the others with a large angle. The impact of this distribution of coercive field appears clearly in Fig.VI.7. For an applied field close to -0.8T (which stands for magnetic particle coercivity as seen in Fig.VI.6), a non-null magnetostriction is found. As that applied field is decreasing, the magnetostriction is reaching a minimum value. This means that the number of particles which have changed their magnetization direction is increasing as the applied field is decreasing to larger negative value.

III.2.3. Cycling

Previously we have applied an external magnetic field, first positive, then negative field and finally the applied field was set back to zero. The magnetostriction curve reaches a negative value as the applied field is zero (Fig.VI.7). The coercive field, for hard particles appears symmetrically for an external field of ±0.8T as seen on the magnetization curve (Fig.VI.6). Apparent coercive field corresponds to a minimum on the magnetostriction curve for a negative applied field. Since the demagnetizing field amplitude changes when the composite is strained positively or negatively, the internal fields in the composite (applied field + demagnetizing field) are different in these two cases. We are now interested in the effect of the positive coercive field. Therefore, we have submitted the samples to a full magnetic loop.

The effect of the cycling magnetic field on a sample is presented in Fig.VI.10. Positive fields and negative fields reach maximum absolute values of 1.2 T. For the first magnetic loop (from zero to positive then negative then zero field), the resulting strain is like the one presented in Fig.VI.7.

Growth and saturation of the alternating peak magnetostriction

By increasing the magnetic field from 0 T to +1.2 T, the magnetostriction of the composite is also increasing as seen in Fig.VI.10. When the magnetic field is then decreasing to -1.2 T, the magnetostriction reaches a minimum for an applied field close to -0.8 T. The amplitude of these two magnetostriction peaks are different; when the applied field is positive (from 0 T to +1.2 T) the resulting magnetostriction peak is smaller than the second peak when the applied field is negative (0 T to -1.2 T). The third peak, when the applied field is now again positive, has a higher amplitude than the two previous ones. Peaks amplitude continues to increase until the phenomenon saturates. The positive magnetostriction is also larger than the negative one.

Drop discontinuity effect

In the case of negative strain, a small drop in the magnetostriction curve is observed. This drop is observed when the applied field reaches the particle coercive field; magnetic moments are then reversed, which changes the amplitude of the magnetostriction curve. When the applied field is positive, that drop is smoother than in the case of a negative field. When exposed to a positive field, the composite exhibits a positive strain so that the demagnetizing field is reduced; thus the inner field is reduced. In the same way, when the composite is exposed to a negative field, the composite exhibits a negative strain so that the demagnetizing field is enhanced; thus the inner field is reinforced. The number of reversed moments is therefore lesser in the case of the positive field than

in the case of negative field, since the inner field is different in each case. This can explain the stronger drop of the magnetostriction in the case of the applied negative field.

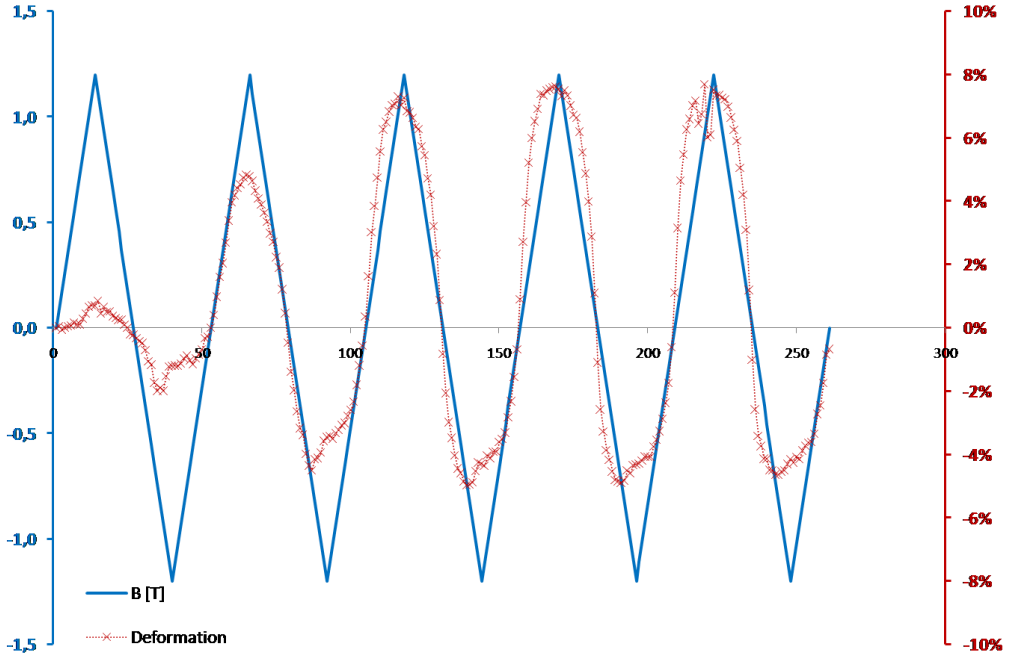

Fig.VI.10 Strain as a function of the applied field, positive and negative alternatively

Necessity of a field reversal for an amplitude evolution

To understand such enhancement of the effective magnetostrictive curve, we did other measurements. First idea was to check the need to change of the applied field sign to exhibit this behavior. The measurement of the magnetostriction of a composite was performed with a magnetic field ranging from 0T to 1.2 T; this sequence of positive field was repeated 6 times, looking for some possible enhancement when cycling with positive field. Then we changed the applied field sign and made a new sequence of three negative peaks of magnetic field. Such sequences of three peaks of magnetic field with same sign then three other peaks with opposite sign were repeated. The corresponding magnetic field is plotted in red in Fig.VI.11. The corresponding strains are also plotted in Fig.VI.11. As expected the magnetostriction curves sign is the same as the applied field sign. No enhancement in the strain is observed when six first positive peaks were performed. Cycling positive amplitude of magnetic field does not change the resulting amplitude of the strain. Then the next sequence of three negative peaks has been operated with the same amplitude: from 0T to -1.2 T.

Negative strain was observed, as a consequence of the negative applied field. Negative strains were larger than positive strain found in the first magnetostriction curves. Moreover, a higher absolute value for the first negative peak is found as compared to the two followings negative peaks. The enhancement is only observed when the applied field has changed its sign. This behavior was confirmed in different subsequent cycles.

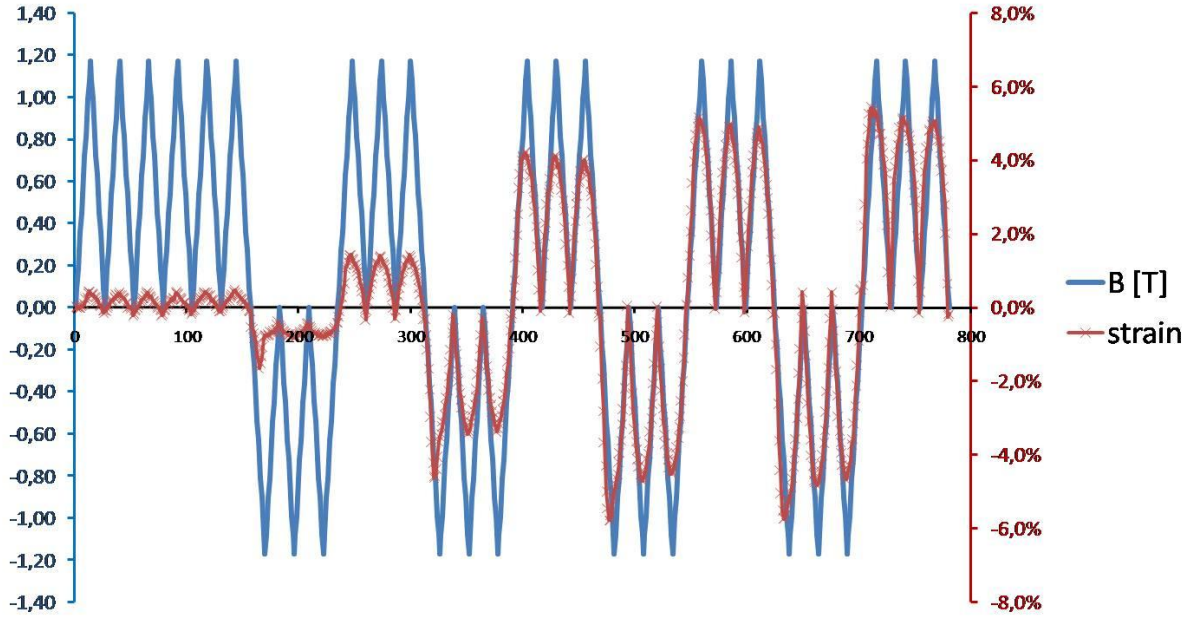

Fig.VI.11 Strain as a function of the applied field, which was packed by sequence of 3 positive peaks and 3 negative peaks

Evolution of the drop effect

In Fig.VI.11, we could see that the first peak of the negative value was larger than the 2 following peaks whereas this difference was not found in the case of positive peaks. To highlight this phenomenon, the 3 strain peaks of negative sequences (0 to -1.2 to 0 Tesla) were superimposed on the same plot in Fig.VI.12.a. We confirm that the first curve reaches as larger value of strain as compared to the 2 followings.

Before these three negative sequences, the applied field was positive. Going from positive field values to negative values induces a change of the sign of the magnetization as the inner field reaches the coercive field of the particles. Reversing magnetization of some of the particles reduces the average magnetization and hence the average coupling and magnetostriction. The difference between the 2nd and the 1st curve can be viewed as the amount of particles that reversed their magnetization. The 2nd and 3rd curves present a similar shape as no more reversal occurs.

Fig.VI.10 & fig.VI.11 show that the increase of the magnetostriction curve becomes lower and lower as the magnetic field is cycling and finally a maximum amplitude of that strain is reached. Fig.VI.12b presents the different negative magnetostriction curves observed just after the reversal of the sign of the magnetic field sequences. Those first peaks of negative magnetostriction present a drop in their shape (as described above) and also evolve after each reversal of the sign of the magnetic cycles, getting smoother and smoother. This suggests that the number of particles which reverse their magnetization is lower and lower as the number of alternating field is larger.

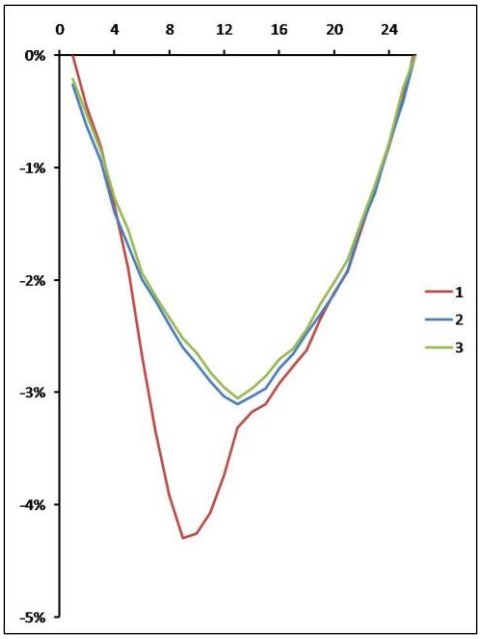

Fig.VI.12a: Three consecutive negative field sequences

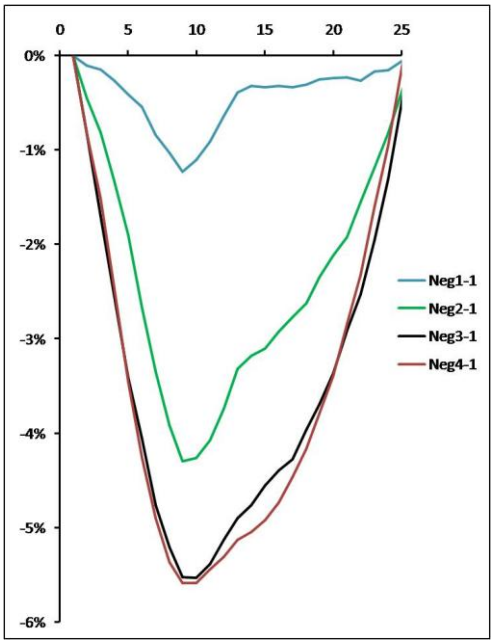

Fig.VI.12b: Comparison between the first negative sequences observed after each magnetic field reversal

Necessity to reach the coercive field

In the above observations, we have suggested that the evolution of the magnetostriction cycles is connected to some reversal of particles magnetization. The next experiment was therefore made to determine whether the enhancement process appears only when an applied negative field that reaches the coercive field is needed or not.

The fig.VI.13 presents the magnetostriction curve of a sample exposed to a homogeneous field with alternating values. In the first part of the experiment, the amplitude of the

negative field was B_0 = -0.55 T and the amplitude of the positive field was B_0 = +1.2 T. This cycle was applied 3 times to verify whether any increase of the magnetostriction maximum occurs or not.

Then, larger negative values were set at B_0 = -0.9 T with the positive applied field still set at B_0 = + 1.2 T. The sample was submitted 3 times to that cycle to check whether any increase of the magnetostriction maximum occurs or not. The last cycles were performed with an applied field ranging values between B_0 = -1.2 T and B_0 = + 1.2 T.

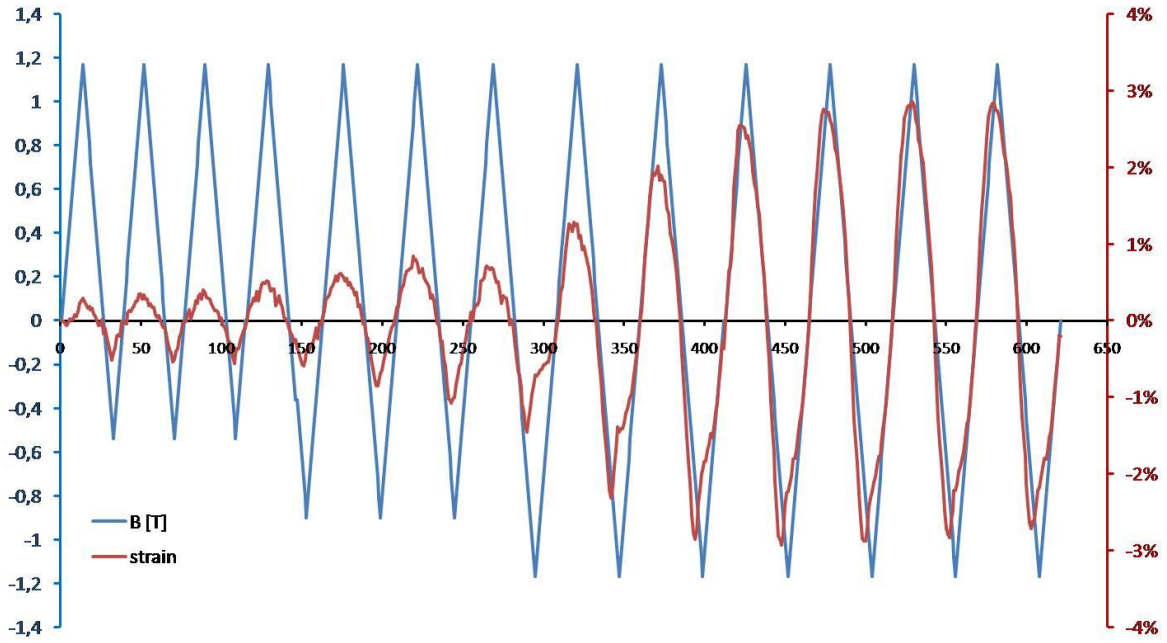

Fig.VI.13 Strain as a function of an alternating applied field. Negative field amplitude increases in 3 steps

In the first part, when the negative values are limited to -0.55 T, the amplitude of the maximum negative magnetostriction is constant and no drop is observed. The applied negative field is therefore shown to be too weak to activate some magnetization reversal.

In the second part, when the negative magnetic field being set to -0.9T (stronger than the coercive field but close to it), a slight enhancement of the positive strain and the negative strain is observed.

Then, in the last part of the experiment, with a negative field down to -1.2 T, a clear evolution effect is observed (increasing amplitude of the maximum magnetostriction). The drop in the negative value of the strain is also clearly observed.

From all the above experiments, the phenomenon of enhancement of the magnetostriction seems to appear when a large enough negative field is applied. The coercive field value is observed to be that needed value.

When a negative field is applied, the composite is contracted as a consequence of the torque acting on the ferromagnetic particles. That contraction reduces the aspect ratio of the composite, resulting in a larger demagnetizing field. The internal field reverses the magnetization of some particles. When the applied field is going back to positive value, the composite is elongated also due to interaction of the particles with the applied field. The aspect ratio becomes larger, than in the case of the contracted composite, which induces lower demagnetizing field and thus a lower internal field. Symmetrical applied field, positive and negative, results into a non-symmetrical internal field due to the elongation and contraction of the composite. The consequence is a non-symmetrical behavior of the magnetization, hence the magnetostriction curve. This non-symmetrical magnetostriction also impact on the magnetization. The result of that complex phenomenon is the enhancement of the magnetostriction curve as the applied field is cycling.

III.2.4. Influence of the cylinder radial field

We have just presented a model of hard magnetic composites in which the particles magnetizations are oriented in any direction. The magnetostriction of such composite was then treated as the interaction of the particles with the local field. This local field was only considered as an axial field. However, for cylindrical samples, the demagnetization field has also a radial component which should be taken into account in our model.

III.2.4.1. Local magnetic field

Demagnetizing field is the field created on a point by the magnetized matter; in a case of an ellipsoid this field is entirely oriented in the opposite direction of the magnetization. However, this field is generally more complex for others geometry. In chapter 4, we have presented the demagnetizing field of the cylinder as a combination of an axial field (eq.IV.11) and a radial field (eq.IV.12); the internal field is then expressed as the summation of the applied field along the cylinder axis and the demagnetizing field with its 2 components:

$$\vec{H}_{\text{int}} = (H_0 + H_{d\_z})\vec{u}_z + H_{d\_r}\vec{u}_r \qquad \text{eq.VI.17}$$

That demagnetizing field in a cylinder is mainly located close to the top (and bottom) edge where the equivalent magnetic charges $(\vec{M} \cdot \vec{n})$ are located. Due to the symmetry, the field on the cylinder axis has no radial component; on the contrary that field component becomes stronger far from this axis. The radial component is then mostly in the neighborhood of the cylinder corner.

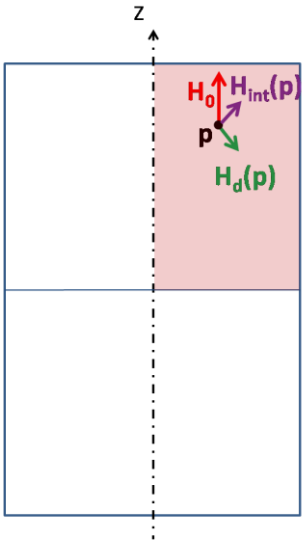

Fig.VI.14a: The local magnetic field $H_{int}(p)$ inside the cylinder : axial applied field H_0 and a local two-components demagnetizing field $H_d(p)$

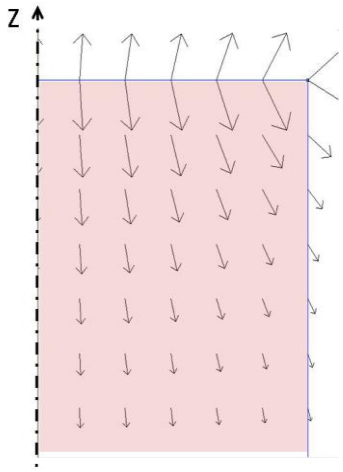

Fig.VI.14b: Local two-components demagnetizing field $H_d(p)$

Both the magnetization and the demagnetizing field are non-homogeneous. However, it is possible to locally correlate the demagnetizing field to the average magnetization M, through local demagnetizing coefficients Nzz and Nrz with:

$$\vec{H}_{\text{int}} = (H_0 - N_{zz}M_{composite})\vec{u}_z - N_{rz}M_{composite}\vec{u}_r \qquad \text{eq.VI.18}$$

A change in the applied field results in a change of both the amplitude and the direction of the inner field. The axial and radial components of the inner field change due to the change of the composite magnetization but the axial component will also change due to the change in the applied field. Axial

and radial components of the inner field have different field dependence behavior. Thus, an increment of the applied field result in a change of direction of the inner field: that field is “turning”.

III.2.4.2. Anisotropic magnetization

Unlike composites based on iron particles, this radial component becomes really important for composite based on hard magnetic particles, like the MQP-S-11-9. The difference appears since the magnetic behavior of iron particles and MQP-S-11-9 possess different magnetocrystalline anisotropies: it is much larger for hard magnetic particles than for soft particles.

The magnetocrystalline anisotropic energy in a magnetic material is defined as the energy paid to rotate the magnetization relatively to the crystal axes. Expression of that energy depends on the considered lattice; cubic, quadratic hexagonal [Mag1]… Whatever the lattice is, the first order expression of the energy is usually a function of the azimuthally rotation of the magnetization:

$$E_A = K_1 \sin^2(\theta) + \ldots \qquad \text{eq.VI.19}$$

K_1 is an anisotropic constant. The term of next higher degree, K_i i>1, are generally small compared to K_1. In the case of a soft material as Iron, this anisotropic constant is much lower than for a hard material:

	$Iron$	$Nd_2Fe_{14}B$
$K_1[kJ/m^3]$	48	4900

Hence, the magnetization’s direction of hard particles is considered to be fixed at low field and remains frozen unless a stronger magnetic field is applied, bringing enough energy to rotate the magnetization along that field.

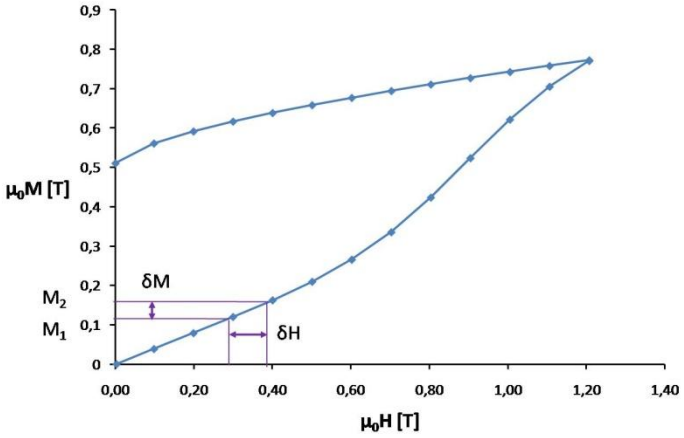

Fig.VI.15: Anisotropic magnetization of the MQP-S-11-9

The change of magnetization of such particle resulting from a change of applied field is expressed as:

$$\vec{M}_2 = \vec{M}_1 + \delta\vec{M} \qquad \text{eq.VI.20}$$

This equation means that the new state of magnetization results from the previous one plus an increment of magnetization. This infinitesimal change of magnetization δM is expressed as a function of the viewed field:

$$\delta\vec{M} = \chi\delta\vec{H}_{\text{int}} \qquad \text{eq.VI.21}$$

A change in the value of the external field results into a change of direction and amplitude of the inner field. Therefore, a particle which has still a magnetization frozen in one direction will experience a torque that depends on the external field. That torque still tends to align the magnetization towards the local inner field as seen in Fig.VI.16.

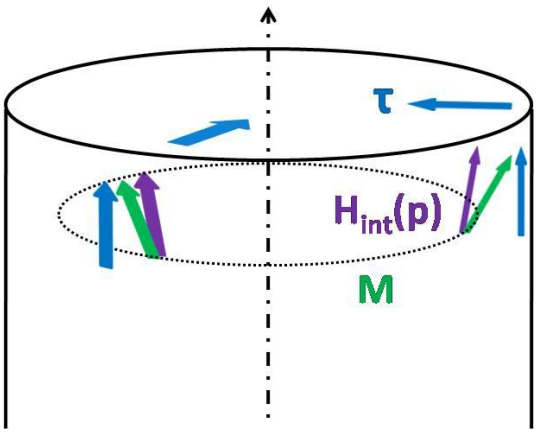

Fig.VI.16a: Shear stress due to the magnetic torque acting within the cylinder in a case of a positive viewed field

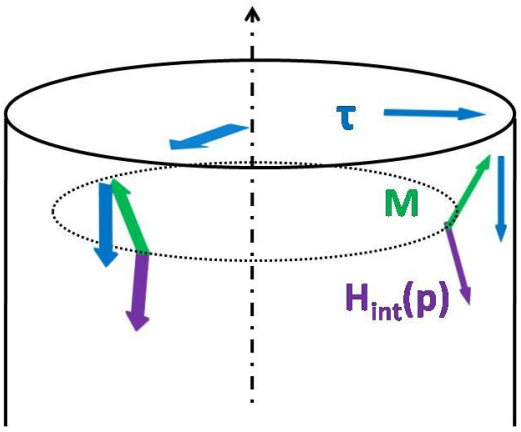

Fig.VI.16b: Shear stress due to the magnetic torque acting within the cylinder in a case of a negative viewed field

In Fig.VI.16a, the inner magnetic field is positive yielding to a positive torque acting on the particles. The opposite case is presented in Fig.VI.16b where the inner field is negative. This torque effect occurs thanks to the radial component of the inner magnetic field and to the hard magnetization of the particles.

This magnetic torque is then converted into a shear stress. This phenomenon will strain the cylinder in different way with respect to the sign of the inner magnetic field, and more specifically to the applied field.

III.2.4.3. Experimental

In order to test the effect of this radial field on a magnetized sample shape, a composite filled with 20% (vol.) hard particles MQP-S-11-9 has been prepared. The cylinder thickness is 40mm and the diameter is 12mm. A magnetic field was applied along the cylinder axis of the sample. The magnetic field values were 0, 1.2 T and -1.2 T. The resulting strain due to the radial component of the inner field occurs in the corner of the cylinders as expected from the Fig.VI.14b. Pictures, Fig.VI.17.a,b and c, were taken during the experiments in this area for each of these magnetic field values.

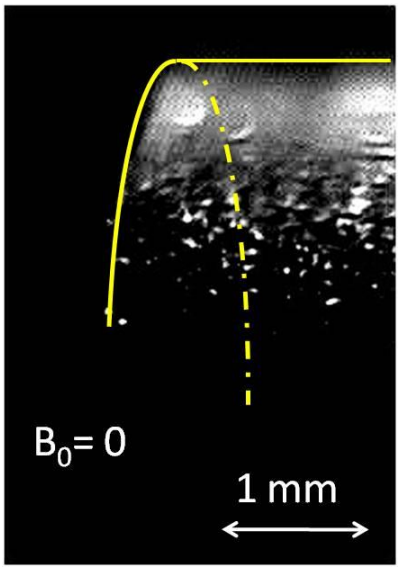

Fig.VI.17.a : composite filled with 20% (vol.) MQP-S-11-9 particles without magnetic field

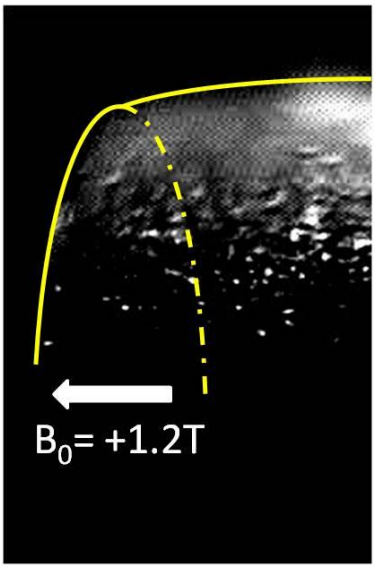

Fig.VI.17.b : composite in a positive magnetic field

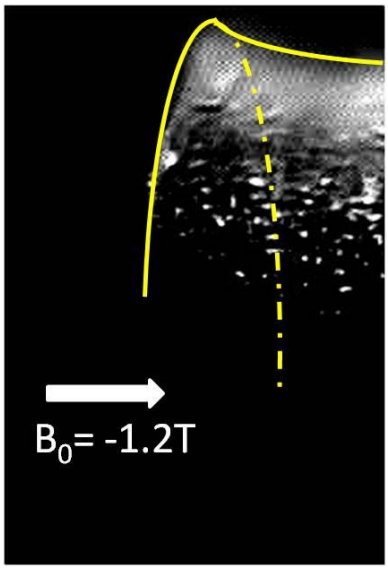

Fig.VI.17.c : composite in a negative magnetic field

In fig.VI.17, the effect of that radial field on the change of shape is presented. In fig.VI.17.a, no magnetic field is applied, the cylinder is at rest. When submitted to a positive external field, relatively to the first magnetization, the sample elongates as described before, but it also becomes barrel-shaped, as seen in Fig.VI.17.b, due to the radial component of the inner field. The composite magnetization reaches a remnant state when the applied field goes down to zero. When the applied is negative, the average magnetization of the composite is still positive; the stresses induce a diabolo type shape as seen in Fig.VI.17.c.

IV. Conclusion

The above experiments present the strain of composite of hard magnetic particles embedded in a soft elastic matrix under a homogenous magnetic field. Hard magnetization of such particles plays an important role on the magnetostriction curve of the composite. A direct effect of the external field is recorded: the strain is either positive or negative with respect to the applied magnetic field sign as expected from Lanotte's model based on magnetic torque. Elongation or compression of the

length of the composite is driven with regards to the sign of the applied field and to the particles magnetization. It should be noticed that the elongation of the composite placed in a homogeneous field was alike piezomagnetism: a linear curve of strain versus applied field is measured; this result is different from the case of composite filled by soft particles which behaved as magnetostriction: a quadratic curve.

The total inner field has an effect on the magnetic torque experienced by particles. Pure effect of the demagnetizing field was measured when the external field was set back to zero: the magnetization reached a positive remnant value resulting into a negative remnant demagnetizing field yielding to a composite compression. In the range of the experimental magnetic field, ±1.2T, the demagnetizing field also provides a new effect. When the applied field is negative, the demagnetizing field, which is still negative, reinforces the inner field: coercive field of particles was easier to reach for negative values than for positive field values. In the case of a positive applied field, the demagnetizing field was still negative which reduced the inner field and coercive field of particles was harder to reach.

Due to that non-symmetrical inner field, to the distribution of magnetic particles and to the coercive value of the magnetic particles, a cycling effect was experimentally highlighted: as the applied field changes its sign, the magnetostriction is enhanced. This phenomenon appears only if the inner field goes above the coercive field of the hard ferromagnetic particles.

The effect of the whole demagnetizing field in the cylinder, including both axial and radial components, was also recorded. The radial component, localized in the cylinder corner, is impacting on the shape of the composite. The cylinder shape becomes like a barrel for a positive applied field and like a diabolo for a negative field.

References:

[Gua1]: Magnetostrictive effect of magnetorheological elastomer, Xinchun Guan, Xufeng Dong, Jinping Ou, *Journal of Magnetism and Magnetic Materials* 320 (2008) 158

[Bed1]: The Giant linear magnetostriction in elastic ferromagnetic composites within a porous matrix, S. Bednarek, *Journal of Magnetism and Magnetic Materials* 301 (2006) 200

[Lao1]: Sate of the art and development trends of novel nanostructured elastomagnetic composites, L. Lanotte, G. Ausanio, C. Hison, V. Iannotti, C. Luponio, C. Luponio Jr., *Journal of Optoelectronics and Advanced Materials* 6 (2004) 523

[Lao2]: Influence of particle pre-orientation on elastomagnetic effect in a composite material of ellipsoidal Ni microparticles in a silicone matrix, L. Lanotte, G. Ausanio, V. Iannotti, C. Luponio Jr., *Applied Physics A* 77 (2003) 953

[Mag1]: Magnetism I-Fundamentals, E. du Tremolet de Lacheisserie, D. Gignoux, M. Schlenker, Springer-Verlag New York Inc. (2004), #ISBN-10: 0387229671, #ISBN-13**:** 978-0387229676

Chapter 7

Thermal effect on the Magnetostriction

I. Introduction

In the previous chapters, we studied the deformation of Fe/Silicone composite as a function of the applied magnetic field, the sample shape and the filling factor. Filling factor is a parameter that determines the magnetic stress and the Young modulus. The temperature is another parameter which determines the level of the magnetic stress and mechanical response. In this chapter, we will focus on thermal behavior of the magnetostriction. The magnetization and elastic modulus are affected when the temperature is changed: at increasing temperature, both the magnetic force and the stiffness decrease resulting in opposite effects on the sample. To study the thermal behavior of the deformation, composites have been made using two different types of ferromagnetic particles and matrix in order to separate the role of these two effects.

I.1. Thermal consideration

I.1.1. Thermal magnetization of the particles

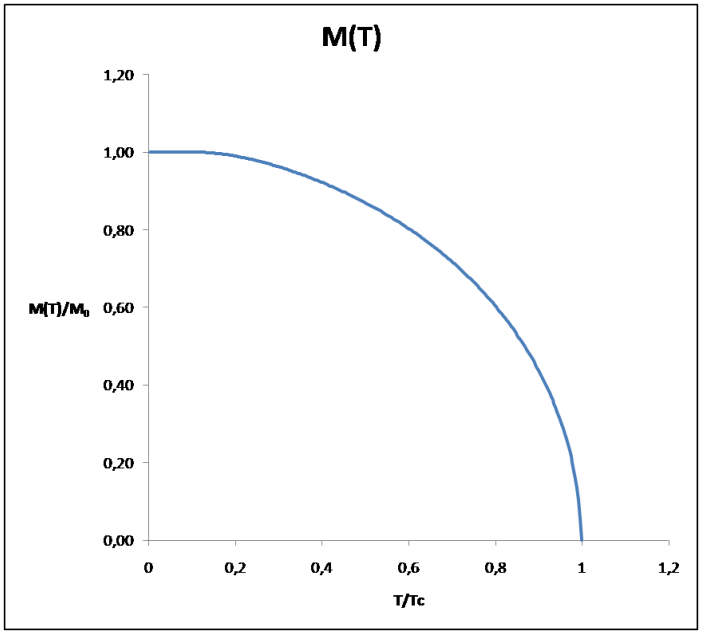

Fig.VII.1: Thermal dependence on the spontaneous magnetization

Ferromagnetic interactions in magnetic materials lead to a spontaneous magnetization. Because of the competition between thermal energy and the magnetic energy, this spontaneous magnetization is reduced when temperature increases as illustrated in Fig.VII.1. At 0K, the spontaneous magnetization is maximum and at the so-called Curie temperature T_c, this spontaneous magnetization disappears. This Curie temperature is characteristic of the each magnetic material.

In this chapter, two ferromagnetic materials are used: namely Iron and Gadolinium. Iron has a high T_C compared to Gadolinium, which yields to an almost constant magnetization at room temperature. Gadolinium magnetization is highly dependent on temperature when measurements are performed close to room temperature: close to T_C of Gadolinium [Ell, Bou]:

$$\begin{array}{lll} & Fe & Gd \\ T_C[°K] & 1043[Mag1] & 295[She] \end{array}$$

Iron thermal expansion coefficient (TEC) is 11.7 $10^{-6}K^{-1}$ (at 293K) [Bor] while for gadolinium TEC is known as 9 $10^{-6}K^{-1}$ [Eng]. In the following experiments, those intrinsic thermal expansion coefficients are neglected because of their small values as we did before for the intrinsic magnetostriction of the ferromagnetic particles, when the magnetostriction of the composite was considered.

I.1.2.Thermomechanical behavior of the matrix

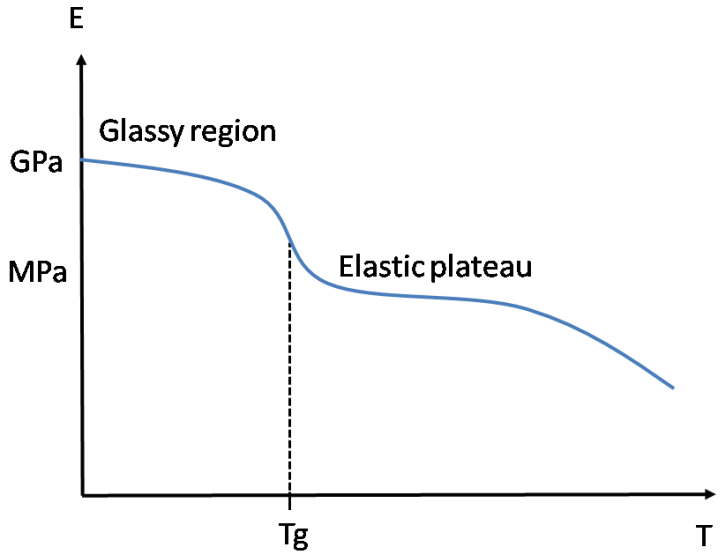

Fig.VII.2: Schematic thermal dependence of Young modulus of amorphous polymlers

The behavior of the Young modulus *E* of an amorphous polymer is drastically temperature dependent. At low temperature, the polymer is glassy and brittle; *E* is almost constant with typical values of few GPa. At higher temperature, the polymer reaches its so-called glass-rubber transition, which corresponds to a modulus drop by around 3 decades within a temperature increase of 20-30K for polymers lightly cross-linked as for the silicone matrix used here. Further another temperature range where the Young modulus remains almost constant corresponds to the rubber plateau, where the elastic behavior results from the polymeric chain conformational entropy. Thus, the rubber plateau exhibits a Young modulus of some MPa. The glass transition is characterized by temperature T_G. T_G is characteristic of a given polymer to its molecular weight (Fig.VII.3), and is independent of filler content, at least for particles in the µm range [Pau].

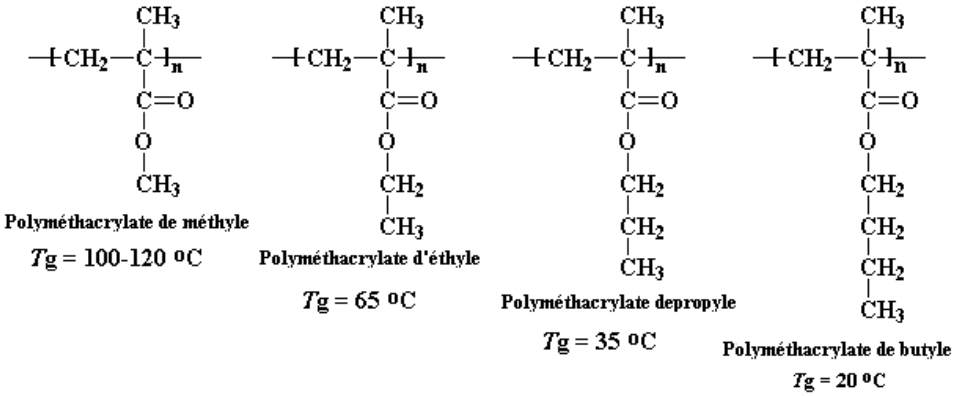

Fig.VII.3: Glass transition for different methacrylate

In the experiments described above and below, we used a silicone characterized by a low $T_{G,}$ which corresponds to a soft elastic behavior at room temperature.

According to literature, this silicone TEC is around 10^{-5} K^{-1} [Han1, Han2]. These polymers TEC even decreases at increasing filling factor [Sim].

II. Experimental

II.1. Strain measurement

II.1.1. Principle

Sample dilatation device was modified to allow thermal measurements. As seen in Fig.VII.3, a thermocouple (type T) is inserted in the sample holder to record temperature during the experiment. The thermocouple, being in contact with the sample, the recorded temperature is set to be the sample temperature. The temperature is assumed to be homogeneous inside the samples during the experiment. The sample and its support are surrounded by a glass tube (ϕ_{int}=3mm, ϕ_{ext}=3.4mm, L=190mm) to play the role of thermal chamber. Magnetostriction curve is recorded using the CCD camera through the transparent glass tube. Cooled air is injected from the top of the tube. The Cooled chamber initially cooled down is then closed by a cover. It is then warmed up to room

temperature by natural thermal exchange with laboratory atmosphere. The warm up temperature was recorded versus time and is plotted in Fig.VII.4.

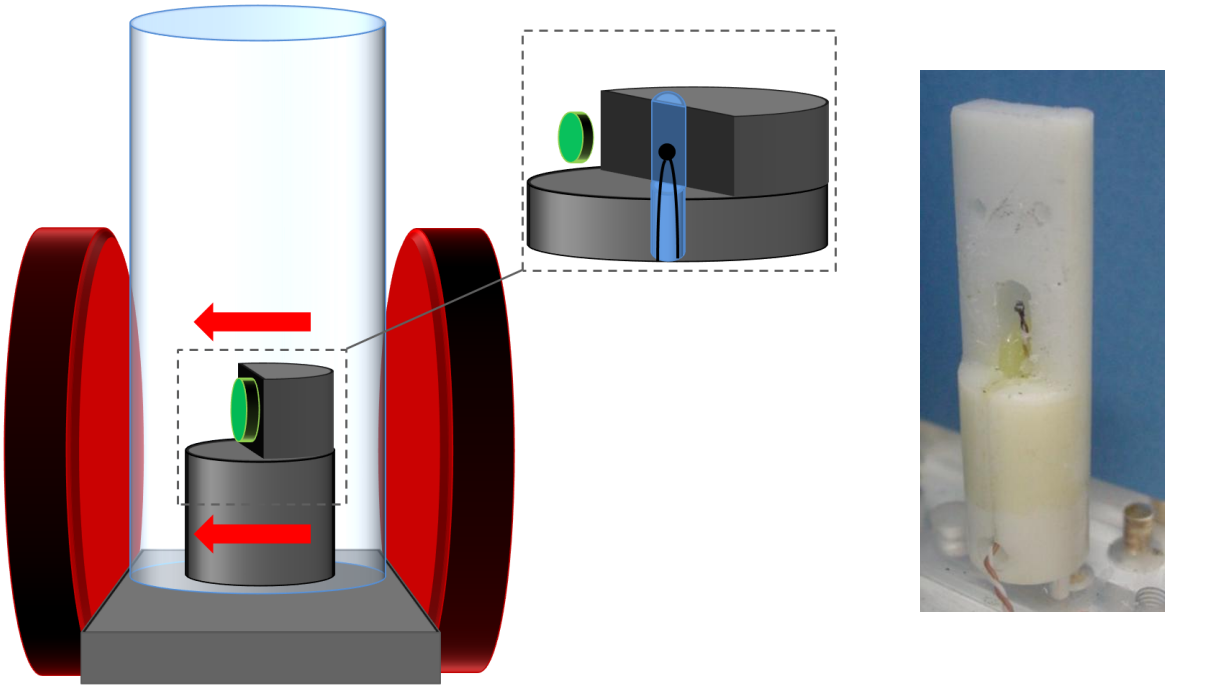

a b

Fig.VII.3: Device modified for thermal measurements

Thermal cycle was repeatable as seen in Fig.VII.4; both experiments with Fe or Gd composite have the same kinetics.

The Fe/silicone and the Gd/silicone samples were cylinders with diameter and thickness equal to 12mm and 4 mm respectively. Gadolinium, 99.9 % pure powder ALFA AESAR, was provided by VWR with a maximal particles size of 325 mesh. The filling factor of the Iron/silicone sample was 27.4%, whereas the filling factor of the Gadolinium/silicone sample was 26.6%.

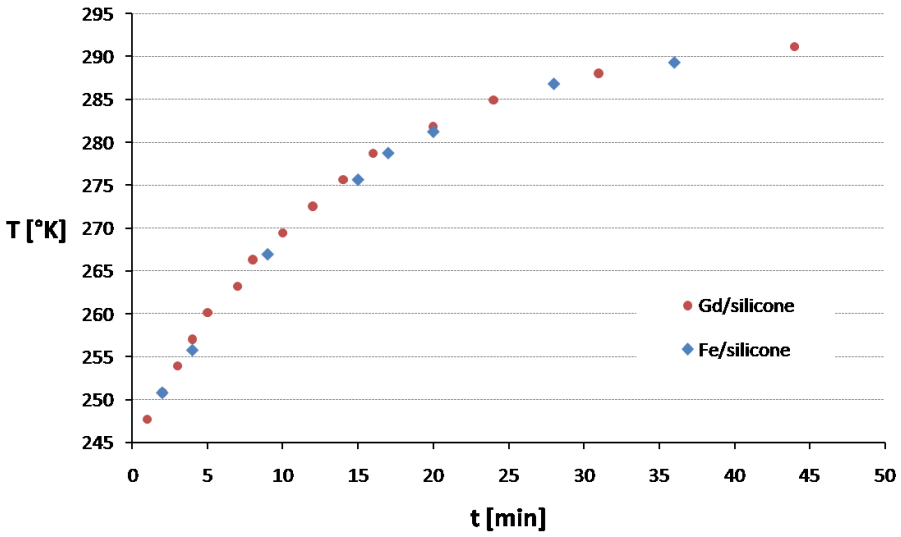

Fig.VII.4: Temperature versus time during experiments

When the thermal chamber starts to warm up, temperature is changed from 245K to 260K in 5 minutes, yielding to a maximal heating rate of 0.05Ks^{-1}. Approaching the room temperature, the heating rate decreases to a lower value, between the 25th and 45th min of the experiment, temperature increased from 285K to roughly 290K; the heating rate in this temperature interval is 0.004Ks^{-1}.

II.1.2. Magnetostriction curves

First experiments were carried out on the Fe/silicone sample. A magnetostriction curve was recorded for an applied field of 0T and of 1.2T. First experiment shows the silicone based composite dependence versus temperature, when the magnetic field is null. Following experiments were made for both Fe/silicone Gd/silicone samples, under a magnetic field of 1.2T.

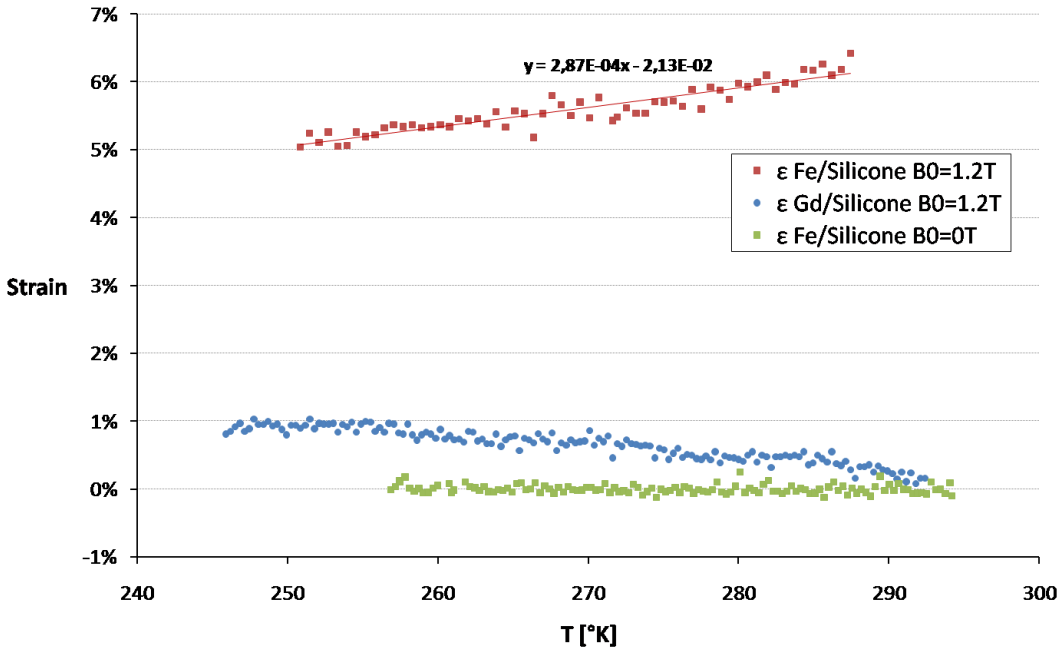

Fig.VII.5: Strain versus temperature for composite based on silicone

Fig.VII.5 presents the thermal behavior of composite with the silicone matrix. If the applied field is turned off, for soft ferromagnetic particles like Iron, no magnetic stress is induced, hence no strain was measured. Only the thermal dilatation occurs; experimental data are provided between 257K and 294K, so that the thermal dilatation is expressed as:

$$\varepsilon_T = \alpha_T \Delta T = 2.1 \cdot 10^{-5} \times 37 = 7.77 \cdot 10^{-4} \approx 0.08\%$$

This value was obtained for TEC of a pure silicone. As previously said, this coefficient is smaller for filled elastomers. For the iron-filled composite the measured curve was nearly zero without magnetic field. If the magnetic field is turned on, iron is magnetized. For temperature ranging from 250K to 290K, the iron magnetization is almost constant, leading to nearly constant induced magnetic stress acting. Strain increases with temperature because of the temperature dependence on the Young modulus. In this case, the strain temperature dependence is purely due to the matrix thermo-mechanical behavior.

In the case of soft ferromagnetic particles like Gadolinium and for temperature ranging from 250K to 290K, where the gadolinium magnetization is strongly temperature sensitive, the magnetic stress also depends on temperature. The strain is dependent on both the magnetic thermo-mechanical behavior for such composite.

III. Discussion

The magnetostriction was found as:

$$\varepsilon_{zz} = \frac{\mu_0 n_{sample} (\phi \cdot M^{sat}_{particle})^2}{2E(\phi)} \qquad \text{eq.VII.1}$$

In this expression, 2 parameters are temperature dependent, magnetization (Fig.VII.1) and the Young modulus (Fig.VII.2). Therefore, eq.VII.1 can be written accounting for temperature as follow:

$$\varepsilon(T) \propto \frac{(M^{sat}_{particle}(T))^2}{E(T)} \qquad \text{eq.VII.2}$$

From this equation, we can write the strain temperature dependence:

$$\frac{\partial \varepsilon_{zz}}{\partial T} = \frac{\mu_0 n_{sample} \phi^2}{2} \left[2M_s \left. \frac{\partial M_s}{\partial T} \right|_{E_0} - \frac{M_s^2}{E^2} \left. \frac{\partial E}{\partial T} \right|_{M_s} \right] \qquad \text{eq.VII.3}$$

$$\frac{\partial \varepsilon_{zz}}{\partial T} = \varepsilon_{zz} \left[2 \left. \frac{\partial M_s}{M_s \partial T} \right|_{E_0} - \left. \frac{\partial E}{E \partial T} \right|_{M_s} \right] \qquad \text{eq.VII.4}$$

Thus, for a temperature increment of *ΔT*, both magnetization and Young modulus will change by *ΔM* and *ΔE* respectively, and we can write the relative magnetostriction for a temperature change as:

$$\frac{\Delta \varepsilon_{zz}}{\varepsilon_{zz}} = \left[2 \left. \frac{\Delta M_s}{M_s} \right|_{E_0} - \left. \frac{\Delta E}{E} \right|_{M_s} \right] \qquad \text{eq.VII.5}$$

In the case of the Iron/Silicone composite, eq.VII.5 can be simplified taking; within the temperature range [250K to 285K]. The value of the magnetization $\mu_0 M_{sat}$ of Iron [Mag1] is 2.18T at 0K and *2*.16T at 300K leading to a relative decrement of 1% to the magnetization, so that the relative change of

magnetization can be neglected unlike the Young modulus in the elastic plateau. Eq.VII.5 simplifies to:

$$\frac{\Delta\varepsilon_{zz}}{\varepsilon_{zz}} = -\frac{\Delta E}{E} \qquad \text{eq.VII.6}$$

The strain variation of the Fe/Silicone is mainly due to the decrease of Young modulus with temperature.

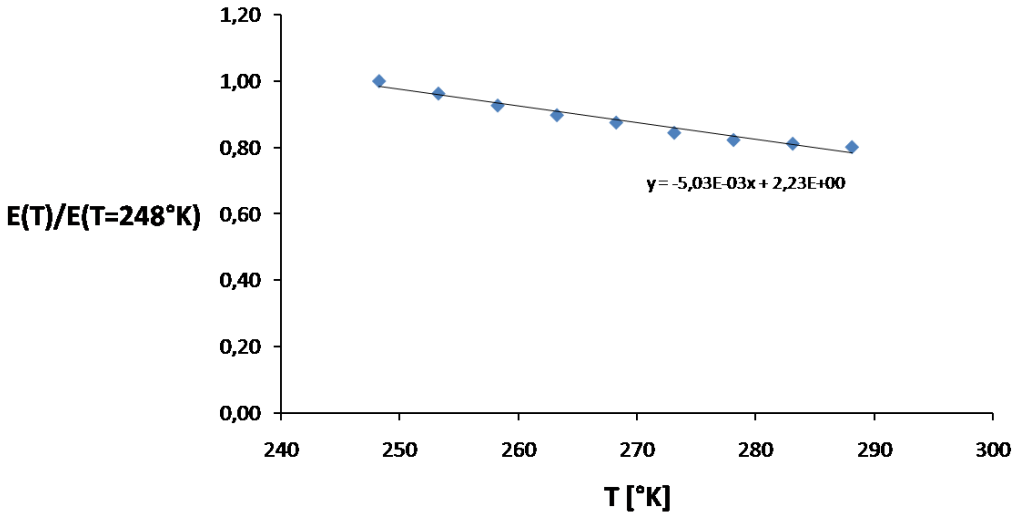

Fig.VII.6: Young modulus of the silicone-filled composite

Strain for the Fe/Silicone sample is plotted in Fig.VII.5 for temperature between 250K and 290K. The thermal dependence of the elastic modulus for the composite is plotted in Fig.VII.6 for temperature ranging from 248K to 288K. Those values are normalized relatively to the lowest measured Young modulus, the one measured at 248°K. The relative Young modulus decreases in the same interval of temperature with a slope of -5.03 K^{-1}, yielding to a relative shift of -20%.

The strain slope of the Fe/Silicone is 2.88 $10^{-4}K^{-1}$ when exposed to the magnetic field with an initial values of 5.2% (T=250K) yielding to a relative increase of +18.6%.

Since the two values are quite similar, a good agreement between experimental data and eq.VII.6 is found. This discussion can be generalized for all temperature above the 250K. Fig.VII.7 presents the variation of the Young modulus and the variation of the Fe/Silicone composite strain versus temperature. Though experimental relative variations of strain are spread around the

modulus relative variation, fitting these data by linear shows that strain and Young modulus fit perfectly well.

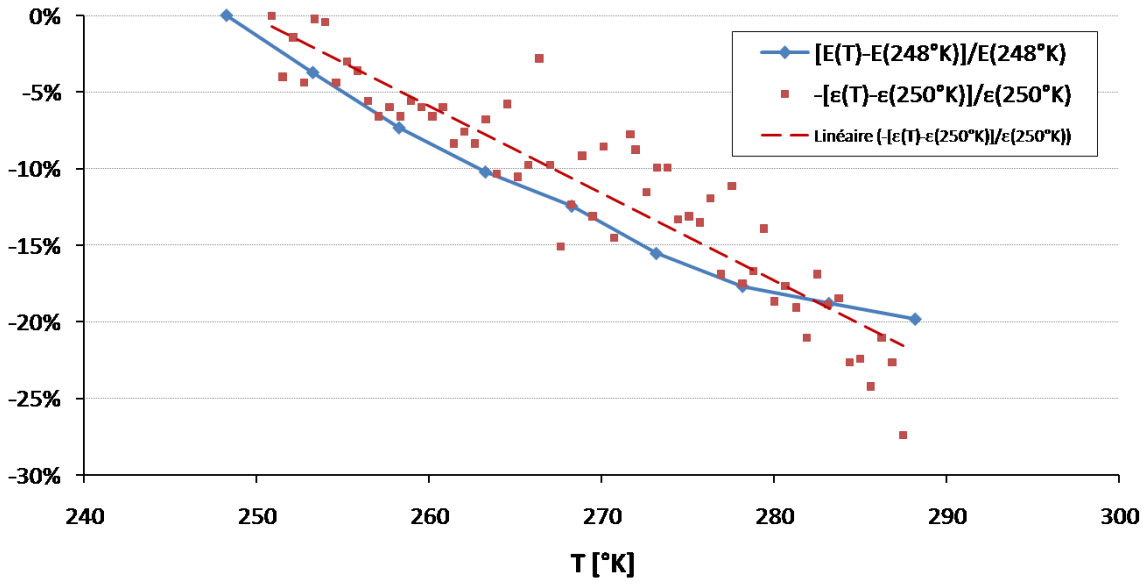

Fig.VII.7: Relative variation of Young modulus and strain versus temperature

In the case of the thermal magnetostriction of Gd/Silicone sample, the behavior is more complex. Close to its Tc, the gadolinium magnetization is highly temperature dependent. The magnetic stress has a non-null value only for temperature below T_C.

For temperature $T \lesssim T_c$, the ferromagnetic magnetization can be written as [Mag]:

$$\frac{M_S(T)}{M_S(T=0)} = A\left(1-\frac{T}{T_C}\right)^{\beta} \qquad \text{eq.VII.7}$$

Where β is a critical exponent predicted to be 0.5 in the Landau transition model [Mag1], but experimental data, for a given element, are generally lower than this value [Kit]. *A* is a correlation coefficient.

Sheng has measured the magnetic critical exponent for a gadolinium sample and found out a 0.31 value and a Curie temperature Tc = 295K [She]. Therefore, a theoretical expression of the thermal magnetostriction of the Gd/Silicone composite, just below the Curie temperature, can be written as:

$$\varepsilon(T) = \frac{n_{sample}\mu_0}{2} \frac{A^2 M_{sat\_Gd}^2 (T=0)\left(1-\frac{T}{T_C}\right)^{2\beta}}{E(T)} \qquad \text{eq.VII.8}$$

Eq.VII.8 provides the thermal strain of a magneto-elastic sample. Young modulus is found to be linear versus the temperature whereas the magnetization behaves as a power-law. The resulting strain has a non-linear dependence with respect to temperature. Experimental data and the theoretical expression, eq.VII.8, are plotted versus the temperature in Fig.VII.8.

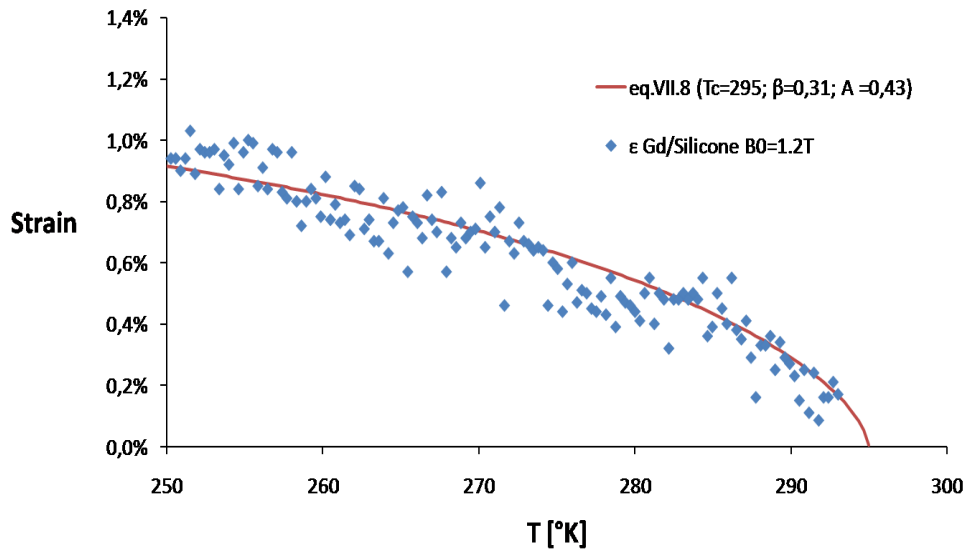

Fig.VII.8: Thermal magnetostriction of Gd/silicone composite versus the temperature. Blue dots are experimental data and the red curve is plotted using eq.VII.8

A regression curve is built using eq.VII.8 and with: Tc = 295K and β=0.31. Those parameters were kept because they are directly linked to the thermal behavior of the magnetization. We also set the $\mu_0 M_{sat}(T=0)$ for gadolinium as 2.66 T [Mag1]. Young modulus thermal dependence was supposed to be the same as for the Fe/silicone composite (Fig.VII.6). However, in order to take into account the

difference in the filling factors of the two composite, we used eq.V.20 & eq.V.24. Thus, for Fe/Silicone composite filled by 27.4 %vol., $E(\phi)/E_0$=4.12. For Gd/Silicone composite filled by 26.6 %vol., $E(\phi)/E_0$=3.9.

The constant *A* was used as a free parameter and set as 0.43, which is close to the Sheng value of 0.49. A good agreement is also found for this thermal composite behavior.

IV. Conclusion

In this chapter, we succeeded in measuring the strain temperature dependence of ferromagnetic particles embedded in a silicone matrix. Thermal dependence is mainly due to the elastic dependence of the matrix filled by iron particles. Those particles have no significant change in magnetization close to room temperature. To improve the model, a composite based on Gadolinium was tested and also provided a good agreement with the model.

To complete the model, measurements made on other matrices with glass transition in the same temperature range should be very interesting. We could obtain an exact compensation of both effects, leading to a constant strain in a given temperature range, like the Invar.

References:

[Ell]: Magnetic properties of rare earth metals; R. J. Elliott, Plenum Publishing Company Ltd. New York (1972); # ISBN-10: 0306305658 # ISBN-13: 978-0306305658

[Bou]: Susceptibilité magnétique du Gadolinium pur en fonction du champ dans la région de réorientation de spins; A. Bourkaa, P. Vajda, J.N. Daou, *Journal de Physique IV* 02 (1992) 133

[Mag1]: Magnetism I-Fundamentals, E. du Tremolet de Lacheisserie, D. Gignoux, M. Schlenker, Springer-Verlag New York Inc. (2004), #ISBN-10: 0387229671, #ISBN-13**:** 978-0387229676

[She]: New Technique for the measurement of Magnetic Critical Exponent β*, Ping Sheng, C. N. Manikopoulos, T. R. Carver, *Phys. Rv. Lett*. 30 (1973) 234

[Bor]: Ferromagnetism, Richard M. Borzorth, John Wiley & Sons Inc; New York 1993; # ISBN-10: 0780310322; # ISBN-13: 978-0780310322

[Eng]: Engineering toolbox, http://www.engineeringtoolbox.com/linear-expansion-coefficients-d_95.html

[Pau]: Influence des renforts sur l'évolution en température du module d'Young de différents composites à matrice polymère, S. Pautrot, F. Lagattu, P. Gadaud, *Annales de chimie* 28 (2003) pp. 43-52

[Han1]: Polymer Handbook 4th edition, Brandrup, J.; Immergut, Edmund H.; Grulke. John Wiley & Sons, 1999; # ISBN -10**:** 0471166286; # ISBN -13**:** 978-0471166283

[Han2]: Handbook of composites 2nd edition p.365. Edited by S.T. Peters; Chapman & Hall, London 1998; # ISBN 0 412 54020 7

[Sim]: Thermal characterization of Al2O3 and ZnO reinforced silicone rubber as thermal pads for heat dissipation purposes; L.C. Sim, S.R. Ramanan, H. Ismail, K.N. Seetharamu, T.J. Goh, *Thermochimica Acta* 430 (2005) 155–165.

[Kit]: Introduction to Solid State Physics 5th edition, Charles Kittel, Dunod 1994 #ISBN-10**:** 2100497103; #ISBN -13**:** 978-2100497102

Conclusion

Embedding ferromagnetic particles, which are weakly magnetostrictive but highly magnetic, in a soft elastic matrix generates an apparent magnetostriction of the composite when submitted to a homogeneous magnetic field. If the classic magnetostriction arises from the coupling between the ferromagnetic interaction and the elastic coefficient of a crystal lattice, the observed strain of such composite was found as a consequence of dipolar interaction between the ferromagnetic particles. If the largest magnetostrictive, called giant, reached a deformation in the order of 0.1%, the combination of that dipolar interaction and the low value of the Young modulus of the matrix results in a larger magnetostriction, two orders of higher magnitude, when compared to those giant magnetostrictive materials. By the magnetostriction that arises from the dipolar interactions, two main parameters have to be considered to analyze the magnetically induced deformation, namely (i) the shape effect and (ii) the particles concentrations within the composite. It is worthy to notice that the dipolar energy density depends on the sample shape. Forces are located close to the boundaries of the magnetic material. In this work, most our samples were cylindrical. Axial forces act on the two disks and radial forces act on the lateral surface. Axial forces and radial forces result in the cylinder elongation. The magnetic energy (more precisely the demagnetizing energy density) decreases as the composite elongates because its aspect ratio increases during the deformation. Thereby, a flat sample will present a larger strain than a long one, at constant amount of particles. Thus, we succeeded in recording a strain of 9.2 % for a 30% filled composite with an external field of 1T. The second parameter is the particles concentration within the matrix. A magnetic moment creates a dipolar force on every other moment and each of those other moments is also creating a force on that moment The effective magnetic force acting on the composite, in the saturation state, is proportional to square of the filling factor : $F_{mag} \sim \phi^2$. The elastic response being controlled by the Young modulus is therefore also affected by the filling factor. If the magnetic force is easily expressed as a function of the filling factor, the Young modulus of the composite have to be defined by more complex expression in regards to the amount of particles. Young modulus, like thermal/electric conductivity of composite, is highly dependent on the filling factor; low filling are having a simple expression, whereas for larger values a relationship accounting for the percolation must be chosen. The percolation of stiff particles generates a limitation of the macroscopic strain. The conversion of

the demagnetizing energy into mechanical energy is shown to be optimal for a filling factor defined by the half of a maximum packing fraction which in our case was found for 54%vol. yielding to an optimal filling factor of 27%.

Unlike to a composite filled with soft magnetic particles where the strain is a quadratic function of the magnetization, composite filled with hard magnetic particles were found to present linear behavior relative to the applied field. Positive applied filed yields to positive strain and reciprocally negative field yields to a negative strain. Moreover, strain of such composite presents a memory effect: the strain at a given applied field depends on the previous state of magnetostriction. Magnetization of hard particles is usually symmetric versus the applied field, but for an elastic composite, particles are magnetized by non-symmetrical process: such composite elongates in positive applied field while they contracted when submitted to a negative field; the demagnetizing field being shape dependent has different amplitude in those 2 cases; magnetic particle inside the composite sees a non-symmetrical field. An enhancement of the strain results of this phenomenon. Filing factor has an effect on the magnetization of the composite and on the Young modulus; temperature also rules these parameters value leading to a temperature dependence on the strain. Examples of thermal behavior have been presented in the last chapter. The temperature behavior of the magnetostriction was measured. Further experiments would complete it; as for instance the behavior near the glass transition temperature, which is characterized by a drastically stiff change. By tuning these different, parameters, materials with original temperature behavior could be probably designed.

In this thesis, measurements were made in static field. A next study of the magnetostriction could investigate the effect of dynamic fields. The strain amplitude depends on frequencies and on the stress. Applying a static magnetic field elongates the material; dynamic magnetic field would therefore strain the composite with respect to the frequency. Moreover, for material with low damping and at the resonating frequencies the amplitude of the strain is maximal, larger than static strain.

Applications of such magnetostrictive materials are transducers/sensors because of their large strain range. However, the hysteresis may be an important issue for commercial devices, which needs repeatable strain. A surface chemical treatment of the particles might improve adhesion with the polymer reducing the damage at this interface when the composite is strained.

Annexes

I. Calculation of the force on the lateral boundary:

The general case of a lateral boundary is treated here. As described in chapter 3, we consider a magnetic moment surrounded by a half magnetic spherical shell. Magnetization direction is along u_z. On that surface, we can set an outward normal unit vector as seen on fig.A.1.

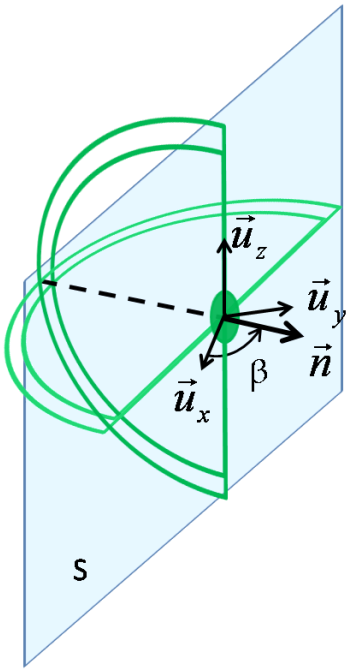

Fig.A.1. Lateral boundary defined by its normal outward unit vector

This vector is written as:

$$\vec{n} = \cos(\beta)\vec{u}_x + \sin(\beta)\vec{u}_y \qquad \text{eq.A.1}$$

As discussed in the 3rd chapter, only f_x and f_y components of the force are non-null. Then the force has to be written as:

$$\vec{F} = f_x\vec{u}_x + f_y\vec{u}_y \qquad \text{eq.A.2}$$

The interval of integration for the angle θ remains unchanged, namely from 0 to π. On the contrary, the angle φ ranges from β+π/2 to β+3π/2. Using the following integral:

$$\int_0^{\pi} \sin(\theta)[1-5\cos^2(\theta)]\sin(\theta)d\theta = -\frac{\pi}{8} \qquad \text{eq.A.3}$$

the two f_x and f_y components of the force are:

$$\int_{\varphi}\int_{\theta} f_x(\theta,\varphi)\sin(\theta)d\theta d\varphi = -\frac{\pi}{8}\int_{\beta+\frac{\pi}{2}}^{\beta+\frac{3\pi}{2}} \cos(\varphi)d\varphi = \frac{\pi}{4}\cos(\beta) \qquad \text{eq.A.4}$$

$$\int_{\varphi}\int_{\theta} f_y(\theta,\varphi)\sin(\theta)d\theta d\varphi = -\frac{\pi}{8}\int_{\beta+\frac{\pi}{2}}^{\beta+\frac{3\pi}{2}} \sin(\varphi)d\varphi = \frac{\pi}{4}\sin(\beta) \qquad \text{eq.A.5}$$

The radial amplitude term is:

$$\int_e^d A_r r^2 dr = \frac{1}{e} - \frac{1}{d} \qquad \text{eq.A.6}$$

with *e* the length characterizing the exclude volume of the considered moment and *d* is the distance between that moment and the shell. Going back to the force acting on the magnetic moment, which is the product of the radial and angular term, we have both f_x and f_y components negative. Rewriting the eq.A.2 as:

$$\vec{F} = -\frac{\pi}{4}\left(\frac{1}{e} - \frac{1}{d}\right)(\cos(\beta)\vec{u}_x + \sin(\beta)\vec{u}_y) \qquad \text{eq.A.7}$$

$$\vec{F} = -\frac{\pi}{4}\left(\frac{1}{e} - \frac{1}{d}\right)\vec{n} \qquad \text{eq.A.8}$$

A magnetized material experiences force on its boundaries. On surface parallel to the magnetization direction, that magnetic force is always directed toward the material core. Magnetized material experiences a contraction from all its boundaries parallel to its magnetization direction.

Introduction

Le but de cette thèse est la mesure et la description de la magnetostriction apparente de composites placés dans un champ magnétique homogène. Les composites étudiés sont des composés de particules ferromagnétiques (principalement du fer) dispersées dans une matrice élastique. La déformation d'un tel matériau nécessite un couplage entre celui-ci et le champ magnétique externe. Ces matériaux sont aussi appelés matériaux actifs. La déformation induite a été étudiée depuis la découverte de la magnetostriction et de la piézoélectricité, il y a près de deux cent ans. L'amélioration de ces propriétés a d'abord été explorée par des approches métallurgiques. Néanmoins les constantes élastiques de ces alliages, généralement de l'ordre de 100 GPa, en limite la déformation. Une autre solution, qui consiste a disperser des particules magnétiques dans une matrice de faible module élastique, a été récemment proposée. Les élastomères organiques sont donc des candidats idéaux de par leur module de Young de quelques MPa. Ces matériaux, résultant du mélange de particules ferromagnétiques (ou ferroélectriques) dans une telle matrice polymère sont appelés "Magneto (Electro) Rheological Elastomers" ou M.R.E.

Dans des travaux précédents, une élongation de 4.81% a été observée pour un composite contenant 15% (vol.) de particules de fer et une porosité de 45% (vol.), soumis à un champ de 8 Tesla, alors que la matrice n'est pas magnétique et que la magnetostriction du fer est très faible (valeur maximale de l'ordre de 10^{-5}). La déformation du composite est de 4 ordres de grandeur supérieure à celle de la phase magnétique. Si le phénomène observé est bien la déformation d'un matériau en présence d'un champ magnétique externe, à l'instar de la magnetostriction d'un cristal ferromagnétique, l'origine physique de cette déformation est différente. Elle est ici la conséquence de l'interaction de particules magnétiques placées dans une matrice élastique souple. On gardera malgré cette remarque, le terme de magnetostriction dans la suite de cette thèse.

Les alliages à base de terre rare possèdent une amplitude magnetostriction de l'ordre de 10^{-3}, qualifiée de "giant magnetostriction". La magnetostriction apparente des composite M.R.E. est encore beacoup plus grande que ces matériaux magnétostrictifs classiques ; le phénomène est donc qualifiée de "huge magnetostriction".

Les mécanismes a l origine de cette magnetostriction apparent sont détaillés dans les chapitres suivants.

Résumé des chapitres

Chapitre 1:

Le premier chapitre présente le point de départ de cette étude, les lois du magnétisme et de l'élasticité, nécessaires pour les chapitres suivants, sont introduites ici. Une brève présentation des M.R.E. et leurs propriétés magnéto-élastiques présentées dans ce chapitre constituent la base bibliographique de ce travail. Diverses études ont démontrés l'effet d'un champ magnétique inhomogène sur ces matériaux ; ils s étirent vers les champs intenses ou encore présentent une augmentation du module de Young (l'effet « delta-E ») lorsqu'ils sont exposés à un champ magnétique. La déformation en champ homogène a été étudiée pour différents types de M.R.E. Les composites dont les particules sont distribuées aléatoirement dans la matrice tendent à s'allonger dans la direction du champ magnétique alors que ceux ayant les particules formant des alignements parallèles au champ se contracte sous l'effet de ce champ.

Chapitre 2:

Le second chapitre présente la méthode de préparation des composites ainsi que les techniques expérimentales utilisées au cours de cette thèse. Les particules sont d'abord mélangées dans la matrice liquide puis l'addition du durcisseur permet l'obtention d'échantillons de formes diverses suivant le moule utilisé. La mesure d'aimantation est faite en utilisant un dispositif de balance de Faraday. L'échantillon est placé dans un gradient de champ magnétique créant une force sur cet échantillon, cette force est enregistrée via la mesure du poids apparent sur une balance placée dessous. Un électro-aimant générant un champ magnétique statique maximal de 1,2 T a été utilisé pour les mesures de magnetostriction. La déformation de l'échantillon est ensuite déterminée à l'aide d'une caméra et d'un traitement numérique. Le module de Young des composites est mesuré par mesure mécanique dynamique (DMA).

Chapitre 3:

Le troisième chapitre traite de l'origine de cette magnetostriction apparente. Un calcul basé sur les interactions dipolaires entre les particules est effectué. Une carte des forces est ainsi obtenue

pour une distribution de particules dans un cylindre. Cette carte montre des forces de traction sont concentrés sur les bords supérieurs et inferieurs du cylindre alors que des forces de compression le sont sur la surface latérale de ce cylindre; il est notable que la résultante des forces au sein du cylindre est nulle. Cette projection des forces sur un plan axisymétrique du cylindre est ensuite utilisée dans un logiciel de calcul par élément fini (FEM) pour évaluer la déformation résultante. La déformation obtenue par ce calcul est en bon accord avec la mesure de magnetostriction d'un échantillon, sans paramètres ajustables.

Chapitre 4:

Dans le chapitre 4, l'aimantation du composite est étudiée. L'aimantation en fonction du champ magnétique externe est décrite par 2 paramètres: le coefficient de champ démagnétisant à champ faible et l'aimantation à saturation pour les champs plus intenses. Ces 2 paramètres sont étudiés expérimentalement et théoriquement pour divers taux de particules. L'aimantation à saturation du composite est simplement celle du matériau ferromagnétique, quelle que soit la distribution de ces particules. Le coefficient de champ démagnétisant dépend du taux de particules mais aussi de la distribution et de la forme des particules.

Chapitre 5:

Dans ce chapitre, nous donnons une expression de la magnetostriction du composite à partir des différent paramètres macroscopiques : module de Young de la matrice, aimantation des particules et le taux de particules. Ce modèle est basé sur la conversion d'énergie magnétique, et plus précisément de l'énergie démagnétisante, en énergie élastique. En effet cette énergie démagnetisante dépend de la forme de l'échantillon et décroit au fur et à mesure que l'échantillon s'allonge. L'effet de forme initiale de l'échantillon est prédit et vérifié expérimentalement. L'effet du taux de particules est aussi traité dans ce chapitre ; à taux croissant de particules dans le composite, l'aimantation et le module de Young augmentent et sont donc en compétition quant à l'évolution de la déformation. Ainsi, passé un certain seuil, le module de Young augmente plus fortement et limite par conséquent l'amplitude de déformation. L'expression choisie pour exprimer ce module de Young dépend de la concentration. A l'instar de la conductivité thermique ou électrique dans un composite, le module de Young s'exprime simplement pour de faible taux de charge mais augmente fortement pour de plus grand taux de charge : dans ce cas une expression prenant en compte l'effet de

percolation des particules est plus pertinent. Cette percolation e particules dures génère une limite dans la déformation macroscopique de la déformation. La déformation de composite est optimale pour un taux de charge étant la moitié de la concentration maximale, qui dans notre cas fut mesurée à 54%vol., ce qui définit ce taux optimale à 27%.

Chapitre 6:

Dans ce chapitre, les particules ferromagnétiques des composites ont un comportement magnétique dur. Contrairement aux composites contenant des particules magnétiques douces où la déformation était toujours positive, la déformation est du signe du champ appliqué et présente un comportement piézomagnétique pour de faible valeur de champ. De plus, une amplification de la déformation est observée à mesure que les champs positifs et négatifs sont alternés. Cet effet apparaît si le champ appliqué est supérieure au champ coercitif des particules dures. Enfin, l'effet de la composante radiale du champ interne du composite cylindrique est décrit. Cette composante radiale crée une composante radiale de déformation.

Chapitre 7:

Dans ce dernier chapitre, l'effet de la température sur la déformation est décrit. L'aimantation des particules ferromagnétiques et le module de Young de la matrice sont dépendant de la température. Deux types de composites ont été étudiés ; les premiers sont renforcés par des particules de fer qui possède une température de Curie très supérieurs aux températures de nos expériences. Les seconds sont renforcés par des particules de gadolinium ayant une température de Curie proche des températures expérimentales. La déformation des composites ayant des particules de fer augmente avec la température qui n'agit que sur le module de Young. La déformation de composite avec des particules de gadolinium diminue et tends vers zéro à mesure que la température approche la température de Curie de ces particules.

Conclusion

Les composites constitués de particules ferromagnétiques, très faiblement magnétostrictifs mais possédant une forte aimantation à saturation, distribuées dans une matrice élastiquement douce se déforment quand ils sont placés dans un champ magnétique homogène. La déformation observée résulte des interactions dipolaires entre les particules. Alors que la plus forte valeur de déformation atteinte par des alliages à base de terre rare ne dépasse pas 0,1%, la déformation atteinte par les composites M.R.E. parvient à atteindre des amplitudes de 2 ordres supérieures en combinant les propriétés de ses constituants. Les forces sont localisées près des surfaces du composite ; des forces de traction agissent sur les 2 surfaces supérieures et inférieures du cylindre alors que des forces de compression agissent sur la surface latérale ; la combinaison de ces forces crée l'allongement de ce cylindre. Pour analyser la déformation de ces composites exposés à un champ externe, deux effets sont étudiés en particulier ; (i) l'effet de du facteur de forme et (ii) le taux de particules dans le composite. Il est important de noter que l'énergie dipolaire dépend de la forme du de l'échantillon considérée. L'énergie magnétique, plus précisément l'énergie démagnétisante décroit lors de l'allongement du composite du fait de l'augmentation de son facteur de forme. Par conséquent, un échantillon "plat" s'allongera plus fortement en valeur relative qu'un échantillon "long", pour un même taux de particules. Nous avons ainsi réussi à mesurer une déformation de 9,2 % pour un composite chargé à 30% placé dans un champ externe de 1T. Le paramètre clé est le taux de particules dans le composite. L'interaction des particules ayant leur aimantation à saturation est de proportionnelle au carré de ce taux de particules. La réponse élastique, contrôlée notamment par le module de Young, est aussi dépendante de la concentration des particules dans le composite. En utilisant un modèle empirique pour évaluer le module de Young des composites, on a pu prédire une valeur optimale du taux de particules et la vérifier expérimentalement en mesurant la déformation en fonction de ce taux.

Dans le cas de composites renforcés par des particules magnétiques douces la déformation ne dépend pas du signe du champ appliqué. Au contraire, en remplaçant ces particules douces par des particules dures, la déformation est, du même signe que le champ appliqué. Un champ positif allonge le composite alors qu'un champ négatif le contracte. L'aimantation de particules magnétiquement dures est normalement symétrique vis-à-vis du champ externe. Ce n'est pas le cas dans les matériaux composites élastiques. L'allongement du composite en champ externe positif et la contraction en champ externe négatif induisent des amplitudes du champ démagnétisant

différentes. Les particules magnétiques voient un champ local non symétrique. Une augmentation de l'amplitude de déformation a été observée au cours de cycles successifs à même amplitude du champ.

Enfin, à l'instar du taux de particules qui modifie l'aimantation du composite et son module de Young, la température influe aussi sur ces deux paramètres. La déformation dépend donc de la température. Le comportement de la magnetostriction en température est présenté dans le dernier chapitre de la thèse. L'effet de la température de Curie a ainsi été démontré expérimentalement. D'autres expériences sur l'effet de la température de transition vitreuse, pour laquelle la valeur du module de Young change radicalement, compléteraient la présentation sur le comportement thermique de la déformation. En jouant sur ces deux paramètres, des matériaux aux caractéristiques thermiques originales pourraient être conçus.

Dans cette thèse, la magnetostriction a été mesurée en champ magnétique statique. Il serait donc intéressant d'étudier l'effet de champ magnétique dynamique. La déformation des élastomères dépend de la fréquence de la sollicitation. Un champ dynamique pourrait aussi apporter une nouvelle contribution, liée à la fréquence de cette sollicitation, à la magnetostriction apparente. (De plus, pour des pièces constituées de matériaux présentant un faible amortissement, et à leur fréquence de résonance, l'amplitude de déformation est maximale et plus importante que la déformation statique.)

L'utilisation comme actionneur ou comme détecteur sont des applications possibles de ces nouveaux matériaux magnétostrictifs due à leur grande déformation. Néanmoins, l'hystérésis observé, mais non étudié ici, reste encore un problème majeur à leur emploi dans des dispositifs industriels. Son origine ne peut qu'être liée à des mécanismes d'endommagement à l'interface particules-matrice (ce que confirme l'étude bibliographique). Des traitements chimiques des particules peuvent améliorer l'adhésion avec le polymère et ainsi diminuer l'amplitude de cette hystérésis.

Abstract:

This thesis is aimed to measure and explain the elongation of M.R.E. placed in a homogenous magnetic field. M.R.E. is material consisting in ferromagnetic particles embedded in an elastic matrix. Combination of a silicone, with low elastic modulus (E_0=0.14 MPa), and Iron particles, characterized by a high saturate magnetization ($\mu_0 M_{sat}$=2.14 T), allows large deformation (some percents) when placed in the applied field $\mu_0 H_0$=1.2 T. Coupling of the dipolar forces calculation between the particles, randomly distributed in a cylinder-shape volume, with strain calculus, using F.E.M. software, is a good agreement with a magnetostrictive experiment. Magnetized sample get a so-called "demagnetizing" energy bounded to it shape: "flatter" samples yields to a larger demagnetizing energy than longer ones. Composite magnetization has been investigated in this thesis through 2 parameters: the saturate magnetization and the effective demagnetizing coefficient. Experiments, carried on samples with different shapes, show the effect of the demagnetizing energy, flattest sample (with aspect ratio c/a =0.3) exhibits the largest strain of 10%. A model, based on the competition of the demagnetizing energy and elastic energy, during the strain, accounts for this shape effect. That model also deals with the filling factor impact on the strain. An optimal filling factor of 27% has been measured and predicted.

Magnetostriction of composites with hard magnetic particles was investigated as function of the applied field. Due to the magnetization hysteresis loop of those particles, a "memory effect" was found in the magnetostriction.

Finally, elastic modulus and particle magnetization are both temperature dependent. The temperature behavior of the magnetostriction is measured. By tuning these parameters, materials with different temperature behavior could be designed.

Résumé:

Le but de cette thèse est l'étude expérimentale et théorique de l'élongation de M.R.E. (Magneto Rheological Elastomer) placé dans un champ magnétique homogène. Ces matériaux sont constitués de particules ferromagnétiques distribuées au sein d'une matrice élastique. La combinaison d'une matrice de silicone de faible module de Young (E_0=0,14 MPa) combinée à la forte aimantation des particules de fer ($\mu_0 M_{sat}$=2,14 T) permet d'atteindre des déformations de plusieurs pourcents, pour un champ appliqué $\mu_0 H_0$=1,2 T. Le calcul des forces dipolaires entre les particules, distribuées aléatoirement dans un volume de forme cylindrique, couplé à un calcul de déformation (utilisant un logiciel F.E.M.) est en accord avec la mesure de magnetostriction. Un échantillon aimanté acquiert une énergie magnétique dite « démagnétisante » liée à sa forme : un échantillon « plat » aura une énergie démagnétisante plus importante qu'un échantillon « long ». L'aimantation d'un composite a été étudié dans cette thèse via 2 paramètres : l'aimantation à saturation et le coefficient de champ démagnétisant effectif. La mesure de déformation faite sur des échantillons de différentes formes montre l'effet de cette énergie démagnétisante : l'échantillon le plus plat (de facteur de forme c/a=0.3) se déforme ainsi jusqu'à près de 10 %. Un modèle basé sur la compétition entre l'énergie démagnétisante et l'énergie élastique, pendant la déformation, donne des valeurs de déformation prenant en compte cet effet de forme. Ce modèle prend en compte aussi l'effet de la fraction volumique sur la déformation du composite. Une concentration optimale de 27 % a été mesurée et prédite.

La magnetostriction de composites avec des particules magnétiques dures a aussi été mesurée en fonction du champ. L'effet de l'hystérésis de ces particules génère un "effet mémoire" à la courbe de magnetostriction.

Enfin, le comportement thermique de la magnetostriction de ces composites a été mesuré. La constante élastique de la matrice et l'aimantation des particules sont des fonctions de la température. Le rôle de ces paramètres permet de concevoir des matériaux avec différentes propriétés thermiques.